

The Preparation and Characterization of Hydroxyapatite Bioceramic Implant Material

**By
Rukiye Çiftçiođlu**

**A Dissertation Submitted to the
Graduate School in Partial Fulfillment of the
Requirements for the Degree of**

MASTER OF SCIENCE

**Department : Materials Science and Engineering
Major : Materials Science and Engineering**

**Izmir Institute of Technology
Izmir , Turkey
January, 2000**

We approve the thesis of Rukiye ÇİFTÇİOĞLU

Date of Signature

.....


28. 01. 2000

Assoc.Prof. Dr. Şebnem HARSA

Supervisor

Department of Food Engineering

.....


28. 01. 2000

Prof. Dr. Semra ÜLKÜ

Co-Supervisor

Department of Chemical Engineering

.....


28. 01. 2000

Asst.Prof.Dr. Funda TIHMİNLİOĞLU

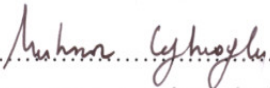
Department of Chemical Engineering

.....


28. 01. 2000

Asst.Prof.Dr. Barış ÖZERDEM

Department of Mechanical Engineering

.....


28. 01. 2000

Prof. Dr. Muhsin ÇİFTÇİOĞLU

Head of Interdisciplinary

Materials Science and Engineering Program

ABSTRACT

The use of hydroxyapatite (HA) powders and ceramics as a biomaterial was investigated in this work. A commercial HA powder was used for the preparation of HA ceramics and the adsorption of Bovine Serum Albumin (BSA) onto HA has been investigated.

The powder and the sintered ceramics were characterized by TGA, DTA, Optical Microscopy, Microhardness Tester, XRD, and FTIR. The sintering studies have shown that it was possible to prepare porous ceramics above 800°C and dense ceramics at 1200-1250°C range. The HA powder lost about 5.5% by weight during heat treatment up to 1000°C and 80% of this weight loss is due to adsorbed water. The particle size of the powder was determined to be submicron whereas the grain sizes of the 1250°C sintered ceramic was in the 1-5 μm . range. A maximum Vickers Hardness of 585 Hv was determined for the 1250°C sintered 97.2% dense ceramic. XRD patterns of the powder and the 1250°C sintered ceramic were identical and almost phase pure. A small CaO peak was detected in the samples which was believed to be remnants of the powder preparation process.

The adsorption of BSA onto HA has been studied as a function of time, protein concentration, pH, ionic strength, and HA solids loading. Adsorption experiments were also conducted with commercial alumina and zirconia ceramic powders. Uptake curves have shown that the adsorption process was almost completed in less than ten minutes. Adsorption isotherms at different pH (4.5-7.4) have been obtained and analyzed using the Langmuir model. The Langmuir parameters q_m (maximum amount of protein adsorbed, mg BSA/g HA) and K' (affinity constant, ml/mg BSA) have been calculated. q_m decreased from 119 to 61.3 with the increase in pH from 4.7 to 7.4. A maximum of 46.1 for K' was determined at pH=5.6 and K' had the lowest value of 3.5 at pH=7.4. Electrostatic attractions were held responsible for the K' maximum at pH=5.6 since HA and BSA surfaces are oppositely charged. The presence of a considerably high amount of BSA adsorption on the HA surface at pH=4.7 where the protein should have close to zero net charge was attributed to hydrophobic effects. The amount of adsorption at equilibrium in the 4.5-5.8 pH range was determined to be twice of that in the 6-8 pH range. Almost 100% of the protein was recovered with a HA solids loading of 750 mg HA/50 ml solution at equilibrium for an initial BSA concentration of 1 mg BSA/ml solution.

ÖZ

Bu çalışmada hidroksiapatit (HA) tozu ve seramiklerinin biyomalzemeler olarak kullanımını incelendi. HA seramiklerinin hazırlanması ve Bovin Serum Albumin (BSA) proteininin HA tozu üzerinde adsorpsiyonunun incelenmesinde ticari bir toz kullanıldı.

HA tozu ve hazırlanan seramikler TGA, DTA, Optik Mikroskop, Mikrosertlik Cihazı, XRD, ve FTIR gibi tekniklerle karakterize edildi. Sinterleme çalışmaları 800°C'nin üstünde gözenekli seramiklerin ve 1200-1250°C aralığında yoğun seramiklerin hazırlanmasının mümkün olduğunu gösterdi. Hidroksiapatit tozu 1000°C'ye kadar yapılan termogravimetrik analizde toplam yaklaşık 5.5% ağırlık kaybetti ve bunun yüzde 80'inin adsorplanmış su olduğu sonucuna varıldı. Toz tanecik boyutunun mikronaltı ve 1250°C'de sinterlenmiş yoğun seramikteki grain boyutunun 1-5µm aralığında olduğu saptandı. Maximum Vickers sertliği 97.2% yoğun seramikte 585 Hv. olarak ölçüldü. Tozun ve yoğun 1250°C seramiğinin XRD desenleri özdeş ve saf tek faza oldukça yakın bulundu. Toz hazırlamadan kaynaklandığı düşünülen şiddeti düşük bir CaO faz piki iki örnekte de gözlemlendi.

BSA'nın HA üzerinde adsorpsiyonu zaman, protein konsantrasyonu, pH, iyonik güç ve HA katı yüklemesinin fonksiyonları olarak incelendi. Adsorpsiyon deneyleri ticari zirkonya ve alümina seramik tozlarıyla da sınırlı olarak yürütüldü. Alım eğrileri adsorpsiyonun on dakikadan az sürelerde tamamlandığını gösterdi. Değişik pH'lerde (4.5-7.4) belirlenen adsorpsiyon izotermi Langmuir modeli kullanılarak analiz edildi. Langmuir parametreleri q_m (maksimum adsorblanan protein miktarı, mg BSA/g HA) ve K' (afinite sabiti, ml/mg BSA) hesaplandı. Solüsyonun pH değerinin 4.7'den 7.4'e değişimiyle q_m değerinin 119'dan 61.3'e düştüğü saptandı. Maksimum K' parametresi pH'da 46.1 ve minimum K' pH=7.4'de 3.5 olarak saptandı. K' parametresinin pH=5.6'daki maksimum değerinden zıt yüklü yüzeylere sahip HA yüzeyi ve BSA protein molekülleri arasındaki elektrostatik çekimlerin sorumlu olduğu sonucuna varıldı. Protein moleküllerinin sıfıra yaklaşık net yüke sahip olduğu pH=4.7'de gözlenen göreceli olarak büyük miktardaki BSA adsorpsiyonunun nedeni hidrofobik etkilerle açıklanabilir. Denge durumunda adsorplanan toplam protein miktarı 4.5-5.8 pH aralığında 6-8 pH aralığındakinin iki katı olarak bulundu. 1 mg BSA/ml solüsyon başlangıç BSA konsantrasyonuna sabit bir ortamdan proteinin yaklaşık 100%'ünün 750 mg HA/50 ml solüsyon katı yüklemesinde katı tarafından alındığı bulundu.

TABLE OF CONTENTS

LIST OF FIGURES.....	viii
LIST OF TABLES.....	xi
CHAPTER I : INTRODUCTION.....	1
CHAPTER II: BIOMEDICAL MATERIALS.....	5
2.1 Classification of Biomaterials.....	5
2.2 Biofunctionality and Biocompatibility.....	7
2.2.1 Biofunctionality.....	8
2.2.2 Biocompatibility.....	9
2.3 Structure and Properties of Hard Tissues (Bone and Teeth).....	12
2.3.1 Composition and Structure	12
2.3.2 Mechanical Properties of Bone and Teeth.....	15
2.4 Bioceramics.....	18
CHAPTER III: PROCESSING AND PROPERTIES OF HA.....	24
3.1 Calcium Phosphate Ceramics.....	24
3.2 HA Powder Processing.....	25
3.3 Sintering of HA Powders.....	29
3.4 Characterization of Powders and Ceramics.....	33
3.5 Applications of HA Ceramics	37
CHAPTER IV: ADSORPTION.....	38
4.1 Definition and Types of Adsorption-Adsorbents	38
4.2 Adsorption Equilibria.....	41
4.3 Adsorption Kinetics.....	43
4.4 Batch Adsorption.....	45

4.5 Protein Adsorption.....	46
4.5.1 Proteins.....	46
4.5.2 Bovine Serum Albumin (BSA).....	48
4.5.3 Adsorption of Proteins on Solids.....	49
CHAPTER V: EXPERIMENTAL.....	57
5.1 Materials.....	57
5.2 Methods.....	59
5.2.1 Sintering Studies and Characterization.....	59
5.2.2 Adsorption Studies.....	60
CHAPTER VI: RESULTS AND DISCUSSION.....	63
6.1 Characterization and Sintering of HA Powders-Ceramics	63
6.2 Adsorption of BSA on HA and ceramic powders	73
CHAPTER VII : CONCLUSIONS AND RECOMMENDATIONS.....	88
REFERENCES.....	91
APPENDIX A.....	95
APPENDIX B.....	97

LIST OF FIGURES

Figure 1. Difference in human survivability in year 2000 versus 1900.	2
Figure 2. Effect of aging on strength of bone for men and women. Inserts.....	2
show loss of trabecular bone with age, which increases fracture probability.	
Figure 3. Organization of a typical bone.....	14
Figure 4. Sagittal section of a molar tooth.....	15
Figure 5. Stress as a function of strain and strain rate for human compact bone.....	16
Figure 6. Bioactivity spectrum for various bioceramic implants: (A) relative rate.....	22
of bioreactivity and (B) time dependence of formation of bone bonding at an implant interface, where A is 45S5 bioactive glass, B is KGS glass-ceramic, C is S53P4, D is A/W glass-ceramic, E is dense synthetic HA, F is KGX glass-ceramic, and G is Al_2O_3 .	
Figure 7. Comparison of interfacial thickness of reaction layer of bioactive	22
implants bonded to bone or thickness of nonadherent fibrous tissue in contact with inactive bioceramics in bone.	
Figure 8. Sequence of interfacial reactions involved in forming a bond between.....	23
bone and a bioactive glass.	
Figure 9. Schematic of crystal structure of hydroxyapatite (a)hexagonal,.....	24
(b)monoclinic.	
Figure 10. Calcium phosphate equilibrium phase diagram (10).....	30
Figure 11. Variation of shrinkage(\circ) and relative density(\blacktriangle) of the HA.....	32
ceramics as a function of temperature (19).	
Figure 12. Densification and HA yield as a function of temperature. (\blacksquare).....	32
Apparent density, (\square) HA/[HA+TCP] ratio as a percentage (20).	
Figure 13. X-Ray Diffraction patterns of three powders in the as-received	34
condition (21).	
Figure 14. X-Ray Diffraction patterns of three powders after heat treatment.....	34
at $1280^\circ C$ (21).	

Figure 15. FTIR spectra of HA powders heat treated in the 1000-1500°C range (22).	35
Figure 16. Variation in hardness with sintering temperature: □ A; ♦ B; ○ C (21).	36
Figure 17. Common adsorption isotherms.	42
Figure 18. The two major types of protein structure with variations: (a) fibrous and (b) globular (30).	47
Figure 19. Adsorption isotherms for BSA onto titanium: pH dependence (35).	50
Figure 20. Effect of pH on equilibrium adsorption isotherms (a) for BSA and (b) for Hb on HA-ulragel in KP buffer 10 mM. Continuous lines correspond to Langmuir equation (36).	51
Figure 21. Time profiles for the adsorption of BSA (0.1 g/l and 0.5 g/l) on titanium, pH 6.8 (35).	54
Figure 22. Adsorption isotherms for BSA onto hydroxyapatite (37).....	55
Figure 23. The weight loss curve of HA powder up to 1000°C.	64
Figure 24. The DTA curve of HA powder up to 1300°C.	64
Figure 25. The X-Ray Diffraction patterns of HA powder (upper) and HA pellet heat treated at 1250°C (bottom).	66
Figure 26. The variation of sintered density and pore content (as percent of theoretical density) of HA pellets with sintering temperature.	67
Figure 27. The variation of Vickers Hardness (Hv) of HA pellets with sintering temperature.	67
Figure 28. Optical microscope pictures of HA powders (750X).	69
Figure 29. Optical microscope pictures of the surfaces of 1250°C sintered HA pellets, 750 and 1500X.	70
Figure 30. FTIR spectra of as-received HA powder.	71
Figure 31. FTIR spectra of HA pellet heat treated at 800°C for 2 hours.	71
Figure 32. FTIR spectra of HA pellet heat treated at 1250°C for 2 hours.....	72
Figure 33. Uptake of BSA by HA at pH=4.7.....	73
Figure 34. Uptake of BSA by HA at pH=5.6.....	74
Figure 35. Uptake of BSA by HA at pH=6.6 with $p_0=1$ mg BSA/ml ...	74
Figure 36. Uptake of BSA by HA at pH=7.4	75
Figure 37. Uptake of BSA by HA at various pH values, $p_0=1$ mg BSA/ml	76

Figure 38. Uptake of BSA by alumina and zirconia powders at pH=4.5 and HA.....	76
powders at pH=4.7 for comparison purposes ($p_0=1$ mg BSA/ml sol.)	
Figure 39. Adsorption isotherms for BSA onto HA for different pH values.....	77
Figure 40. Adsorption isotherms for BSA onto HA at pH=7.4 for tris, NaP	82
and SBF buffer solutions.	
Figure 41. Adsorption isotherms for BSA onto alumina and zirconia powders.....	83
at pH=4.5 and HA powders at pH=4.7 for comparison purposes.	
Figure 42. Double reciprocal plot for BSA adsorption on HA at pH =7.4.....	84
Figure 43. The variation of affinity constant with pH for BSA adsorption on HA.....	84
Figure 44. The variation of maximum adsorption capacity with pH for BSA.....	85
adsorption on HA.	
Figure 45. The variation of amount of BSA adsorbed on HA with pH	86
($p_0=1$ mg BSA/ml sol.).	
Figure 46a. The variation of final concentration of BSA in solution with HA.....	87
solids loading (pH=4.7 and $p_0=1$ mg BSA/ml sol.)	
Figure 46b. The variation of percent adsorbed BSA in the solution with HA	87
solids loading (pH=4.7 and $p_0=1$ mg BSA/ml sol.).	
Figure 47a. Calibration curve for direct procedure of Lowry assay.	95
Figure 47b. Calibration curve for indirect procedure of Lowry assay.....	95
Figure 48. Double reciprocal plot for BSA adsorption on HA at pH =5.6.....	97
Figure 49. Double reciprocal plot for BSA adsorption on HA at pH = 6.6.....	97
Figure 50. Double reciprocal plot for BSA adsorption on HA at pH = 4.7.....	98
Figure 51. Double reciprocal plot for BSA adsorption on zirconia at pH = 4.5... ..	98

LIST OF TABLES

Table 1. Biomedical materials and applications.	5
Table 2. Composition of bone.	13
Table 3. Mechanical properties of a compact bone.	16
Table 4. Mechanical properties of dentine and enamel.	17
Table 5. Clinical uses of bioceramics (10).	20
Table 6. Types of bioceramic tissue attachment and bioceramic classification.	21
Table 7. Mechanical properties of dense HA and porous HA.....	37
Table 8. The general characteristic features which distinguish physical and chemical adsorption.	39
Table 9. Protein structure.	48
Table 10. Properties of Hydroxyapatite.	57
Table 11. Properties of Bovine Serum Albumin.	57
Table 12. Ion concentration (mM) of simulated body fluid (SBF) and human blood plasma (44).	58
Table 13. The Langmuir parameters of the equilibrium data for BSA/HA adsorption.....	78

CHAPTER I

INTRODUCTION

Humans begin to age from the moment they are born. We face diseases and accidents which do damage our bodies. Our bodies are all made of materials; if not of conventional materials like metals, polymers, ceramics or composites; biomaterials. These materials, just like the other well accustomed materials performing in extreme environments do break, wear out or crack.

The use of various drugs like antibiotics, vaccines, antiseptics etc. during the 20th Century has increased the life expectancy of humans to a very attractive age. At the beginning of the century about 60% of human beings didn't live long enough to see their 10th birthday and almost none had celebrated their 70th birthday as seen in Figure 1 (1). In the year 2000 we live on the average about 70 years and a significant number of people celebrate their 90th and 100th birthday.

This increase in life expectancy poses one of the major problems that faces humans in the 21st century. As we age our bodies deteriorate and many of us will outlast our "bodyparts". The quality of our connective tissues, particularly our skeletal tissues begin to decline. The strength of the bones decrease as we age as shown in Figure 2 (1). The loss of bone strength is especially serious for females and may be up to 40-50% by the age of 60-70.

The solution to the above problem during the past 30 years have been the use of artificial materials called "Biomaterials" or "Biomedical Materials" to repair or replace diseased, damaged or aged body parts. Currently there are 45 different body parts that can be replaced by biomaterials in USA.

Biomaterials are synthetic polymers, metals, ceramics, inorganics and natural macromolecules (biopolymers) that are manufactured or processed to be suitable for use in or as medical devices or prostheses. About 11 million people in USA have at least one medical device and 6 million of these people have been using fixation devices (usually fracture fixation) (2). More than 200,000 people a year receive a hip prosthesis (1). About 1 million teeth have been saved by using bioactive glasses.

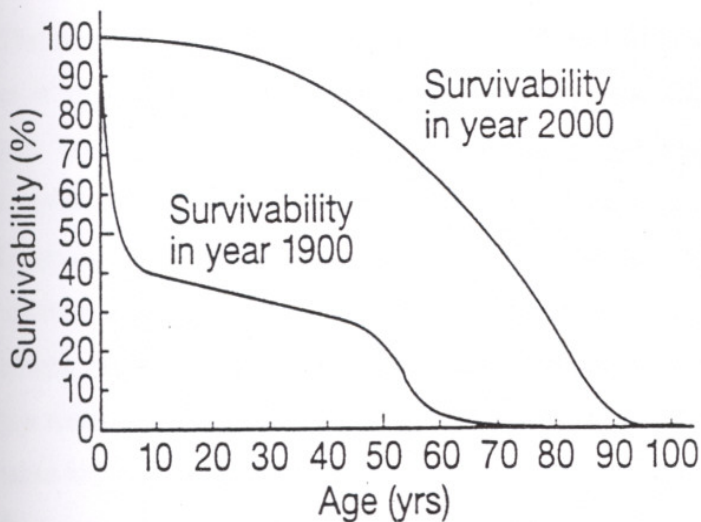


Figure 1. Difference in human survivability in year 2000 versus 1900.

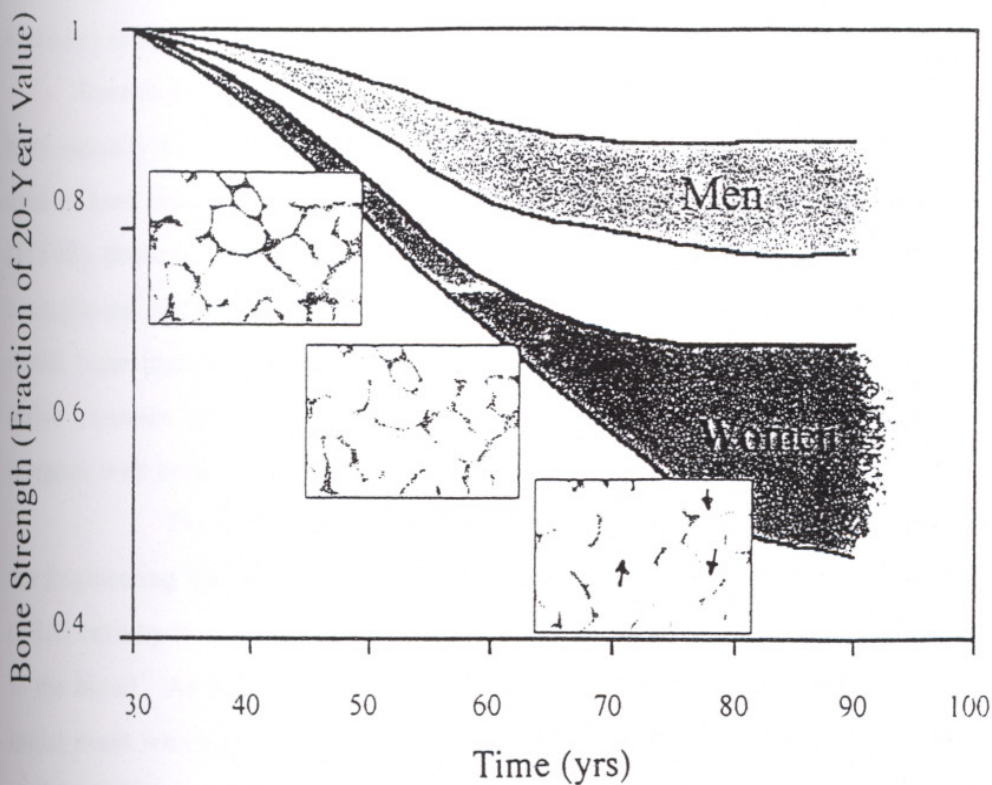


Figure 2. Effect of aging on strength of bone for men and women. Inserts show loss of trabecular bone with age, which increases fracture probability.

The extent of interest in biomaterials research can be stated by the increase in the number of centers conducting R&D on bioactive ceramics. The number of these centers increased from 6 in 1980 to 35 in 1988 (3). Biomaterials R&D necessitates an interdisciplinary effort of scientists, engineers, biochemists and clinicians. These interdisciplinary teams use biomaterials to fabricate artificial organs, medical devices, and drug delivery systems. As an example to the interdisciplinary teamwork for the optimization of total joint replacement, a large number of factors related with biology, materials mechanics, chemical structure, surface science, and environmental sciences have to be taken into consideration (4).

Biofunctionality and biocompatibility of medical and dental materials is of extreme importance for their performance. Biofunctionality may be considered in relation to a set of properties which allow a device to perform a function, whereas biocompatibility refers to the ability of the device to continue to perform that function effectively for as long as necessary in or on the body (5).

Ceramics which are used to repair and reconstruct diseased or damaged parts of the body (usually hard tissues such as bone and tooth) are called as bioceramics. Ceramics used in hard tissue replacement involve four different tissue attachment mechanisms (3). [1] Fully dense inert ceramics that attach to bone by either a press fit, bone ongrowth onto a roughened surface or attachment via a cementing agent, [2] Porous inert ceramics into which bone ingrowth occurs creating a mechanical attachment, [3] Fully dense surface active ceramics which attach to bone via a chemical bond, [4] Resorbable ceramics that integrate with bone and eventually are replaced by bone.

This work constituted the preliminary stage of an ongoing DPT Project at the Engineering Faculty of İZTECH. In this study adsorption of Bovine Serum Albumin (BSA) onto hydroxyapatite have been investigated. Albumin is the most abundant protein in the blood. As soon as implant is placed within the body an interface is created. The initial event which takes place will be the adsorption of proteins from the blood onto the surfaces within seconds of contact. The presence of adsorbed protein layer is important in mediating cellular response to the implant. Proteins can regulate cell adhesion and subsequent tissue attachment to implant. Hydroxyapatite was chosen because biological

apatite is the major constituent of hard tissues of bone and teeth. Apatites are also excellent biomaterials due to their biocompatibility and bioactivity. The effects of a number of parameters such as pH, buffer type, and protein concentration on the adsorption of BSA onto HA have been investigated. Isotherms have been analyzed using the Langmuir model, which is important in providing quantitative data such as maximum capacity of HA and affinity constant.

HA powder was also pressed and sintered in the 800-1400°C range for the formation of dense-porous implants. The sintered densities and microhardnesses of the sintered HA pellets have been determined.

CHAPTER II

BIOMEDICAL MATERIALS

Synthetic polymers, metals, ceramics, inorganics and natural macromolecules (biopolymers) that can be implanted for long-term use (e.g. artificial hip) or short-term use (e.g. intravenous catheter) which will come in contact with cells, proteins, tissues, organs and organ systems are called as biomaterials or biomedical materials. These materials are manufactured or processed to be suitable for use in or as medical devices or prostheses. In most cases they are used as a component in a medical device. The form of the material, how it interfaces with the tissue, and its time of use will determine the required materials properties. No single material is suitable for all biomedical applications. Ceramics, glasses and glass-ceramics are generally suitable for repair and replacement of hard tissues whereas polymeric materials are the choice of material for cardiovascular system applications.

2.1 Classification of Biomaterials

Biomedical materials can be classified according to their applications or the type of materials. Such a classification based on the type of material is given in Table 1 along with the application areas (6).

Table 1. Biomedical materials and applications.

Material	Application
Nondegradable Synthetics – Commodity Polymers	
Polyamides	Sutures
Polycarbonates	Housing materials
Polyesters	Vascular grafts
Polyformaldehyde	Heart valve stents
Polyolefins	Sutures, mesh for hernia repair
Polyvinyl chloride	Tubing, blood bags

Nondegradable Synthetics – Value-added polymers

Fluorocarbons

Hydrogels

Polyolefin elastomers

Polyurethanes

Silicones

Ultrahigh molecular weight polyethylene

Biodegradables

Albumin, cross-linked

Collagen/gelatin, cross-linked

Polyamino acids

Polyanhydrides

Polycaprolactones

Poly(lactic/glycolic acid) copolymers

Polyhydroxybutyrates

Polyorthoesters

Biologically derived materials

Bovine carotid artery

Bovine ligaments

Bovine pericardium

Human umbilical vein

Porcine heart valve

Bio-derived macromolecules

Chitosans

Collagen

Elastin

Gelatin, cross-linked

Hyaluronic acid

Tissue adhesives

Cyanoacrylates

Fibrin glue

Molluscan glue

Metal and Metallic alloys

Cobalt chrome molybdenum alloys

Nitinol alloys (shape memory alloys)

Stainless steels

Titanium and titanium alloys

Ceramics, inorganics, and glasses

Vascular grafts

Contact lenses, catheter coatings

Tubing, artificial heart bladder

Catheters, artificial heart bladders

Soft tissue reconstruction, tubing

Acetabular cup

Vascular graft coatings, cell encapsulation

Soft tissue reconstruction,

Vascular graft coatings

Controlled release, cell adhesion peptides

Controlled release

Controlled release, bone plates

Sutures, bone plates

Controlled release, bone plates

Controlled release, bone plates

Vascular grafts

Ligaments

Pericardial substitute, heart valves

Vascular grafts

Heart valves

Experimental, wound dressing,

Controlled release

Soft tissue injectables, coatings, wound dressing

Experimental, coatings

Artificial heart bladder coating

Coatings, wound dressing, surgical non-adhesion

Wound closure, microsurgery

Vascular graft coating

Enhancement of cell adhesion

Orthopedic and dental implants,

Vascular stents

Heart valve stents

Orthopedic wire

Orthopedic wire

Artificial heart housing, heart valve stents

Aluminum, calcium and phosphorous oxides	Degradable bone filler, enhanced bone growth
Bioglass	Bioactive phosphorous calcium glass, orthopedic coating
Glass ceramics	Encapsulation of implantable medical electronics
High density alumina	Acetabular cup, ball of hip prosthesis
Hydroxyapatite	Bioactive ceramics, orthopedic coating, bone fillers
Carbons	
Glassy carbons	Fibers for orthopedic composites
Pyrolytic(low temperature isotropic) carbon	Heart valves , dental implants
Ultralow temperature isotropic carbon	Coatings on heat sensitive polymers
Passive Coatings	
Albumin	Thromboresistance
Alkyl chains	Adsorbs albumin for thromboresistance
Fluorocarbons	Reduced drag for catheters, thromboresistance
Hydrogels	Reduced drag for catheters, thromboresistance
Silica-free silicones	Thromboresistance, improved wound healing for soft tissue reconstruction
Bioactive coatings	
Anticoagulants, e.g., heparin and hirudin	Thromboresistance
Antimicrobials	Infection resistance
Bioactive ceramics and glasses	Bone adhesion and formation, soft tissue adhesion
Cell adhesion peptides	Enhanced cell adhesion, epithelium, endothelium
Cell adhesion proteins	Enhanced cell adhesion, epithelium, endothelium
Negative surface charge	Thromboresistance
Thrombolytics	Thromboresistance

2.2 Biofunctionality and Biocompatibility

The performance of medical and dental materials is controlled by two sets of characteristics, those which determine the ability of a device to perform the appropriate and specified function and those which determine the compatibility of the material with the

body. The two terms, biofunctionality and biocompatibility, are used to represent these characteristics. These two terms are related very closely. Biofunctionality may be considered in relation to a set of properties which allow a device to perform a function while biocompatibility refers to the ability of the device to continue to perform that function effectively and for as long as necessary in or on the body (5). The most important properties which contribute to biofunctionality and biocompatibility will be discussed in the following sections.

2.2.1 Biofunctionality

The reasons for using biomaterials and their expected functions determine the parameters of biofunctionality. The conditions which require the use of biomaterials may be grouped as follows:

- Gross congenital (from birth) defects cause functional deficiencies,
- Developmental defects with functional consequences,
- Diseases which lead to irreversible changes in the tissues,
- Gradual loss of tissue,
- Tissue injury requiring temporary support while healing takes place,
- The desire to deliver drugs in a controlled manner,
- Psychological problems and aesthetic reasons.

The functional requirements of the materials include the following:

- Load transmission and stress distribution: This will be the major function of any device used to replace or augment part of the musculoskeletal system. The stress fields are often complex because of multiple points at which forces are exerted on parts of this system, directed by muscles via a number of points of attachment. It is one of the most important features of the functioning of any device within this system that the device disturbs the pattern of load transfer as little as possible since the structure of bone is intimately related to the stress fields. The usual parameters of mechanical properties such as compressive, tensile, shear strengths are all important. Since devices are often meant to function for many years within this dynamic situation, both fatigue and creep performance are of uttermost significance. Impact strength and fracture toughness may also be critical. The main

point of this issue is the particular need for bone replacement or augmentation devices to be “iso-elastic” with the adjacent bone. Cortical bone has a Young’s Modulus in the region of 20 GPa as an example. This is not easily achieved in high strength materials.

- Articulation: All joint replacements require low friction, low wear, articulating surfaces to allow movement. Low coefficients of friction are difficult to obtain with synthetic materials and engineering structures. Most joint replacements rely on a combination of one extremely hard surface, usually of a highly polished alloy or oxide ceramic and one of a polymer. Wear will limit the lifetime of prosthesis. Wear has been one of the most important failure modes of tooth filling materials, too (5).
- The control of blood and other fluid flow, simple space filling, generation and application of electrical stimuli, transmission of light and sound , the handling of drugs and other substances and guided tissue regeneration are some of the other important functional requirements.

2.2.2 Biocompatibility

Biocompatibility is the acceptance of an artificial implant by surrounding tissues and by the body as a whole. The implant should be compatible with tissues in terms of mechanical, chemical, surface and pharmacological properties.

At the simplest level, it could be stated that biocompatibility means a total absence of interaction between material and tissue. The concept that, the more inert the material the more tolerant will be the body to that material, implies that the body effectively ignores the material, which is passively tolerated rather than actively incorporated. No device placed within the body can be considered as truly incorporated if it is ignored. Long term performance and stability usually require intimate acceptance. The material and tissue should interact in the most appropriate way to maximize the effective incorporation of the material into the relevant tissues and to ensure stability. If stated in other terms, compatibility can be defined as “the ability of a material to perform with an appropriate host response in a specific application” (5).

It is concerned with all aspects of the interaction that occur but focuses on the development of the response of the tissues. This host response controls the performance of the patient following placement of the implant. Host response, however, itself is controlled by the characteristics of material and especially its chemical stability in the body. The susceptibility of the material to degradation and the effect such degradation has on the tissue are the important, central features of biocompatibility.

The environment of the body is an aqueous medium, extremely well buffered so that pH is maintained at around 7.4 and it is held at constant temperature (37°C). The saline solution is an excellent electrolyte and facilitates electrochemical mechanism of corrosion and hydrolysis. There are also many molecular and cellular species in the tissues which have the ability to catalyze certain chemical reactions or rapidly destroy certain components identified as foreign. Degradation of materials such as metals and polymers takes place in this aggressive environment.

The response of the body is a complex issue which could be dealt with in a number of ways. The important parameters which influence the response of the tissues include the type of tissue that is in contact with the material, the physical and chemical characteristics of the material and the general status of the host. There are different types of responses that are seen with varying distance from the surface .

There will be some initial interfacial reaction between blood and the implant with proteins being adsorbed on the implant surface. Proteins may be able to influence corrosion and degradation processes. All cellular activity near an implant surface will be related to the implant via a proteinaceous interface (5).

In order to implant a material in the tissue, some surgical intervention is required. This surgical procedure will itself result in a wound healing process. The tissue response to the material can therefore be seen as a modification of the wound healing process. The tissue will respond to damage through a well defined procedure involving two phases. The first phase, inflammation, is the initial reaction of the body to injury that involves localized changes to the microvasculature and the cellular composition of the tissue. The second phase is the repair phase in which the tissue attempts to restore the damage.

Generally the body's reaction to foreign materials is to get rid of them. The foreign material could be extruded from the body if it can be moved, or walled off if it can not be

moved. If the material is particulate or fluid, it will be ingested by the giant cells (macrophages) and removed. These responses are related to the healing process of the wound. A typical tissue response is that the polymorphonuclear leukocytes appear near the implant followed by the macrophages. However, if the implant is chemically and physically inert to the tissue, the foreign body giant cells may not form and only a thin layer of collagenous tissue encapsulates the implant. If the implant is either a chemical or a physical irritant to the surrounding tissue, inflammation occurs in the implant site. Inflammation will delay the normal healing process resulting in granular tissues. The degree of tissue response varies according to both physical and chemical nature of the implants (7).

If there is any interfacial reaction resulting in the release of any products in the tissue, the distribution of those products must be of great significance to the body as a whole. These products may passively diffuse through the tissue under a concentration gradient but there are more active methods of distribution in the tissue that are more significant. Soluble components may rapidly gain access to the vasculature, can readily spread in the blood stream, could then reach many organs and tissues throughout the body. In some cases they are tolerated without adverse effects, but they may have great effects, with possible systemic effects of biocompatibility.

The events that occur at the material-tissue interface could be controlled. In the field of blood compatibility, it is a widely used technique to administer systemic anticoagulants to patients receiving certain heart valves. The possibility of modifying such materials by using bioactive material interfacial reactions is especially significant and may be controlled. One of the best examples to this possibility is the use of HA and other calcium based materials to actively encourage bone regeneration at implant surfaces. Modification of polymer surfaces to improve their compatibility with blood is another significant example. In more general terms, there are possibilities of incorporating in or attaching to the surfaces of biomaterials agents like anti-inflammatory drugs or growth factors which are able to influence processes of inflammation and repair. It is important to note that not only the characteristics of the material and the device but also the host variables control events.

The barrier to the successful common use of medical devices is the poor understanding of biocompatibility. Success with more sophisticated performance is likely to be achieved when the details of biocompatibility are fully understood (5).

2.3 Structure and Properties of Hard Tissues (Bone and Teeth)

It is important to know the physical, chemical, and mechanical properties of the hard tissues because they provide quantitative parameters necessary for successful fabrication of artificial bone replacement implants. The hard tissues, i.e., bones and teeth, are ceramic-organic composites with complex microstructure (8). Their primary function is "load carrying".

2.3.1 Composition and Structure

Bone is a composite material made up of collagen protein fibers threading through hydroxyapatite $\text{Ca}_{10}(\text{PO}_4)_6(\text{OH})_2$. HA makes up about 69 wt % of bone structure and in crystallized or amorphous form provides stiffness to the bone. Collagen fibers make up about 20 wt % of bone and in a bundled array of cross-linked helical polypeptide strands, provide extra strength allowing bones to flex under stress (9). Water makes up 9 wt % of bone. Composition of bone is given in Table 2 (7). There are other mineral ions such as citrate ($\text{C}_6\text{H}_5\text{O}_7^{4-}$), carbonate (CO_3^{2-}), fluoride (F^-) and hydroxyl ions (OH^-) which may produce some of the subtle differences in microstructural features of bone. The diameter of the collagen microfibrils vary from 100 to 2000 nm. HA crystals present in the form of plates or needles are about 40-60 nm long, 20 nm wide and 1.5-5 nm thick. They are deposited parallel to the collagen fibers. The mineral phase present in the bone is not a discrete aggregation of the HA crystals. It is made up of a continuous phase.

The mineral-containing fibrils are arranged into lamellar sheets (3-7 μm) that run helically with respect to the long axis of the cylindrical osteons (or some times called Haversian system). The osteon is made of 4 to 20 lamellae that are arranged in concentric rings around the Haversian canal. Osteons are typically 150 to 250 μm in diameter.

Between these osteons the interstitial systems are sharply divided by the cementing line. The metabolic substances can be transported by the intercommunicating pore system known as canaliculi, lacunae, and Volkmann's canals, which are connected with the marrow cavity. The various interconnecting systems are filled with body fluids and their volume can be as high as 19 % (8). The external or internal surface of the bone are called periosteum and endoseum, respectively, and both have osteogenic properties.

Long bones such as the femur contain cancellous (or spongy) and compact bone. A schematic anatomical view of a long bone is shown in Figure 3 (8) . Cancellous bone is a cellular material consisting of a connected network of rods or plates. Low density, open cell, rod-like structures develop in regions of low stress while high density, closed cell, plate-like structures occur in regions of higher stress (8).

Table 2. Composition of bone.

Components	Amount (wt%)
Mineral (apatite)	69
Organic matrix	22
Collagen	(90-96 % of organic matrix)
Others	(4-10 % of organic matrix)
Water	9

Although bone seems lifeless, it actually is made up of a very alive porous framework that is constantly rebuilding itself. Bone tissue replaces itself through the action of cells called osteoblasts that produce acids to dissolve (resorb) HA and enzymes to break down collagen . The resulting release of calcium and proteins prompts osteoblasts to lay down new matrix that mineralizes and forms hydroxyapatite and collagen. Some growth factors either increase or decrease bone remodelling. Blood vessels run through the bone framework , too, carrying many different compounds that organize bone remodeling, such

as calcitrol, calcitonin, parathyroid, and prostaglandins. Beneath all of that is the bone marrow that creates the osteoblasts and osteoclasts as well as the red and white cells (9).

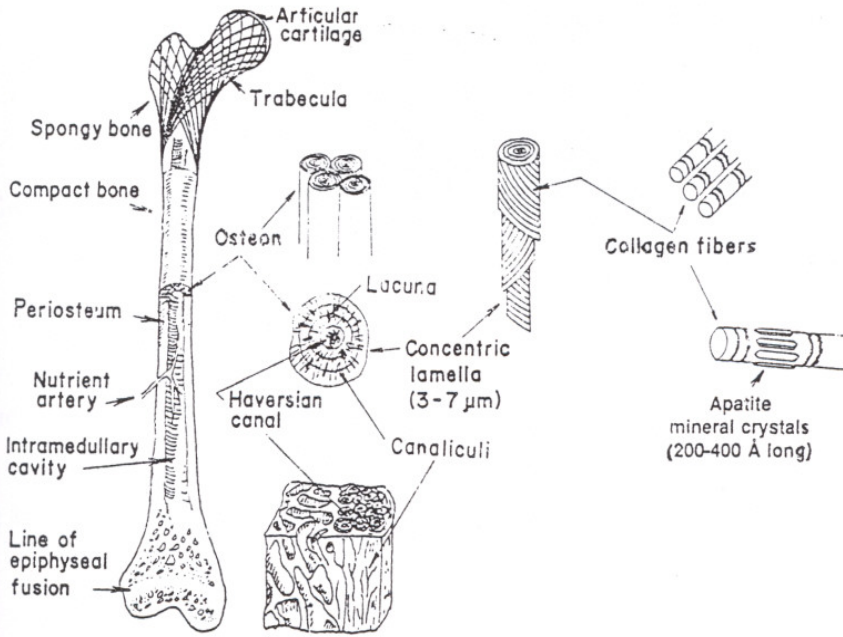


Figure 3. Organization of a typical bone.

All teeth are made of two portions: the crown and the root. The root is placed in a socket called the alveolus in the maxillary (upper) or mandibular (lower) bones. A sagittal cross section of a permanent tooth is shown in Figure 4 (8) to illustrate various structural features. The enamel is the hardest substance found in the body and consist almost entirely of calcium phosphate salts (97 wt %) in the form of large apatite crystals. The remaining 3 wt % consists of organic substances and water. Dentine is another mineralized tissue and has similar composition and physical properties of a compact bone. Dentinal tubules contain collagen fibrils penetrating every part of dentine. Cementum covers most of the root of the tooth and is made of coarsely fibrillated bonelike substances. The periodontal membrane is made of mostly collagenous fibers plus glycoproteins (7).

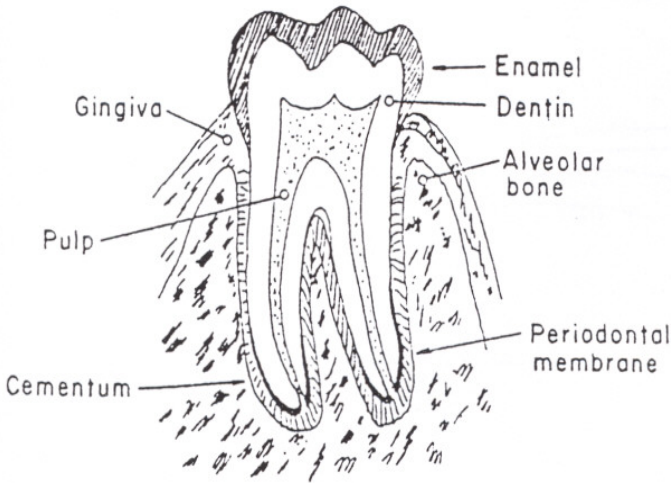


Figure 4. Sagittal section of a molar tooth.

2.3.2 Mechanical Properties of Bone and Teeth

As with most other biological materials, the properties of bone and teeth depend largely on the humidity, mode of applied load, rate of loading, and direction of the applied load. As a ceramic-organic composite, bone exhibits high toughness and relatively high modulus. High toughness is related to the presence of collagen, and complicated fibrous microstructure. The effect of rate of loading on the bone is shown in Figure 5.

Young's modulus, the ultimate compressive and yield strength all increase with increased rate of loading as seen in the figure. However, the failure strain and the fracture toughness of the bone reach a maximum and then decrease. This implies that there is a critical rate of loading (7). Bone is a tough material at low strain rates but fractures more like a brittle material at high strain rates. Highly mineralized bone has a higher modulus of elasticity and bending strength but lower toughness. This illustrates the importance of the organic phase in providing toughness and energy absorption capability in bone. The mechanical properties of human compact bone are summarized in Table 3 (8).

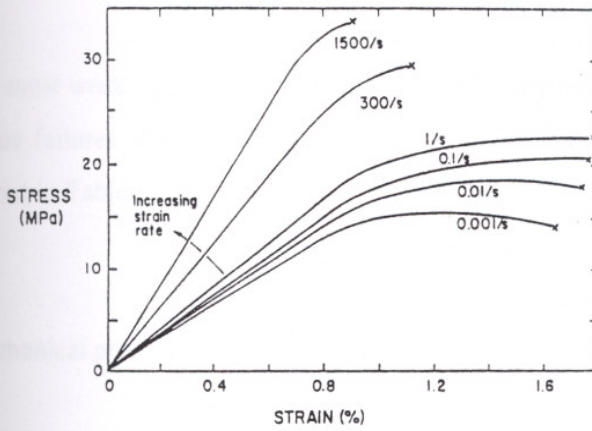


Figure 5. Stress as a function of strain and strain rate for human compact bone.

Table 3. Mechanical properties of a compact bone.

	Test direction related to bone axis	
	Parallel	Normal
Tensile strength (MPa)	124 – 174	49
Compressive strength (MPa)	170-193	133
Bending strength (MPa)	160 ^a	
Shear strength (MPa)	54	
Young's modulus (GPa)	17.0 – 18.9	11.5
Work of fracture (J/m ²)	20 – 27 (Random)	
	6000 (low strain rate)	
	98 (high strain rate)	
K _{1c} (MPa.m ^{1/2})	2 – 12	
Ultimate tensile strain	0.014-0.031	0.007
Ultimate compressive strain	0.00185-0.026	0.028
Yield tensile strain	0.007	0.004
Yield compressive	0.010	0.011

^a Direction of measurement not specified

Teeth must work under a stress of about 20 MPa, applied about 3000 times per day, without fatigue failures and only with moderate wear. The mechanical properties of teeth are summarized in Table 4 (8).

Table 4. Mechanical properties of dentine and enamel .

	Dentine	Enamel
Compressive strength (MPa)	250-350	95-350
Proportional limit in compression (MPa)	160-170	70-350
Young's modulus in compression (Gpa)	11-17	9-84
Tensile strength (MPa)	21-53	10
Young's modulus in tension (GPa)	11-19	
Flexural strength (MPa)	245-268	76
Young's modulus in bending (GPa)	12	131
Shear strength (MPa)	69-147	64-93
Proportional limit in shear (MPa)	60	
Shear modulus (GPa)	6	
Work of fracture (J/m ²)	200-500	13 ^a 200 ^b

^a Measured parallel to prism orientation.

^b Measured perpendicular to prism orientation.

ANKARA YÜKSEK TEKNOLOJİ ENSTİTÜSÜ
REKTÖRLÜĞÜ
Kütüphane ve Dokümantasyon Daire Başkanlığı

2.4 Bioceramics

Specially designed ceramics have been used in the innovative repair or reconstruction of diseased or damaged parts of the body improving the quality of life and in some cases the length of life for thousands of people in the last couple of decades of the 20th century. These ceramic materials are called as bioceramics. Bioceramics used for the repair of the musculo-skeletal system may be bioinert (e.g., alumina and zirconia), resorbable (e.g., tricalcium phosphate), bioactive (e.g., hydroxyapatite, bioactive glasses and glass-ceramics) or porous for tissue ingrowth (hydroxyapatite-coated metals). Bioceramics can be single crystals (sapphire), polycrystalline (alumina or HA), glass (Bioglass), glass-ceramic or composites (polyethylene-HA).

Bioceramics are generally used as implants to repair parts of the body, usually hard tissues such as bones or teeth, but carbon based ceramics are also used for the replacement of heart valves. Clinical applications of bioceramics are listed in Table 5 (10). These materials have to survive harsh conditions corrosive to most materials, saline solutions at 37°C under variable, multiaxial, cyclical mechanical loads. The use of bioceramics depends on achieving a stable attachment to the connective tissue and a match of the mechanical behaviour of the implant with the tissue to be replaced. Survivability of a bioceramic requires formation of a stable interface with living host tissue. No material implanted in living tissues is inert; all materials elicit a response from living tissue and the nature of this response at the interface directly affects the mechanism of tissue attachment. If the implant material is toxic, the surrounding tissue dies. If it is nontoxic and the material is inert, a fibrous tissue of variable thickness forms. If the material is nontoxic and bioactive, an interfacial bond forms. If the material is nontoxic and dissolve, the surrounding tissue replaces the implant in time. Bioceramics can be classified according to the type of tissue attachment mechanism in line with these responses as summarized in Table 6 (10). The relative level of the reactivities of these four groups of materials along with specific examples of bioceramics is given in Figure 6 (10).

The relative level of reactivity of an implant influences the thickness of the interfacial zone or layer between the material and the tissue. The interfacial zone thickness

of the reaction layer for different bioceramics are given in Figure 7. In the last 20 years, experience on the failure of implant materials has shown that the failure originates from the bioceramic-tissue interface. For inert bioceramics (Type 1), the interface is not chemically or biologically bonded and there is relative movement. The progressive development of a nonadherent fibrous capsule occurs in both soft and hard tissues ("morphological fixation"). Movement at the interface leads to deterioration of the function of both implant and the surrounding tissue. The thickness of the nonadherent capsule varies greatly, depending on both the material and the extent of relative motion.

The concept behind porous bioceramics (Type 2) is the ingrowth of tissue into pores on the surface or throughout the implant. The increased interfacial area between the implant and the tissue, the establishment of the interface in the pores by the tissue results in an increased resistance to the movement of the implant in the tissue. This method of attachment ("biological fixation") is capable of withstanding more-complex stress states. One of the most important limitations to porous implants is that the pores within the material must be bigger than 100-150 μm in diameter in order to provide a blood supply to the ingrown connective tissue.

Resorbable bioceramics (Type 4) are designed to degrade gradually in time and be replaced by the natural host tissue which leads to an almost nonexistent, very thin interface. This looks like the optimal solution to the biomaterial problem if the strength requirements and short term performance requirements are met. Natural tissues can repair themselves and are gradually replaced throughout life by a continual turnover of cell populations. Thus, resorbable biomaterials are based on similar principles of repair that have evolved over millions of years.

Bioactive ceramics attach directly by chemical bonding with the bone. Bonding of bone to bioactive glasses involves 12 reaction stages summarized in Figure 8 (10). The first five stages are very rapid and involve ion exchange of alkali ions with hydrogen ions from body fluids, network dissolution, silica-gel polymerization, and chemisorption and crystallization of the hydroxyl carbonate apatite (HCA) layer.

Table 5. Clinical uses of bioceramics (10).

Application	Materials
Orthopedic	Al ₂ O ₃ Stabilized ZrO ₂ HA* powders Bioactive glass powders
Coatings for bioactive bonding	HA Bioactive glass ceramics
Bone space fillers	Tricalcium phosphate Calcium Phosphate salts
Dental implants	Al ₂ O ₃ HA Bioactive glasses
Artificial tendon and ligament	PLA-carbon-fiber composite
Periodontal pocket obliteration	HA HA-PLA* composite Tricalcium phosphate Calcium phosphate salts Bioactive glasses
Alveolar ridge augmentation	HA HA-autogenous bone composite Bioactive glasses
Maxillofacial reconstruction	Al ₂ O ₃ HA PE*-HA composite Bioactive glasses
Spinal surgery	Bioactive glass-ceramic HA
Therapeutic treatment of tumors	Rare-earth doped aluminosilicate Glasses
Artificial heart valves	Pyrolytic carbon coating
Otolaryngological	Al ₂ O ₃ HA Bioactive glasses Bioactive glass ceramics PE-HA composite

*HA is hydroxyapatite, PE is polyethylene and PLA is poly(lactic acid).

The bonding mechanisms of dense HA implants appear to be very different from those described above for bioactive glasses. A cellular bone matrix from differentiated osteoblasts appear at the surface, producing a narrow amorphous electron dense band only 3-5 μm wide. Collagen bundles appear between this area and the cells. As the site matures, the bonding zone shrinks to a depth of only 0.05-0.2 μm . The result is normal bone attached through a thin epitaxial bonding layer to the bulk implant (3).

Table 6. Types of bioceramic tissue attachment and bioceramic classification.

Type of attachment	Type of bioceramic
Dense, nonporous, almost inert ceramics attach by bone growth into surface irregularities by cementing the device into the tissue, or by press-fitting into a defect (<i>Morphological Fixation</i>)	Al_2O_3 ZrO_2
For porous implants, bone ingrowth occurs, which mechanically attaches the bone to the material (<i>Biological Fixation</i>)	Porous Hydroxyapatite Hydroxyapatite-coated porous metals
Surface-reactive ceramics, glasses, and glass-ceramics attach directly by chemical bonding with the bone (<i>Bioactive Fixation</i>)	Bioactive glasses Bioactive glass-ceramics Dense Hydroxyapatite
Resorbable ceramics and glasses in bulk or powder form Designed to be slowly replaced by bone	Calcium sulfate(plaster of Paris), Tricalcium Phosphate, Calcium phosphate salts, Bioactive Glasses

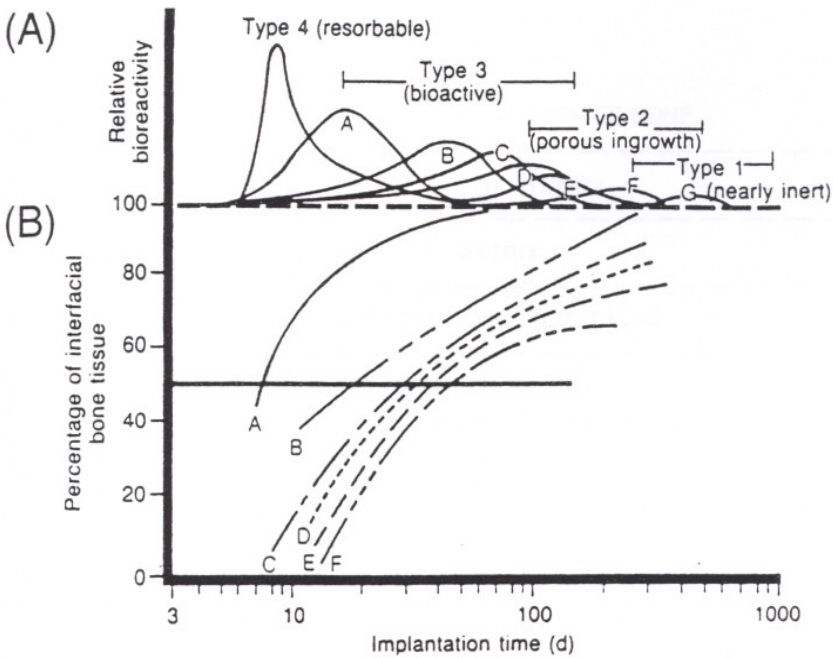


Figure 6. Bioactivity spectrum for various bioceramic implants: (A) relative rate of bioreactivity and (B) time dependence of formation of bone bonding at an implant interface, where A is 45S5 bioactive glass, B is KGS glass-ceramic, C is S53P4, D is A/W glass-ceramic, E is dense synthetic HA, F is KGX glass-ceramic, and G is Al_2O_3 .

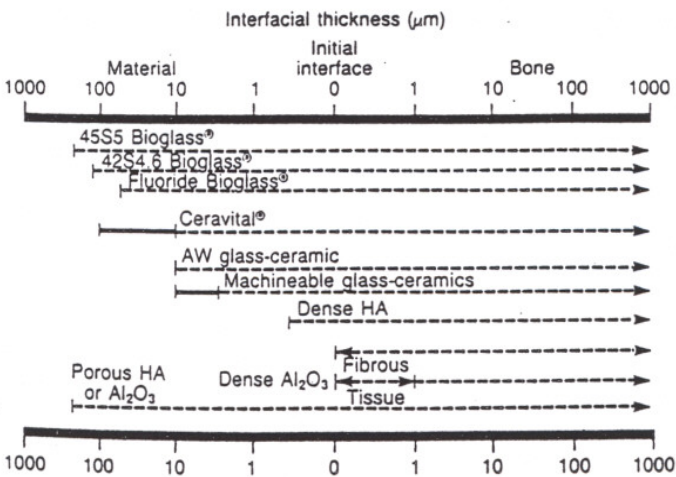


Figure 7. Comparison of interfacial thickness of reaction layer of bioactive implants bonded to bone or thickness of nonadherent fibrous tissue in contact with inactive bioceramics in bone.

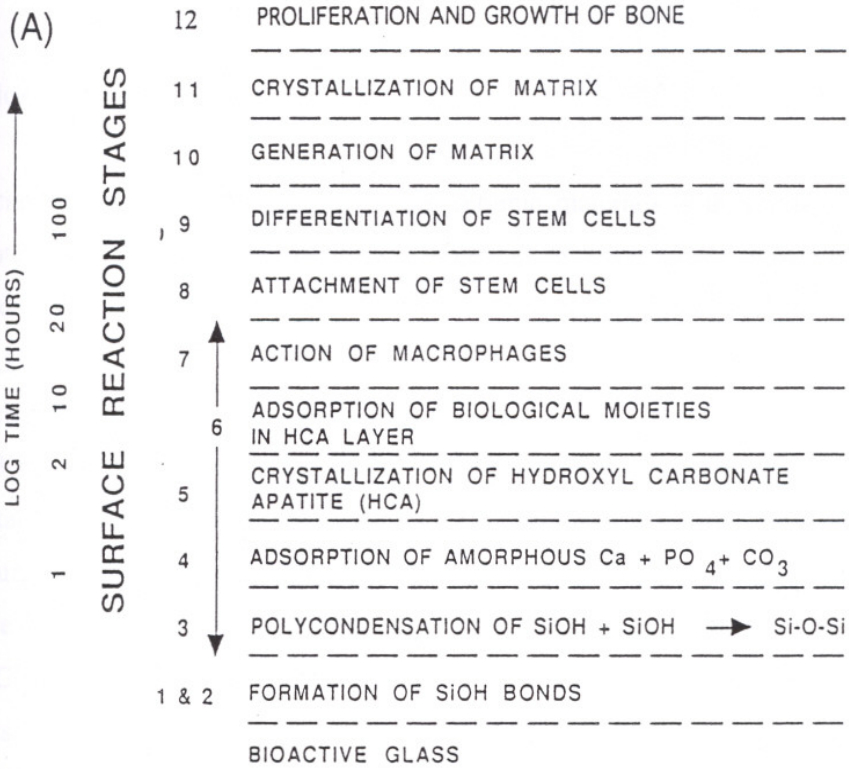


Figure 8. Sequence of interfacial reactions involved in forming a bond between bone and a bioactive glass.

CHAPTER III

PROCESSING AND PROPERTIES OF HA

3.1 Calcium Phosphate Ceramics

Calcium Phosphate Ceramics (CPC) are ceramic materials with varying calcium to phosphate ratios. They have considerable potential as bone substitute materials or as surface on bone – interfacing prostheses, in view of the very favourable response of bone to them(11).

Calcium Phosphate –based ceramics have been used in medicine and dentistry for nearly 30 years. Applications include dental implants, percutaneous devices and use in periodontal treatment, alveolar ridge augmentation, orthopedics, maxillofacial surgery , and spinal surgery. Different phases of CPC's are used depending upon whether resorbable or bioactive material is desired (3).

CPC's with Ca/P ratio in the 1.5-1.67 range are the most interesting and useful materials. Tricalcium phosphate (TCP Ca/P=1.5) and calcium hydroxyapatite (HA Ca/P=1.67) have been widely investigated.

HA is the major mineral component of bones and teeth. It is recognized by the body as the natural ceramic constituent in bones and teeth. It has a hexagonal crystal structure, an ideal chemical formula of $\text{Ca}_{10}(\text{PO}_4)_6(\text{OH})_2$, and ideal weight percentages of 39.9% Ca , 18.5% P and 3.38% OH (4). Schematic crystal structure of HA is shown in Figure 9. (4).

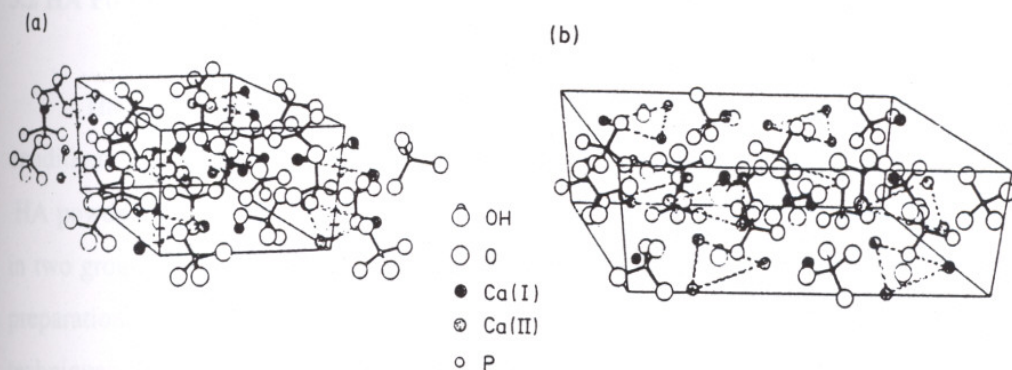


Figure 9. Schematic of crystal structure of hydroxyapatite (a)hexagonal,(b)monoclinic.

Two aspects regarding the crystal chemistry of natural and synthetic apatites should be recognized. First, HA in bone is nonstoichiometric, has a Ca/P ratio less than 1.67 and it contains carbonate ions, sodium, magnesium, fluorine, and chlorine. Second, most synthetic HA's actually contain substitution for the phosphate and/or hydroxyl groups and vary from ideal stoichiometry and Ca/P ratios. Oxyhydroxyapatite $[\text{Ca}_{10}(\text{PO}_4)_6\text{O}]$, α -tricalcium phosphate (α -TCP), β -tricalcium phosphate (β -TCP) or β -Whitlockite $[\text{Ca}_3(\text{PO}_4)_2]$, tetracalcium phosphate ($\text{Ca}_4\text{P}_2\text{O}_9$) and octocalcium phosphate $[\text{Ca}_8(\text{HPO}_4)_2(\text{PO}_4)_4 \cdot 5 \text{H}_2\text{O}]$ have all been detected by XRD, FTIR and chemical analysis (4).

Differences in structure, chemistry and composition of apatites arise from differences in material processing techniques, time, temperature and atmosphere. The stable phases of calcium phosphate ceramics depend considerably on temperature and water content of the environment. At body temperature only two calcium phosphates are stable in aqueous media at $\text{pH} < 4.2$, the stable phase is $\text{CaHPO}_4 \cdot 2 \text{H}_2\text{O}$ (Dicalcium phosphate or brushite, DCP) while at $\text{pH} \geq 4.2$ the stable phase is HA.

At higher temperatures, other phases such as $\text{Ca}_3(\text{PO}_4)_2$ (α -TCP or β -TCP), and tetracalcium phosphate ($\text{Ca}_4\text{P}_2\text{O}_9$). The unhydrated high temperature calcium phosphate phases interact with water or body fluids at 37°C to form HA (3):



3.2 HA Powder Processing

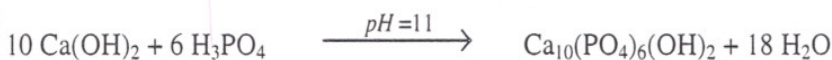
The characteristics of HA powders depend sensitively on the preparation technique conditions e.g. starting materials, pH, temperature, aging time, calcinations conditions etc.

HA powders can be prepared by a series of techniques and these can mainly be classified in two groups as wet and solid state reaction methods. Precipitation, hydrothermal powder preparation and hydrolysis of calcium phosphates are commonly used wet method techniques. Powders with different stoichiometry, morphology, and level of crystallinity can be prepared by using these techniques.

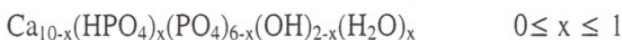
In one of the precipitation techniques powders can be prepared by using CaO and H₃PO₄ as the starting chemicals (12). CaO calcined at 900°C was added to distilled water under constant stirring for the preparation of a Ca(OH)₂ suspension. A H₃PO₄ solution was slowly added to the above solution under vigorous stirring at room temperature. Powders with different Ca/P ratios can be prepared by varying the concentration and the amount of these two solutions.

The pH of the reaction environment was continuously measured during the synthesis and controlled using an aqueous ammonia solution. Powder precursors with atomic Ca/P ratios of 1.5 and 1.55 were obtained without the base addition. Ca/P ratios in the 1.6-1.73 was obtained when the pH of the environment was kept at about 11 by ammonia solution addition (12).

Reaction mixtures were stirred for 4 hours after the addition of the acid. The gelatinous precipitates were aged for 48 hours at room temperature, filtered, washed and dried at 90°C. The dried precursor were subsequently ground in a vibrating mill and calcined at 800°C for 3 hours. The reaction can be expressed as follows for stoichiometric (Ca/P=1.67) HA:



Different Ca/P ratios and crystalline phases can be obtained depending on the amount of Ca(OH)₂ in the solution and the preparation conditions. Ca deficient hydroxyapatite materials can be represented like:



HA powders can also be prepared by using other starting materials through precipitation. 0.2 M Ca(NO₃)₂ and NH₄H₂PO₄ solutions were mixed together and heated in a closed plastic bottle at 50°C with pH adjusted to 12 for three days for the preparation of a HA gel with a Ca/P ratio of 1.8. Ammonia was boiled out, the precipitate was decanted several times, filtered and thoroughly washed with distilled water (13). The wet cake was extruded using syringe into small cylinders and dried at room temperature subsequently calcined at 300-500°C for 5 hrs. The powder was estimated to have a crystallite size of 15-20 nm from its surface (106.2 m²/g) and was not reported to be calcium deficient.

In another study, Bouali et al. (14) synthesized HA powders in basic medium by mixing 0.25 M $(\text{NH}_4)_2\text{HPO}_4$ and $\text{Ca}(\text{NO}_3)_2 \cdot 4 \text{H}_2\text{O}$ solution and warm suspension filtered, heated to 400°C in order to eliminate the ammonium nitrate contained in the precipitation. Hydroxyapatite with Ca/P ratio of 1.64 corresponding to about 10% of tricalcium phosphate was obtained.

Motohiro and co-workers (15) investigated the preparation of HA by a homogeneous precipitation technique. Calcium nitrate (0.01M), diammonium hydrogen phosphate (0,006M) and EDTA (0.012 M) were dissolved in water. Hydrogen peroxide at different levels were added to these solutions. The final mixture was kept at 90°C for 4 h in a constant temperature bath for the synthesis of calcium phosphate powders. Various powders with different chemical compositions and morphologies like spheres, plates, needles etc. were obtained at various pH and hydrogen peroxide combinations.

Platety HA powders were synthesized by hydrothermal processing in alcoholic media. The HA precursor slurry was prepared from $\text{CaHPO}_4 \cdot 2\text{H}_2\text{O}$ and CaCO_3 which were well mixed in a pot mill using ZrO_2 balls in water for 24 hours at 50 rpm. Various kinds of alcohols in different amounts were added to the HA precursor. After controlled to pH 10 by NH_4OH , this mixture was treated in an autoclave with stirring under hydrothermal conditions at 180°C for 5 h to crystallize (16) The peaks of X-Ray diffraction pattern of the precursor were broad which indicates the precursor were not crystallized completely whereas the peaks of X-Ray diffraction patterns of samples treated hydrothermally with alcohols were sharp which indicates samples were well crystallized. IR spectra results showed samples were well crystallized HA containing carbon ions.

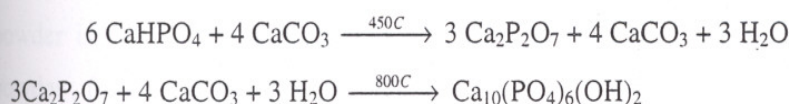
In another study, Monma et. al. (17) studied the conversion of brushite, $\text{CaHPO}_4 \cdot 2 \text{H}_2\text{O}$ (DCPD), into hydroxyapatite (HA) by hydrolysis on the basis of the following two-stage scheme:



Reaction I corresponds to a structural change into the HA structure and Reaction II corresponds to a compositional increase in Ca/P ratio retaining the apatite structure. In

reaction I DCPD was suspended and stirred with magnetic stirrer in distilled water by bubbling nitrogen gas. Reaction temperature and pH were kept within the ranges 40-80°C and 3 to 13 respectively. The reaction pHs were adjusted with ammonium hydroxide. Sample was filtered washed with water and dried at 80°C. In reaction II HA sample was treated at 30 to 50°C for 1 h alkaline solution containing CaCl₂ · 2 H₂O as a Ca²⁺ source for an increase in Ca/P ratio. The resulting sample was filtered, washed and dried in the same manner as in reaction I. In hydrolysis reaction, the complete conversion depended on temperature, pH and time. The higher the temperature and pH were, the easier the Ca/P ratio was increased up to about 1.60. The stoichiometric ratio was obtained at 40°C in 3 hours at pH = 9-10. The HA powders prepared were found to have low crystallinity from XRD characterizations.

Solid state reactions usually give a stoichiometric and well-crystallized HA powder. High temperatures and long heat treatment times are required. Sinterability of these powders is generally low. Arita et al. (18) used dibasic calcium phosphate (DPC : CaHPO₄) and CaCO₃ as starting materials to produce solid state produced HA powder. These powders were mixed at about a ratio of 1.5 for a stoichiometric HA powder and heat treated at temperatures up to 1000°C for 2 hours. Two separate reactions were determined with TGA and DTA analysis with these starting compounds. These reactions were observed to be:



The surface areas of these powders were about 4-6 m²/g with an average particle size of 2 μm.

Sol-gel processing provides an alternative approach to the conventional HA powder synthesis methods. Metal alkoxides [M(OR)_n] are converted into amorphous metal oxide gels through hydrolysis and condensation reactions in sol-gel processing. These gels upon heat treatment at lower temperatures yield ceramics with superior chemical and structural homogeneity (13). Amorphous calcium phosphate (ACP) gel was obtained in ethanol from calcium ethoxide [Ca(OEt)₂] and H₃PO₄ solution. The calcium diethoxide solution was

prepared by the reaction of calcium metal with ethanol for 4 hours at 80°C under nitrogen gas with stirring. H₃PO₄ dissolved in ethanol was added dropwise into the alkoxide solution at temperatures lower than 10°C. A white ACP gel was slowly prepared and further aged at room temperature under flowing nitrogen for 24 hours under constant stirring. The gel-precipitate was centrifuged and dried at 100°C for at 8 hours in an oven. The synthesized ACP powder consisted of primarily nanosized particles in the range of 10-60 nm. The XRD patterns of the powder showed the presence of an amorphous phase when heat treated below 600°C. Heat treatment above 600°C resulted in the formation of crystalline HA with XRD peaks becoming intense with the increase in temperature. The TGA analysis showed a total weight loss of about 20% in the 35- 850°C range with no weight loss above 850°C.

Various other preparation techniques like flux method, electrocrystallization, spray-pyrolysis, freeze-drying, microwave irradiation, mechano-chemical method, and emulsion processing are also known to be used for HA powder preparation (8).

3.3 Sintering of HA Powders

Dense and porous HA ceramics can be prepared by various heat treatment schedules. Dense HA ceramics with superior mechanical properties can be prepared if the starting HA powder is stoichiometric (Ca/P ratio of 1.67). If a higher Ca/P ratio is present in the powder, formation of calcium oxide, Ca(OH)₂-CaCO₃ degrade the mechanical properties significantly. Lower Ca/P ratio causes the formation of TCP(8). Most HA powders can be pressurelessly sintered to about full density in the 1000-1500°C range. Depending on temperature and also partial pressure of water in the sintering atmosphere, different phases can be formed. HA can be formed and is the stable phase up to 1360°C as shown in equilibrium phase diagram for CaO-P₂O₅ with 500 mmHg partial pressure of water given in Figure 10 (3). In the absence of water HA decomposes to TCP and tetracalcium phosphate by the following reaction:



It is often difficult to predict the volume fraction of high temperature phases formed during sintering and their relative stability when cooled to room temperature.

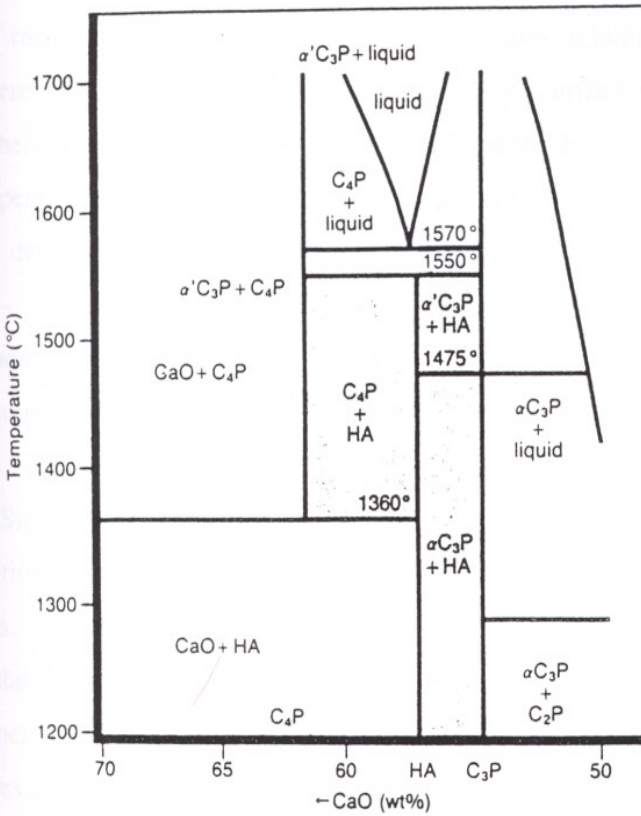


Figure 10. Calcium phosphate equilibrium phase diagram (10).

Green structures were prepared from a commercial (Merck) powder by isostatic pressing at 180 MPa in one of the sintering studies. A pre-sintering stage of 2 hours at 900°C in air was applied. The final sintering was carried out in air for 3 hours at different temperatures in the 1000-1450°C range (19). The variation of relative density and shrinkage as a function of sintering temperature is given in Figure 11. The relative density increased from 57% after pre-sintering to nearly 99% after sintering at 1450°C. Such a density is high in comparison to the values usually reported in literature for HA ceramics sintered at 1300°C. Starting powder has Ca/P ratio of 1.68±0.02 (stoichiometric) and no other phases were detected in the sintered ceramics. The relative density is almost constant in the 1300-

1450°C range at about 99% but the grain size uniformity changes with the increase in temperature. The grains were small with a uniform distribution at 1300°C but the distribution becomes considerably wider at 1450°C.

HA pellets were die pressed at 80 MPa without binders and sintered in the 900-1400°C range with 200°C/h heating and cooling rates in another sintering work (20). All runs were done in a graphite furnace under a pressurized (1 MPa) high purity Argon atmosphere. The relative density and the HA% [as the HA/(HA+TCP) 100] dependences on temperature are given in Figure 12. The sintering curve plateaued at ~1200°C and relative density is about 95%. The density decreased significantly above 1300°C. The HA% - Temperature curve indicated that the critical temperature above which decomposition occurred was 1350°C. Also, comparison of two curves shows that the onset of decomposition corresponded approximately to the drop in density that began at 1300-1350°C.

Sintering atmosphere and schedule, composition-morphology-particle size and its distribution-surface area of powder all have a significant effect on the densification of HA powders. Higher densities can be achieved at lower temperatures by using hot pressing, hot isostatic pressing. Lower densification temperatures result in the formation of ceramics with finer and more uniform grain sizes which leads to ceramics with higher thermal stabilities and better mechanical properties.

Porous HA ceramics can be fabricated by sintering powders with appropriate pore creating additives such as paraffin, naphthalene, polyethylene glycol and hydrogen peroxide which evolve gases at high temperatures. HA can also be cast into CaCO₃ skeleton which is dissolved leaving a porous network. Natural porous materials, like coral skeletons made of CaCO₃, can be converted into HA under hydrothermal conditions (8).

Figure 1

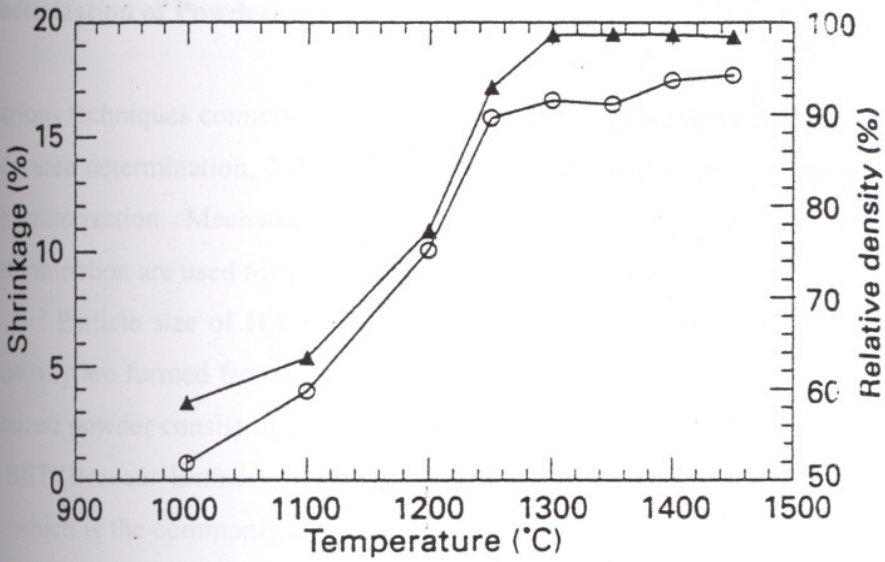


Figure 11. Variation of shrinkage(○) and relative density(▲) of the HA ceramics as a function of temperature (19).

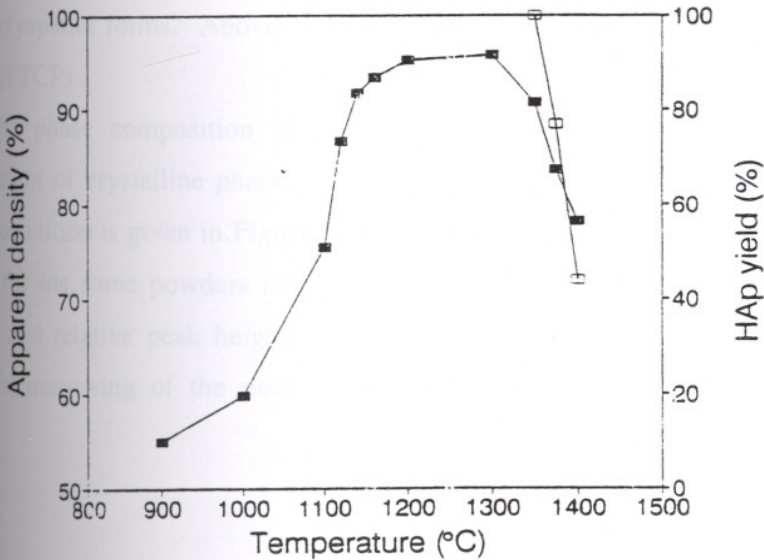


Figure 12. Densification and HA yield as a function of temperature. (■) Apparent density, (□) HA/[HA+TCP] ratio as a percentage (20).

3.4 Characterization of Powders and Ceramics

Various techniques commonly employed in ceramic processing such as particle size and surface area determination, XRD , FTIR, TGA-DTA, SEM, etc. can be used for HA powder characterization. Mechanical testing , optical microscopy, SEM , XRD, FTIR and density determination are used for HA ceramic characterization.

Particle size of HA powders vary depending on the preparation technique. Powders usually are formed from 1-300 μm agglomerates of finer primary particles. Sol-gel synthesized powder consist of nanosized particles with diameter in a range of 150-250 nm.(13). BET (Brunaur-Emmett-Teller) surface area of HA powders are in the range of 3-106 m^2/g which is the commonly used technique for the determination of surface areas of ceramic powders.

As stoichiometric HA is heated from room temperature it may become dehydrated. Between 25 and 200°C adsorbed water is reversibly lost. In the 200-400°C range lattice bound water irreversibly lost causing a contraction of the crystal lattice (4). At temperatures higher than 850°C , a reversible weight loss occurs. If pyrolysis occurs , oxyhydroxyapatite forms. Above 1050°C HA may decompose into $\text{Ca}_3(\text{PO}_4)_2$ (TCP) and $\text{Ca}_4\text{P}_2\text{O}_9$ (TTCP) .

The phase composition of HA is analysed by X-Ray diffractometry for the determination of crystalline phases. The XRD patterns of three synthetic powders in as received condition is given in Figure 13 (21). In comparison Figure 14 shows the patterns obtained for the same powders after heat treatment at 1280°C for 12 hours. The peak positions and relative peak heights for an HA standard is also given in these figures. Significant narrowing of the peak heights after heat treatment was observed in these powders.

IZMIR YUKSEK TEKNOLOJİ ENSTITÜSÜ
REKTÖRLÜĞÜ
Kütüphane ve Dokümantasyon Daire Bşk.

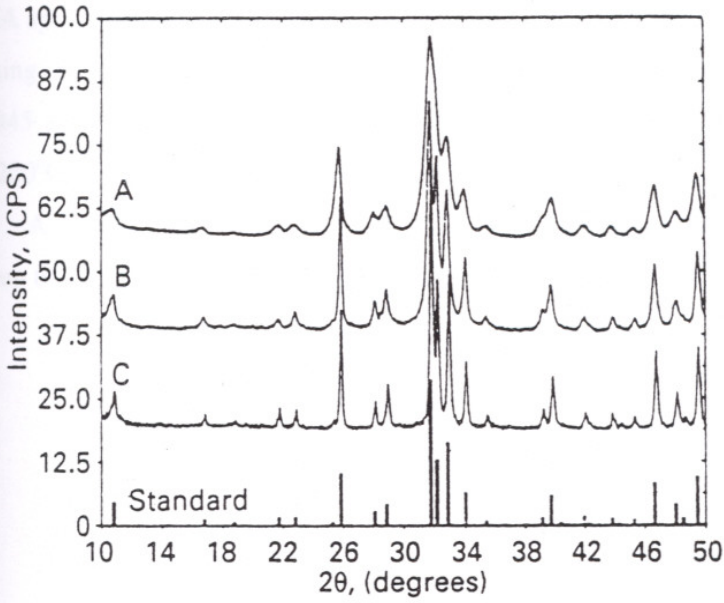


Figure 13. X-Ray Diffraction patterns of three powders in the as-received condition (21).

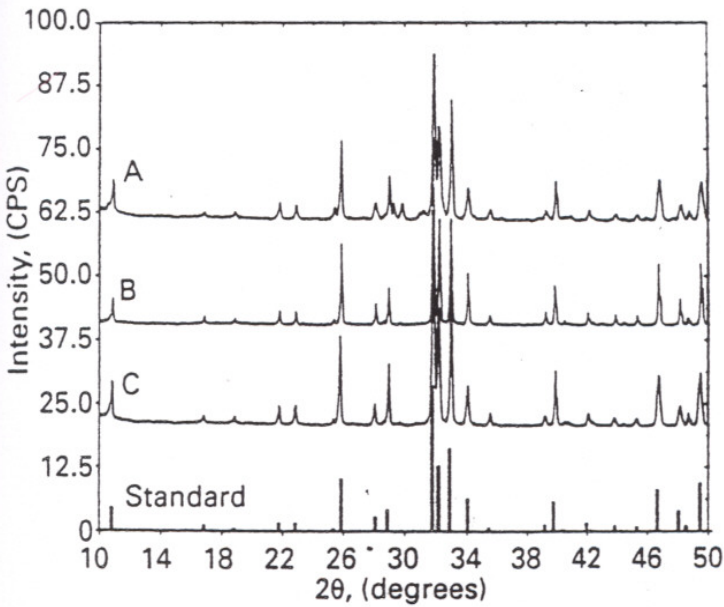


Figure 14. X-Ray Diffraction patterns of three powders after heat treatment at 1280°C (21).

FTIR spectra of HA heated at different temperatures are given in Figure 15 (22). Typical HA spectra is obtained at 1000°C. With the increase in temperature the vibrational and stretching band of OH⁻ at 635 and 3572 cm⁻¹ gradually decrease in intensity and the bands at 945 and 1025 cm⁻¹ corresponding to oxyhydroxyapatite functional group appear around 1200°C. When the temperature is over 1300°C, the vibrational OH⁻ bands disappear. A broad band from 1200 to 950 cm⁻¹ was formed when temperature was increased up to 1400°C which corresponded to TTCP and α-TCP (22).

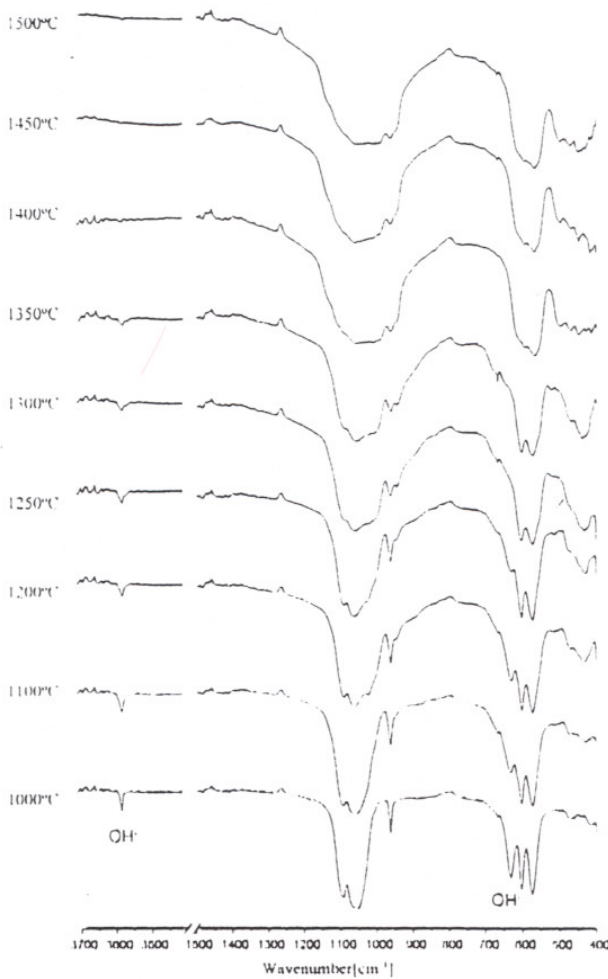


Figure 15. FTIR spectra of HA powders heat treated in the 1000-1500°C range (22).

The variation of Vickers hardness with sintering temperature for HA ceramics obtained from three different HA starting powders with different properties is shown in Figure 16. The hardness of ceramics A and C increased considerably with sintering temperature while the hardness of sample B remained constant at about 50 Hv. Increases in the hardness of sample C was higher than that for sample A. Peak hardness values of 880 Hv and 680 Hv were observed at temperatures of 1265 °C and 1320°C for samples C and A, respectively (21). These differences in hardness values were attributed to the differences in the morphologies and particle-agglomerate sizes of the starting powders. The Vickers hardness was observed to increase steadily up to 1400°C in contrast to fracture toughness with a peak hardness of about 600 Hv at 1400°C. The hardness started to decrease for samples sintered at 1450°C (19).

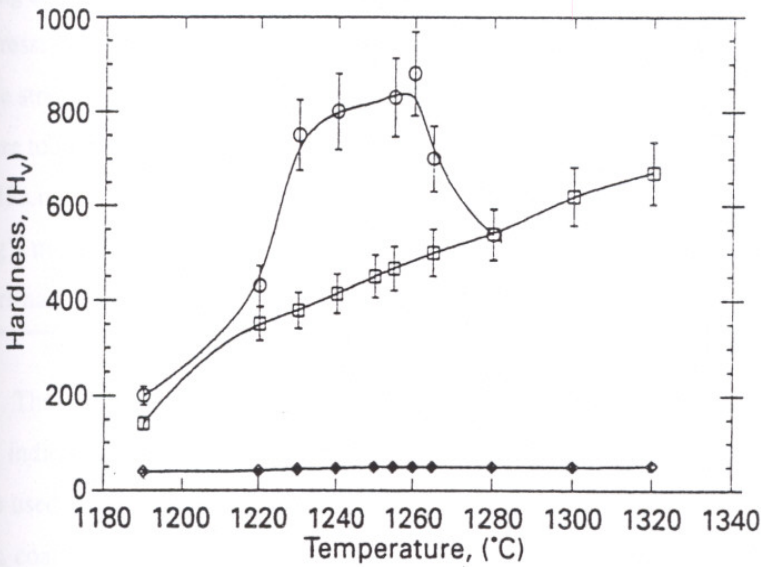


Figure 16. Variation in hardness with sintering temperature: □ A; ♦ B; ○ C (21).

3.5 Applications of HA Ceramics

HA ceramics have been in use in medicine and dentistry for 20 years (3). Application include coatings of orthopedic and dental implants, alveolar ridge augmentation, maxillofacial surgery, otolaryngology, and scaffolds for bone growth and as powder in total hip and knee surgery (Table 5)

HA seems to be the most appropriate ceramic material for artificial teeth and bones due to excellent biocompatibility and bioactivity. Unfortunately, mechanical properties of pure HA ceramics are poor (8). The mechanical properties of HA ceramics are shown in Table 7. The mechanical behavior of HA ceramics strongly influences their application as implant (10) The tensile and compressive strength fatigue resistance depend on total volume of porosity.

Table 7. Mechanical properties of dense HA and porous HA.

Property	Dense HA	Porous HA
Bending strength (MPa)	115-200	2-11
Compressive strength (MPa)	500-1000	2-100
Tensile strength (MPa)	38-300	3
Fracture toughness	0.8-1.2	
K_{Ic} (MPa.m ^{1/2})		
Young's modulus (GPa)	80-110	
Vickers hardness (Hv)	600	

The Weibull modulus (m) of HA implants is low in physiological solutions ($m=12$), which indicates low reliability under tensile loads. Consequently, in clinical practice, HA can be used as powders; small, unloaded implants; dental implants (with reinforcing metal posts); coating on metal implants which is one of the most important application of HA (where bone tissue integrates itself completely with the implant); low loaded porous implants (where bone growth acts as a reinforcing phase); or bioactive phase in a polymer-bioactive ceramic composite.

CHAPTER IV

ADSORPTION

4.1 Definition and Types of Adsorption – Adsorbents

Adsorption is the adhesion of molecules on the surfaces of solids. Adsorption was defined as the enrichment of one or more components in an interfacial layer (23). Solid material on which solutes of interest adhere is called as the “adsorbent”. The material in the fluid phase which is capable of being adsorbed is called the “adsorptive”. The material adsorbed onto the solid is called as the “adsorbate”.

Liquid phase adsorption applications include removal of ; organic compounds from water or organic solutions, colored impurities from organics and various fermentation products from fermentor effluents. Gas phase adsorption applications include removal of ; water from hydrocarbon gases , sulfur compounds from natural gas, solvents from air and other gases.

When the mixture to be separated is brought into contact with another insoluble phase, the adsorbent, and the unequal distribution of the original constituents between the adsorbed phase on the solid surface and the bulk of the fluid permits separation. The adsorption often occurs as a monolayer on the surface of the adsorbent. However, several layers sometimes occur. There are two types of adsorption phenomena : physical and chemical adsorption but there are many intermediate cases.

Physical adsorption is a reversible phenomenon which is a result of intermolecular forces of attraction between molecules of solid and adsorbate. The forces involved in physical adsorption include both Van der Waals forces (dispersion-repulsion) and electrostatic interactions comprising polarization , dipole and quadropole interactions. In the case of some adsorbents with an ionic structure, besides Van der Waals forces , electrostatic interactions are also significant.

Chemisorption is the result of chemical interactions between the adsorbent and the adsorbate. The strength of the chemical bond may vary considerably. The force of

adhesion is usually much greater than that found in physical adsorption (24). Characteristics of these two types of adsorption are given in Table 8 (25).

Table 8. The general characteristic features which distinguish physical and chemical adsorption.

Physical Adsorption	Chemical Adsorption
Low heat of Adsorption (<2 or 3 times latent heat of evaporation)	High heat of Adsorption (>2 or 3 times latent heat of evaporation)
Non specific	Highly specific
Monolayer or multilayer	Monolayer only
No dissociation of adsorbed species. Only significant at relatively low temperatures.	May involve dissociation. Possible over a wide range of temperature.
Rapid, non-activated, reversible. No electron transfer although polarization of sorbate may occur.	Activated, may be slow and irreversible. Electron transfer leading to bond formation between sorbate and surface.

Desorption is opposite of adsorption and the amount adsorbed decreases if the diffusion is in the opposite direction, mass transfer from adsorbent to fluid phase, desorption takes place. When the reverse isotherm does not follow the same path of adsorption, adsorption hysteresis evolves.

Adsorbents must possess certain engineering properties depending upon the application. Many adsorbents have been developed for a wide range of separations. Typically, the adsorbents are in the form of small pellets, beads, or granules ranging from about 0.1 mm to 12 mm in size. The performance of an adsorption process depends heavily on the capacity of the adsorbent.

All adsorbents must have large surface area. The amount they adsorb is roughly proportional to the surface area of the adsorbent, so that they must have porous structures. Pore size and total pore volume of adsorbents are very important as well as the shape of the pores. IUPAC has adapted the following classification of pores according to the width:

Macropores (> 50 nm.)

Mesopores (2-50 nm.)

Micropores (< 2 nm.)

In addition to the above properties, the usefulness of an adsorbent is a function of the following properties:

- Composition
- Hydrophilicity and hydrophobicity
- Ligand or other functional groups
- Mechanical and chemical stability

And also adsorbents used in bioprocesses should be:

- Biocompatible
- Resistant to micro-organisms
- Sterilisable
- Of constant quality.

Different adsorbents utilize different binding mechanisms. Adsorbents can be classified in three main groups (26):

- Inorganic (silica, carbon, calcium phosphate, zeolites, etc.)
- Synthetic polymers or resins (dextran, polysulfone, etc.)
- Composites (silica -dextran)

Inorganic adsorbents such as activated carbon, silica and alumina are generally rigid, stable and available in many sizes and shapes. The selectivity, however, is rather low. Also, regeneration is difficult therefore lifetime is limited. Carbons have nonpolar surfaces that are used to adsorb nonpolar molecules especially hydrocarbons. Activated alumina which has a polar surface is largely used as a desiccant. Silica is also used as a desiccant. HA is used for protein purification.

The most important class of inorganic adsorbents is probably zeolites, a subclass of molecular sieves. They are crystalline aluminasilicates with specific pore sizes located within small crystals.

Synthetic polymers are prepared by polymerizing two major types of monomers. They are available in a gel type and a macroreticular sponge like structure. They are applied in a wide range of applications such as in the recovery of antibiotics, and adsorbing organic and inorganic pigments etc. . Their mechanical strength, especially that of gel type limits their applicability in large scale processes and they are mainly used in chromatography.

The composite adsorbents combine the advantages of the inorganic rigid carrier with the favourable adsorption behaviour of polymeric adsorbents. The inner surface of an inorganic carrier is covered with a very thin layer of an organic material. Composite adsorbents can be applied in the recovery of proteins (26).

4.2 Adsorption Equilibria

The analysis of adsorption is based on equilibria and on mass balance. The equilibria are presented as adsorption isotherms at constant temperature. The amount adsorbed varies with the concentration. This relation between the amount adsorbed on the solid and the concentration in the fluid is called an isotherm.

Typical isotherms for various materials for liquid adsorption are shown schematically in Figure 17 (27). For each isotherm, the abscissa gives the solute concentration in the solution usually in units of mass of solute per volume of solution. The ordinate gives the solute concentration on the surface of the adsorbent most commonly in units of mass of solute per mass of adsorbent. Any isotherm with a downward curvature is referred to as favorable and any isotherm with an upward curvature is referred to as unfavourable.

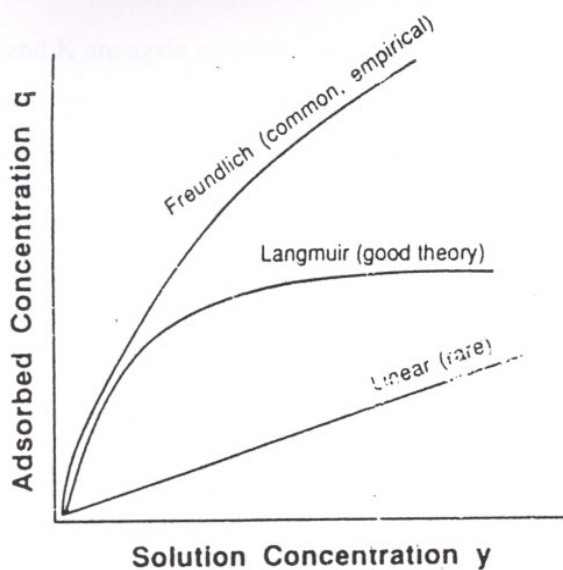


Figure 17. Common adsorption isotherms.

The determination of adsorption isotherms is important in providing data such as maximum capacity of adsorbent and dissociation constant. The linear isotherm can be expressed by an equation similar to Henry's Law:

$$q = Kp \quad (1)$$

where q is the amount of solute adsorbed per amount of adsorbent. p is the solute concentration in solution, K is a constant determined experimentally in volume of solution per mass of adsorbent. This linear isotherm is not common but in dilute region it can be used to approximate data of many systems.

The Freundlich isotherm equation, which is empirical, often approximates data for many physical adsorption system and is particularly useful for liquids.

$$q = Kp^n \quad (2)$$

where K and n are constants and must be determined experimentally if a log-log plot of q versus p is made, the slope is the dimensionless exponent n . The dimensions of K depend on the value of n (27).

The Langmuir isotherm has a theoretical basis and it is given by:

$$q = \frac{q_m p}{K + p} \quad (3)$$

where q_m and K are again constants. The dimensions of q_m and K are the same as those of q and p respectively. K and q_m must be determined experimentally. By plotting $1/q$ versus $1/p$ the slope gives K/q_m and the intercept is $1/q_m$.

q_m = maximum adsorption capacity

q = amount adsorbed at equilibrium

p = concentration of free adsorptive at equilibrium

K = dissociation constant

The assumptions made for Langmuir isotherm:

- only a fixed number of active sites are available for adsorption. A monolayer is formed
- adsorption is reversible
- no lateral interaction between adsorbed molecules
- all adsorption sites are identical
- no change in structure upon adsorption.

4.3 Adsorption Kinetics

To understand the mechanism of adsorption, it is also important to determine the mass transfer rates in a system. Determining the rate of adsorption is useful to know how fast the equilibrium phase is attained. The rate of adsorption is based on mass balances.

Analysis is based on finite rates of mass transfer and an equilibrium isotherm or adsorption kinetics for a certain system.

Differences in rate theory models are mainly due to the differences in describing the mass transfer. Various steps (and resistances) to this mass transfer can exist:

1. Mass transfer from the fluid phase to the external surfaces of the adsorbent particles (film diffusion resistance)
2. Pore diffusion in the fluid phase (pore diffusion resistance)
3. Adsorption reaction at the phase boundaries (surface reaction resistance)
4. Diffusion in the sorbed state (particle phase diffusion resistance) (28).

The rate limiting step may be one or a combination of the above mass transfer steps. For some adsorbents two mechanisms may occur in parallel and the faster controls the rate of adsorption. Each step involves a different concentration driving force and gives rise to a somewhat different form of mathematical result.

In the mathematical modelling of adsorption processes an option is to model a system as realistically as possible taken into account the individual resistances to mass transfer. However, the mathematics involved can be complex and in some circumstances an option may be to use simplified rate equations for the liquid-solid interface mass transfer, essentially combining the resistances to mass transfer to give what are known as lumped parameter models. These simplified models are used especially for well-stirred vessels when adsorbent is homogeneous.

Experimental kinetic data are frequently analyzed with the Langmuir equation. The model assumes that the adsorption can be taken as a reversible mass transfer process in which free adsorbate becomes bound to the adsorbent. The adsorption proceeds at a rate proportional to the product of the concentration of adsorbate in solution and the concentration of unused adsorbent. The reverse rate is proportional to the amount of adsorbate bound to the adsorbent. The rate equation describing the process can be written as:

$$\frac{dq}{dt} = K_a p(q_m - q) - K_d q \quad (4)$$

where p is the concentration of the adsorbate in solution and q is the concentration of adsorbed on adsorbent. K_a and K_d are the forward and reverse rate coefficients and q_m is the maximum capacity of the adsorbent. $K = K_a/K_d$ is the dissociation constant. K_a and K_d include contributions from the individual resistances to mass transfer from the bulk of the mobile phase to the available sites on the adsorption media. K_a , K_d and q_m can be determined from equilibrium and mass transfer rate experiments. Adsorption equilibrium is attained when $dq/dt=0$ and

$$K_a p(q_m - q) = K_d q \quad (5)$$

from this equality: $q = \frac{q_m p}{K + p}$, where K is the dissociation constant. (6)

4.4 Batch Adsorption

Batch adsorption is often used to adsorb solutes from liquid solutions when the quantities treated are small. An equilibrium relation such as Freundlich or Langmuir isotherm and a mass balance are needed. Initial feed concentration (p_o) and the final equilibrium concentration (p). q and q_o are the final and initial concentrations on the adsorbent. W_s is the amount of adsorbent and V is the volume of feed solution.

$$p_o V + q_o W_s = p V + q W_s \quad (7)$$

This equation can be rearranged:

$$q = q_o + \frac{V}{W_s} (p_o - p) \quad (8)$$

If q is plotted against p according to equation 8, the result is a straight line. If the equilibrium isotherm is also plotted on the same graph, the intersection of both lines gives the final equilibrium values of q and p .

When batch adsorption takes place in a well stirred vessel, concentration of the fluid in the vessel decreases with the progress of the process. In this case, the mass balance in the vessel will be expressed in the following form when $q_o = 0$ is considered at $t=0$.

$$q = \frac{V}{W_s} (p_o - p) \quad (9)$$

q can be calculated from the above equation. In the liquid phase adsorption, it is difficult to follow directly the change of amount adsorbed but the progress of adsorption may be traced by observing the concentration changes in the liquid phase as a function of time.

4.5 Protein Adsorption

4.5.1 Proteins

Proteins are built up by amino acids that are linked by peptide bonds into a polypeptide chain. Simple proteins are polymers formed by condensation of amino acids. In protein formation, the condensation reaction occurs between the amino group of one amino acid and the carboxyl group of another, forming peptide bond by the following reaction:



All of the 20 amino acids have in common a central carbon atom (C_α) to which are attached a hydrogen atom, an amino group (NH_2), and a carboxy group (COOH). Amino acids are differentiated according to the R (residue) group attached to the α Carbon through its fourth valency. There are 20 different R groups. Proteins have identical backbone structures. They are distinguished only by the distribution of the variable side chains along the main chain.

Proteins derive their chemical variety from the amino acid composition and the distribution of amino acid residues along the peptide chain. Since the amino acids that make up proteins contain two or more polar or ionogenic functional groups such as $-\text{NH}_2$, $-\text{OH}$, $-\text{COOH}$, and $-\text{SH}$, they are chemically reactive and subject to chemical attack. This sensitivity renders proteins somewhat unstable. Acidic and basic amino acids have side chains that contain ionogenic groups, i.e., terminal $-\text{COOH}$ or NH_2 groups that give the protein its polyelectrolyte character (29). The acid ($-\text{COOH}$) and base ($-\text{NH}_2$) groups of amino acid can ionize in aqueous solution. The amino acid is positively charged (cation) at low pH and negatively charged (anion) at high pH. At an intermediate pH value, the amino acid acts as a dipolar ion which has no net charge. This pH is the isoelectric point, which varies according to the R group involved. The ionogenic groups situated at the surface of the three-dimensional structure of the protein convey the surface properties of the molecule;

which in turn influences how the molecules interact with each other, with other dissolved species in solution.

In addition to the carboxyl and amino groups possessed by all amino acids, The R groups of some acids can ionize. Several of the acids possess nonpolar R groups which are hydrophobic; other R groups are hydrophilic in character.

Amino acids are not the only constituents of all proteins. Most proteins are conjugated usually covalently, to other chemical groups, organic or inorganic, referred to as prosthetic groups. Hemoglobin, the oxygen-carrying molecule in the red cells, is a familiar example of a conjugated protein.

The two major types of protein configuration are fibrous and globular shown in Figure 18 (30). Proteins have molecular weights larger than about 10000, and some protein molecular weights exceed 1 million.

The functional properties of protein depend upon their three-dimensional structure. Three-dimensional structure arises because particular sequences of amino acids in polypeptide chains fold to generate, from linear chains, compact domains with specific three-dimensional structures. Protein structure is summarized in Table 9.

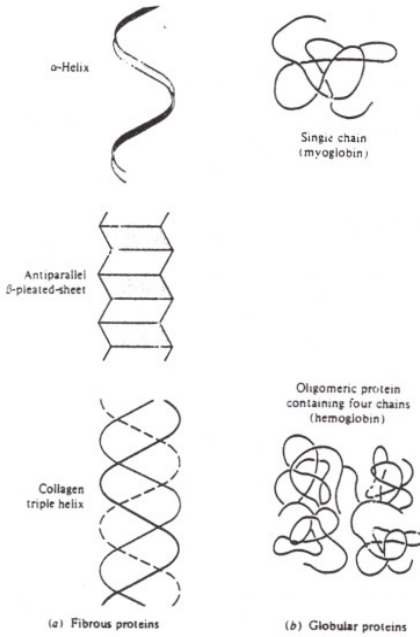


Figure 18. The two major types of protein structure with variations: (a) fibrous and (b) globular (30).

Table 9. Protein structure.

1. Primary	Amino acid sequence, joined through peptide bonds
2. Secondary	Manner of extension of polymer chain, due largely to hydrogen bonding between residues not widely separated along chain
3. Tertiary	Folding, bending of polymer chain, induced by hydrogen, salt, and covalent disulfide bonds as well as hydrophobic and hydrophilic interactions
4. Quaternary	How different polypeptide chains fit together; structure stabilized by same forces as tertiary structure

4.5.2 Bovine Serum Albumin (BSA)

BSA is generally used in biomaterial research and protein adsorption studies since it is very similar to the human serum albumin (HSA) in the sequence of amino acid units and is cheaper than HSA. Serum albumin transports fatty acids in blood. Its molecular weight ranges 66,000- 72,000 Dalton (g/mol). It is ellipsoid with axes of 14x4 nm. Dimensions 4x4x14 nm. Both have 18 amino acids in common arranged differently in the distribution. Both show about 100 carboxylic groups coming from aspartic and glutamic acids, about 100 basic groups from arginine, lysine, histidine and hydroxyl groups of tyrosine. Each molecule has about 17-18 transverse disulphide bridges and only one partially reactive sulphhydryl group (31). BSA is polyelectrolyte so the charge varies with pH. The net charge of molecule is 0 at pI (pH 4.7 ± 0.1). The net charge at pH 5, 6 and 7 is -2, -12 and -18 respectively (32). BSA is available in a highly purified form, easily soluble in water, homogeneous and well-characterized. Serum albumin is the most abundant protein present in the body of all mammalian species. It is present in human serum and in plasma at a concentration of 3.8-5.0 g/dl. This protein has not the highest probability of contact because

of its concentration, but it is the first that can cover a foreign body with released blood. It is considered as the protein that first participates in interaction with the foreign body in the competition with other proteins.

4.5.3 Adsorption of Proteins on Solids

The investigation of the mechanism involved during protein adsorption is of significant interest particularly in pharmaceutical and food industries as well as in biological environment. Adsorption of proteins takes place almost instantaneously when a solid surface comes in contact with a protein solution. The protein film forming may then act as a substratum for subsequent adhesion of other components such as eukaryotic cells or microorganisms. One major area where protein interactions with solid surface is of interest is in the field of biocompatible materials: soft and hard tissue implants and blood compatible materials have been truly investigated. Researchers studying adhesion and behaviour platelets, endothelial cells, fibroblasts and other cells on substrates deal with protein adsorption.

Research on protein adsorption will enable scientists to examine the interactions between blood and implants. It is believed that a layer of adsorbed protein exists on the surface of all implant materials and presence of this preadsorbed protein layer is important in regulating cellular response to the implant. A number of studies have shown that protein like fibronectin, bone morphogenic proteins and some synthetic peptides can regulate cell adhesion and subsequent tissue attachment to materials used as implants and this can lead to an increased rate of normal tissue regeneration (33).

The process of protein adsorption is affected by the properties of the surface, the nature of protein and the solution conditions such as temperature, pH, concentration of protein, solid/liquid ratio, ionic strength, presence of other proteins and time.

The surface of a protein is often complex in nature, with differences in characteristics such as hydrophobicity and charge. This in combination with the fact that many real surfaces are heterogeneous, complicates the prediction of how a protein will interact with a surface. A major factor influencing protein adsorption is the surface energy. Either enthalpy or entropy changes may provide a negative free energy change for the

adsorption of protein onto surfaces. The surface energy can be influenced by re-orientation of surface groups due to changes in environment. It has frequently been reported that hydrophobic surfaces adsorb more protein than hydrophilic ones (34).

Estimating the effect of surface charge on protein adsorption is difficult. Proteins that carry the same net charge as the surface may still bind through local patches of the opposite charge and may adsorb to hydrophilic surfaces with the same charge. This can be explained by conformational changes of the protein. It has been pointed out the groups at a surface of a protein are the ones most likely to interact with a solid surface (34).

The amount of globular proteins adsorbed to most solid surface is usually around or below monolayer of protein. However, sometimes multilayers can occur (35). Adsorption isotherms might feature steps. Discontinuity is shown in the Figure 19. At low BSA concentrations the surface of titanium powder is not saturated and adsorbed molecules are in random orientations on the surface. At coverage is greater than 50%, lateral interactions between the molecules become important. This may produce an ordering effect of the adsorbed protein so the surface has room for more protein to adsorb.

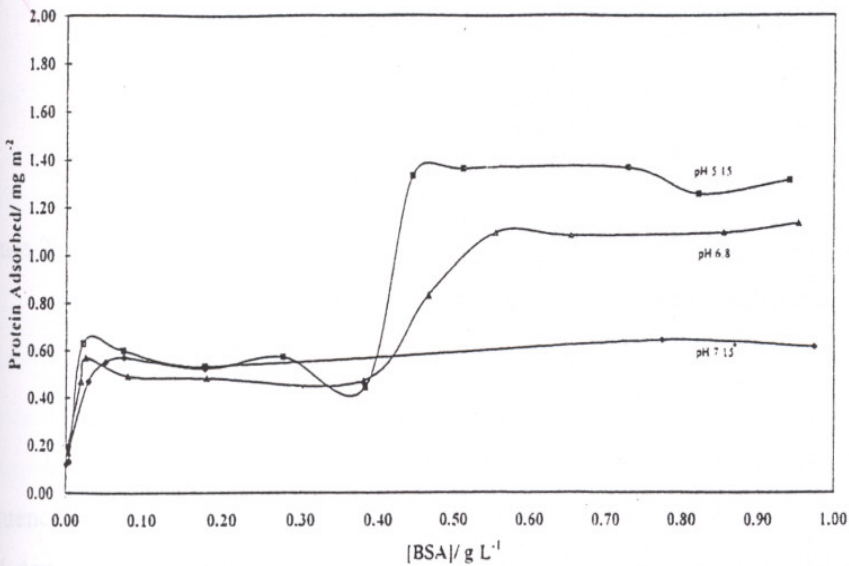
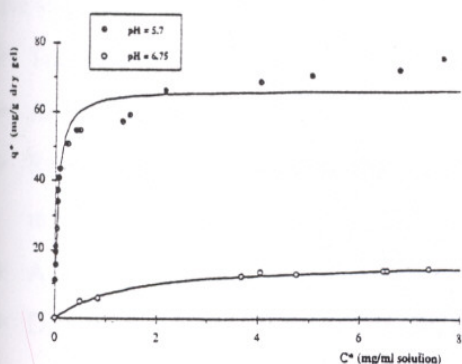
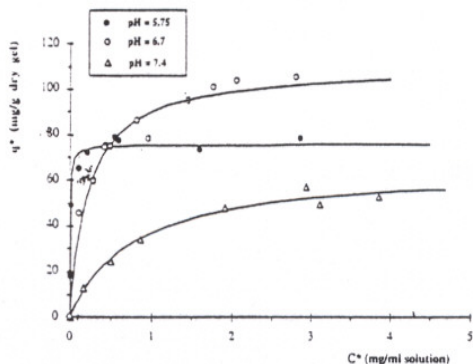


Figure 19. Adsorption isotherms for BSA onto titanium: pH dependence (35).

A maximum in the adsorbed amount is often found around the isoelectric point of protein. The Figure 20 shows the effect of pH on equilibrium adsorption isotherms for BSA and hemoglobin Hb) on HA-ultragel in potassium phosphate (KP) buffer 10 mM. pI of BSA is at pH 4.8 ± 0.1 and pI of hemoglobin is at pH 6.8 Amount of BSA adsorbed is higher for pH 5.7 than for pH 6.75 whereas amount of Hb adsorbed is the highest for pH 6.7 , near the isoelectric point of Hb (pI=6.8). This may be due to a minimum in intramolecular and/or lateral repulsion of the adsorbed protein molecules. At its pI, the molecule presents at a minimum net charge, which minimises electrostatic repulsions with an ionic surface (36).



(a)



(b)

Figure 20. Effect of pH on equilibrium adsorption isotherms (a) for BSA and (b) for Hb on HA-ultragel in KP buffer 10 mM. Continuous lines correspond to Langmuir equation (36).

Electrostatic interactions are screened at high salt concentrations. As this will influence intramolecular, protein-protein and surface-protein interactions. The overall effect will depend on the types of forces governing the protein adsorption. In the adsorption of BSA onto HA powder study; increasing the NaCl concentration resulted in a slight increase in adsorption but the binding affinity decreased (37). In the same study; increasing

CaCl_2 and Na_2HPO_4 concentrations resulted in an increase and decrease in adsorption and binding affinities, respectively (37).

The influence of temperature on adsorption is determined by the thermodynamics for each specific adsorption process; increases as well as decreases in adsorption with increasing temperature have been reported (34). The amount of human serum albumin (HSA) adsorbed onto HA decreased with increasing temperature (38). In contrast, the amount of α -Lactalbumin adsorbed onto hydrophilic chromium increased with increasing temperature. This could be related to conformational changes of the protein in the solution at higher temperatures (34).

Time dependence of adsorption kinetics and conformational change have been investigated by researchers. Total adsorption process is dynamic and may be divided into five steps:

- Transport of the molecule to the adsorbing surface ,
- An attachment step,
- Rearrangement of the conformation of the adsorbed molecule in response to the change in microenvironment,
- A detachment step,
- Diffusion away from the surface (34, 39).

Depending on the system , the transport rate is generally controlled by step 1 or 2.

In order to adsorb, the protein has to be transported from the bulk phase to the surface by diffusion or convection . Even in a well-stirred system there is a stagnant layer close to the surface through which protein has to migrate by diffusion.

Adsorption reaction at the surface can be the rate-determining step. As the surface fills with adsorbed protein, the adsorption rate becomes a function of surface coverage , decrease below the rate of diffusion and becomes surface-reaction controlled. In other systems, the surface reaction can be rate determining throughout the process. This may be due to an energy barrier against deposition (34).

The conformation of the adsorbed protein can be vitally important for its function. Change in conformation can occur immediately upon adsorption but time-dependent conformational changes are also possible. (34).

It is reported that proteins will undergo conformational changes upon adsorption to most materials and cellular interaction will greatly depend on the nature of this conformational change. Not all the changes will be beneficial for cell attachment. The differences in cellular response of different materials suggest that there are differences in the organization of the adsorbed protein layer (33).

Zang et. al. (33) studied the BSA adsorption behaviour of thin films of calcium phosphate (CaP) bioceramic and titanium (Ti). This study showed that the surface composition and structure influenced the kinetics of BSA adsorption and the structure of the adsorbed BSA. CaP surfaces caused more alteration of the structure of adsorbed BSA than the Ti surfaces. Soderquist et. al. (40) investigated the adsorption and desorption of plasma proteins; albumin, γ -globulin, and fibrinogen on copolymer and silicone surfaces. They suggested that there were three distinct processes contributing to the kinetics of uptake/loss of protein on or from polymeric surfaces. Initially, protein adsorbed reversibly. The second stage was characterized by slow change in structure of the adsorbed protein as a function of time. In the final stage, denatured protein was slowly desorbed. Also, the study of adsorption of BSA on titanium powder showed that the time dependence, isotherm and desorption data provide indirect evidence of possible conformational changes in BSA. The time dependence of adsorption of BSA on titanium is shown in Figure 21 (35). As can be seen, the maximum adsorption is reached at 10 and 15 minutes for 0.1 and 0.5 g/l BSA, respectively, after that adsorption decreased and then reached to a steady state. It was suggested that conformational changes in the molecules led to some unfolding, which resulted in an increase in the number of protein sites contacting the surface.

Protein adsorption is often apparently irreversible or partially reversible by dilution (38,34,41). Protein can sometimes be desorbed by changing pH (38,34,41) or increasing ionic strength (37,35,41). The effects of pH and salt concentration are usually more pronounced with hydrophilic surface than hydrophobic ones (34). Protein adsorption is irreversible on hydrophobic surfaces (38,42).

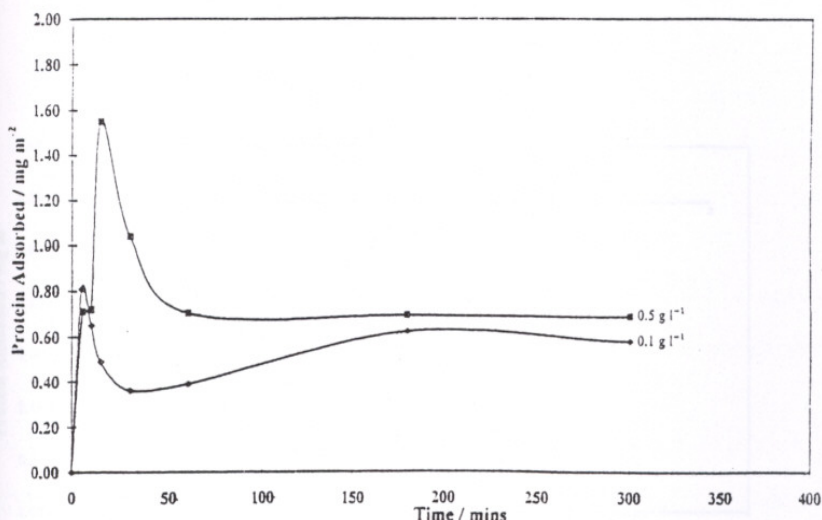


Figure 21. Time profiles for the adsorption of BSA (0.1 g/l and 0.5 g/l) on titanium, pH 6.8 (35).

Desorbed protein may be less prone to adsorb second time because of some conformational changes. In many cases; however, the protein is probably able to recover its native structure.

There have been several attempts to model protein adsorption. Some of models were based on the Langmuir equation which is only applicable to reversible adsorption (34,36). The adsorption process of BSA onto HA is described by the Langmuir model which is depicted in Figure 22 (37). More elaborate model which allowed the conformational changes to proceed to a final stage of totally irreversibly adsorption was presented by Soderquist and Walton (40). Lundström and co-workers worked extensively on developing models of increasing complexity.

Organization and orientation of proteins on a surface is important in processes such as immunological and enzymic activity of the adsorbed protein. The structure of adsorbed proteins differ with a type of adsorbent. Nygren and Stenberg found that the structure of adsorbed fibrinogen on hydrophobic and hydrophilic silica surfaces differed. Arnebrant and Nylander suggested different orientations of insulin on hydrophobic and hydrophilic surfaces. It was suggested that conformation occurred at high protein concentration for fibrinogen and γ -globulin (34).

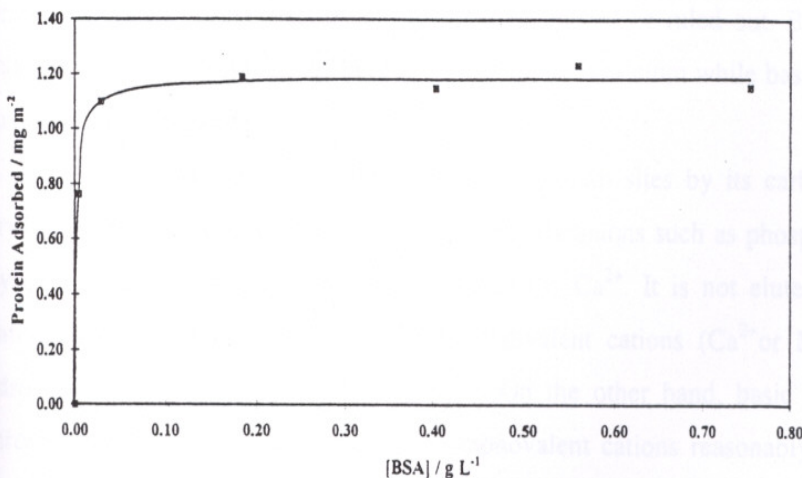


Figure 22. Adsorption isotherm for BSA onto hydroxyapatite (37).

The adsorption behaviour of proteins from blood or plasma and from mixture of blood proteins showed that the composition of the adsorbate changes with time due to the exchange processes on solid surface. The kinetics and sequence of exchange, and hence the adsorbate composition varies with the type of surface and with the degree of dilution of the sample. Exchange reactions are probably general feature of adsorption from complex protein solutions.

Pre-adsorption of a protein which binds strongly to the biomaterial surface and prevents further adsorption can be used to reduce the disadvantageous effects of protein adsorption and to improve the blood-compatibility of biomaterial. However, the risk of protein exchange always exists. For blood-compatible surfaces, albumin is used for this purpose. Thrombosis can also be avoided by coating surfaces with heparin (34).

The development of crystalline calcium phosphate or HA made its use possible in column for protein chromatography. The adsorptive capacity of crystalline calcium phosphate is lower than calcium phosphate gels because proteins cannot penetrate the particles. Limited capacity of crystalline calcium phosphate makes its use in enzyme purification mainly a late-stage procedure.

The mechanism of protein adsorption onto HA is thought to involve both Ca^{2+} and PO_4^{3-} groups on crystal surface. Since these charged groups are closely arranged on the

crystal surface it is likely that dipole-dipole interactions exist between adsorbent and protein although purely electrostatic interactions cannot be ruled out. Bernardi suggested that acidic and neutral proteins bind to hydroxyapatite calcium while basic proteins adsorb to phosphate groups (43).

Acidic proteins would bind chiefly on calcium sites by its carboxylic groups at crystal surfaces at a neutral pH. It is only eluted by anions such as phosphate ions, but not by chloride ions Cl^- which have little affinity for Ca^{2+} . It is not eluted by monovalent cations such as Na^+ or K^+ and furthermore divalent cations (Ca^{2+} or Mg^{2+}) enhance its adsorption and create new adsorption sites. On the other hand, basic proteins, binding through PO_4^{n-} sites, can be displaced by monovalent cations reasonably effectively, and very effectively by Ca^{2+} ions which have a high affinity for the PO_4^{n-} sites (36).

CHAPTER V

EXPERIMENTAL

5.1 Materials

Adsorbent used in this study was a commercial Hydroxyapatite powder (Aldrich Chemical Company). Properties of HA powder are given in the Table 10. Protein used was Bovine Serum Albumin (BSA) from Sigma (A-2153 Product lot 36H1183 initial fractionations by cold alcohol precipitation ,Fraction V minimum (96% electrophoresis) Nitrogen content is 15.88 %) . Properties of BSA are in Table 11.

Table 10. Properties of Hydroxyapatite.

Chemical Formula	$\approx \text{Ca}_{10}(\text{PO}_4)_6(\text{OH})_2$
Molecular weight (g/mol)	1004.6
Density (g/cm ³)	3.16

Table 11. Properties of Bovine Serum Albumin.

Molecular weight (g/mol or Dalton)	66.700
Dimensions (nm)	4 x 4 x 14
Density (g/cm ³)	1.36
Isoelectric point(pI) pH	4.7-4.9

Alumina (Sumitomo AKP-50) and zirconia (Tosoh TZ-3Y) were also used as adsorbents for comparison purposes. Buffer solutions prepared for the adsorption experiments were as follows:

Acetate buffer solution (57.6mM acetic acid and 42.4 mM Sodium acetate in 1000 ml) for pH 4.7

Acetate buffer solution (12.0mM acetic acid and 88.0 mM Sodium acetate in 1000 ml) for pH 5.6

Sodium phosphate buffer solution (2.22 mM Na_2HPO_4 and 6.64 mM NaH_2PO_4 . H_2O dissolved in deionized water and diluted to 1000ml) for pH 6.6

Sodium phosphate buffer solution (5.7 mM Na_2HPO_4 and 3.15 mM NaH_2PO_4 . H_2O dissolved in bidistilled water and diluted to 1000ml) for pH 7.4

Trishydroxymethyl aminomethane buffer solution (50 mM Trishydroxymethyl aminomethane and 34.4 mM HCl acid diluted to 1000ml) for pH 7.4

Simulated body fluid was prepared by dissolving reagent grade chemicals of NaCl , NaHCO_3 , KCl , K_2HPO_4 , $\text{MgCl}_2 \cdot 6 \text{H}_2\text{O}$, $\text{CaCl}_2 \cdot 2 \text{H}_2\text{O}$ and Na_2SO_4 in deionized water and they were added to the solution in the order they are listed (Composition is given in Table 12). The solution was buffered at physiological pH 7.4 at 37°C with 50 mM trishydroxymethyl aminomethane [$(\text{CH}_2\text{OH})_3\text{CNH}_2$] (THAM) and 36.23 mM HCl acid. HCl was added before calcium chloride and THAM was the last reagent added to the solution.

Table 12. Ion concentration (mM) of simulated body fluid (SBF) and human blood plasma (44).

	Na^+	K^+	Ca^{2+}	Mg^{2+}	Cl^-	HCO_3^-	HPO_4^{2-}	SO_4^{2-}
Plasma	142.0	5.0	2.5	1.5	103.0	27.0	1.0	0.5
SBF	142.0	5.0	2.5	1.5	148.0	4.2	1.0	0.5

5.2 Methods

5.2.1 Sintering Studies and Characterization

All powders were uniaxially pressed at 160 MPa. The pressed green pellets were sintered in a high temperature furnace (Carbolite RHF 1600) in air at selected temperatures in the range of 800-1400°C for 2 hours. Heating rate was 4°C/min for 800, 900, 1100, 1250 and 10°C/min for 900, 1200, 1400°C. The sintered ceramics were furnace cooled to room temperature.

HA powder and sintered HA pellets were further characterized by a number of techniques. Weight loss curve of HA powder was determined by thermogravimetric analysis (TGA) using a Shimadzu TGA-51 instrument with a constant heating rate of 4°C/min. up to 1000 °C under a dry N₂ stream.

DTA curve of HA powder was also obtained by using an Shimadzu DTA-50 with a heating rate of 4°C/min to 1300 °C.

The infrared spectra of powder and sintered HA samples were taken by Fourier Transform Infrared Spectrophotometer (FTIR-8201, Shimadzu) using KBr pellet technique. Approximately 4 mg of sample and 0.2 g KBr were mixed and ground in a mortar and this powder mixture was formed as a pellet was by pressing under vacuum (8 tonnes of force).

The phase composition and structure of HA powder and sintered HA at 1250 °C were characterized by X-ray diffraction. (Rigaku D.Max.3C.XRD).

The density of green pellets was determined from weight and dimensions of pellets. The density of sintered samples was measured by Archimede's principle by using a density determination kit (Sartorius BP 2105) and the average density of four samples at each sintering temperature was obtained.

Vickers Hardness (Hv) results were obtained by an indentation method using a Vickers hardness tester (HVS-1000). 5 pyramidal indents were tested on a heat treated pellet to give an overall average hardness value. A load of 2.9421 N was applied for samples sintered at 800, 900, 1000 °C for 15 seconds. Loads of 4.9035 N and 9.8070 N were applied for samples sintered at 1100 and >1100 °C, respectively. The hardness

values of alumina and zirconia pellets sintered at 1450°C were also examined similarly for comparison purposes.

In order to investigate the microstructure of the sintered samples and the powder particle size, an optical microscope (OLYMPUS BX-60) was used.

5.2.2 Adsorption Studies

Adsorption isotherms were obtained in batch mode under constant stirring. 1 gram BSA was dissolved in 40 ml different buffer solution (25 mg BSA/ml buffer) and kept in the refrigerator. A typical adsorption isotherm was obtained as follows:

50 ml buffer solutions with various BSA concentrations (0.1-3 mg BSA/ml) were prepared in flasks. As-received 0.2 gram HA powder was added to these solutions. These samples were incubated in the thermal shaker at 37°C and shaken at 120 rpm for 5 hours. Samples were taken from these solutions and centrifuged for 15 minutes at 4000 rpm (Nüve, NF 815). The supernatant was saved for protein concentration determination which was carried out by Shimadzu UV 1601 UV-Visible spectrophotometer at 750 nm.

Two calibration curves were plotted. The first one obtained by using protein standard (BSA) was plotted using protein assay kit by Sigma Diagnostics. The Lowry method (Appendix A) was employed for the determination of calibration curves and BSA concentration in the solutions.

The standard solutions were prepared by diluting BSA protein standard solution in water to a volume of 1.0 ml in labeled test tubes. 1.0 ml water was added to each labeled test tube blank (2 blanks). The samples were added to labeled test tubes and diluted to 1.0 ml with water. 1.0 ml Lowry reagent solution was added to each test tube and mixed thoroughly. Solutions were allowed to stand at room temperature for 20 minutes. 0.5 ml Folin & Ciocalteu's Phenol Reagent Working solution were added to each tube with rapid and immediate mixing. Solutions were allowed to stand for 30 minutes for color development and they were transferred to cuvetts and the absorbance was measured at a wavelength of 750 nm. A calibration curve was prepared by plotting the absorbance values of the standards versus their corresponding protein concentrations. Concentration was determined from the calibration curve for each absorbance value. These protein

concentrations were further multiplied with the dilution factors in order to obtain the actual protein concentration in the original sample (p).

The second calibration curve for the indirect procedure of Lowry method was prepared. Standards, blanks and samples were prepared in plastic microcentrifuge tubes as described above. 0.1 ml DOC (sodium deoxycholate) solution was added to each tube and solutions were mixed and allowed to stand at room temperature for 10 minutes. Equivalent amount of (0.1 ml) TCA (trichloroacetic acid) solution was then added to each test tube and these solutions were well mixed. These solutions were centrifuged for 15 minutes. The supernatants were decanted and blotted away. The precipitates were dissolved in 1.0 ml Lowry Reagent solution. They were transferred to labeled test tubes and the centrifuge tubes were rinsed with 1.0 ml water. The rinsings were added to their respectively labeled test tubes and solutions were mixed. Then the same procedure was carried out as above. The calibration curves used in this work are given in Appendix A.

After BSA equilibrium concentrations were determined, the amount of BSA adsorbed on HA were calculated from the Equation 9:

$$q = (p_0 - p) \frac{V}{W_s}$$

where p_0 is the initial BSA concentration in the solution, p is the equilibrium BSA concentration, V is the sample volume, and W_s is the amount of HA used. Adsorption isotherms were obtained for each pH value by plotting q (amount of BSA adsorbed on HA, mg/g) versus equilibrium concentration of BSA (p) in the solution. Langmuir model was used to describe adsorption equilibria.

Batch kinetic experiments for various pH (4.7-7.4) and concentrations were carried out to determine the amount of BSA adsorbed on HA, alumina and zirconia against time. 0.2 gram HA was added to protein in 50 ml buffer solution with identical experimental conditions with adsorption isotherm determinations. Samples from the flasks were taken out at certain time intervals, a similar procedure was followed as described earlier in adsorption isotherm experiments and q versus t plots were prepared.

The effect of pH on BSA adsorption onto HA powder was also investigated by adding 0.2 g HA powder into 50 ml various buffer solutions (pH =4.4-8) with 1 mg/ml

BSA concentration following the same procedure. The amount of BSA adsorbed (q) versus pH curve was plotted.

The effect of solid/volume ratios on adsorption was examined by changing the amount of HA powder (0,05-1,5 g), keeping liquid phase constant (50 ml $p_0=1$ mg BSA/ml). These experiments were repeated by changing the amount of liquid (100-5 ml) while keeping the amount of HA powder constant (0.2 g) at pH 4.7 and 37°C. The amount of BSA remaining in solution (p), $(p_0-p)100$ versus mg HA in 50 ml solution curves were plotted. Each adsorption experiment was repeated at least twice.

İZMİR YÜKSEK TEKNOLOJİ ENSTİTÜSÜ
REKTÖRLÜĞÜ
Kütüphane ve Dokümantasyon Daire Bşk.

CHAPTER VI

RESULTS AND DISCUSSION

6.1 Characterization and Sintering of HA Powders-Ceramics

The hydroxyapatite powder used in this work was a commercial powder. Synthesis of HA powders was not included in this work in order to limit the subject although some powder preparation studies was considered in the initial stages of the work. The Ca/P ratio of the powder was not given by the chemical company. The composition was stated to be ~ $\text{Ca}_{10}(\text{PO}_4)_6(\text{OH})_2$. This powder was used in the preparation of ceramics and was characterized along the course of this work.

The thermal behaviour of the powder was characterized by TGA-DTA and these are given in Figures 23 and 24. In order to investigate the phase purity of the powder and sintered dense ceramics X-Ray Diffraction (XRD) patterns of the powder and 1250°C sintered dense ceramic was obtained as given in Figure 25. The sintering behaviour of the powder was investigated by the formation of uniaxially pressed pellets and sintering in the 800-1400°C range. The results of these sintering studies are summarized in Figure 26. The variation of Vickers Hardness of these ceramics are given in Figure 27. The optical Microscope pictures of the powder and the microstructure of the dense 1250°C sintered ceramic are shown in Figures 28 and 29. The FTIR spectra of the powder, the 800°C and 1250°C sintered ceramics are given in Figures 30, 31 and 32.

The total TGA weight loss of the powder is 5.34% of the original weight at the final analysis temperature of 1000°C. The TGA profile has three stages with an initial rapid weight loss up to 300°C where about 80% of the total weight loss occurs. This weight loss can be attributed to the removal of adsorbed H_2O from the powder. This stage is followed by a slower gradual decrease up to 500°C. The weight loss almost ceased in the second stage (500-800°C). About 0.4-0.5% weight loss occurred in the final stage (800-1000°C). This final weight loss may be due to the removal of some CO_3 groups in the powder. This was also supported by a small endothermic peak in the DTA curve at about 900°C. During the sintering experiments additional weight losses was observed at 1400°C with a total weight loss of about 10% for a green pellet. This additional loss is partially due to the

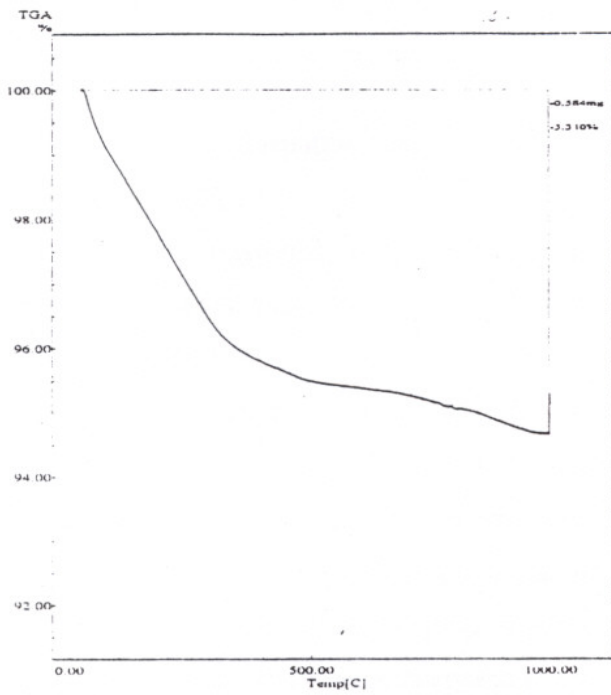


Figure 23. The weight loss curve of HA powder up to 1000°C.

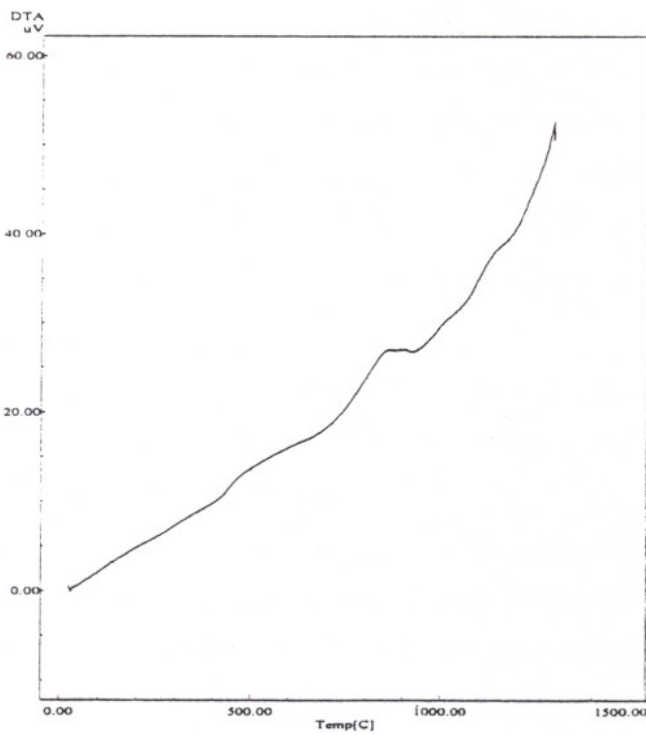


Figure 24. The DTA curve of HA powder up to 1300°C.

binder used in the pellet formation and partially due to the decomposition of HA and removal of OH⁻ groups (22).

The XRD peak positions and relative peak heights for both the powder and the 1250°C sintered ceramic matches to that of a standard (21) with one additional weak peak located at about $2\theta = 37.5^\circ$ in both patterns. This extra peak may be due to the presence of CaO (which has a peak located at about 37.5°) (12). This peak is present in both samples and can be due to the presence of unreacted small quantity of CaO during powder preparation. The full width half maxima of the peaks decrease significantly after heat treatment at 1250°C indicating crystallite-grain growth during sintering. These two patterns also support the idea that the powder crystal structure will be preserved during sintering 1250°C where dense HA ceramics were prepared in this work as discussed in the following paragraphs.

The green densities of the HA pellets were determined to be in the 45-49% of theoretical density from dimension-weight measurements. This represented about 23% shrinkage after sintering at 1250°C to 97%. The sintering-pore content curves given in Figure 26 were plotted as percentages of the theoretical density of HA (3.16 g/cm^3) (10). There are two distinct regions in these curves. In the first region (800-1000°C), the rate of densification is slow followed by a higher rate in the second region (1000-1250°C). The density remains constant at about 97% above 1250°C up to 1400°C. The densities of the pellets sintered at 800°C was about 54% (45-49% green density). The ceramics sintered up to a temperature of 1000°C has >35% porosity and the pore phase most likely is interconnected. The pores in these ceramics most likely is fine and in the submicron range close to the particle size. They are considerably stronger than the green pellets and may have significant applications in this form.

Sintering above 1200-1250°C is pointless if the goal is to prepare dense HA ceramics. An optimum sintering schedule in the 1150-1250°C range can yield dense-defect free-fine grain size ceramics with improved mechanical properties. HA ceramics with controlled porosity and microstructure can be micro-engineered in the 1000-1250°C range where phase transformations-decompositions are absent. The densities of sintered HA ceramics were reported to decrease above 1350°C (20) because of decompositions-phase

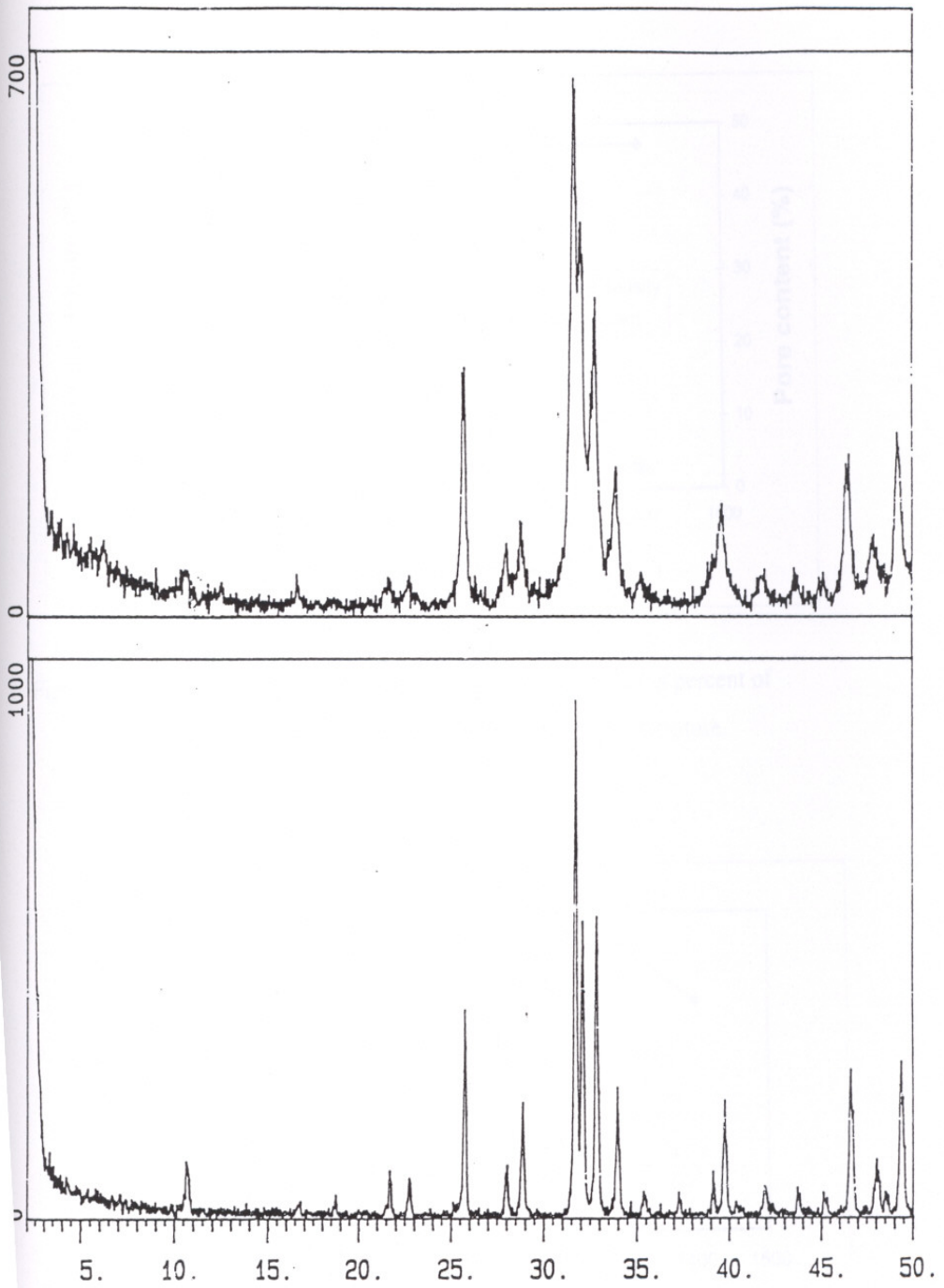


Figure 25. The X-Ray Diffraction patterns of HA powder (upper) and HA pellet heat treated at 1250°C (bottom).

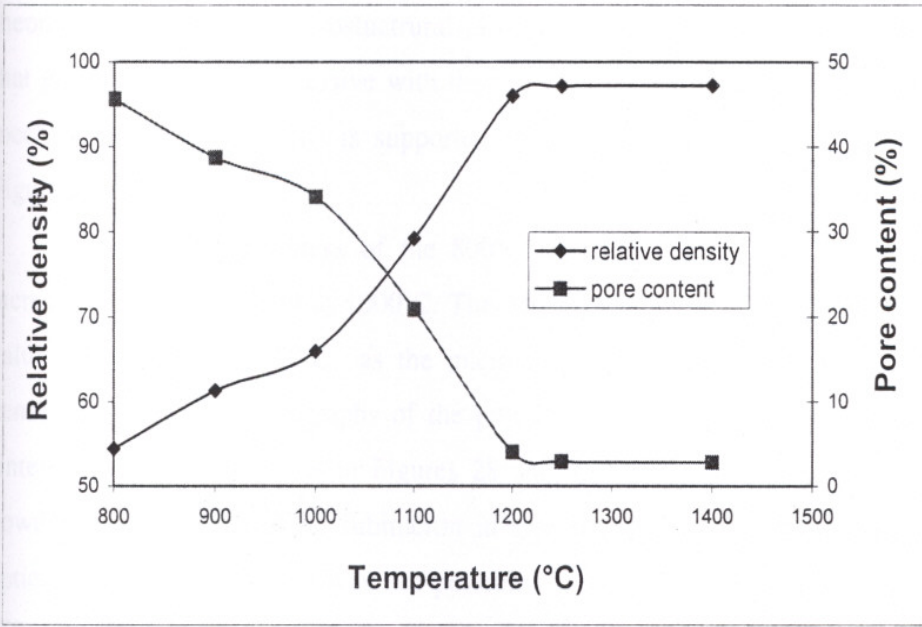


Figure 26. The variation of sintered density and pore content (as percent of theoretical density) of HA pellets with sintering temperature.

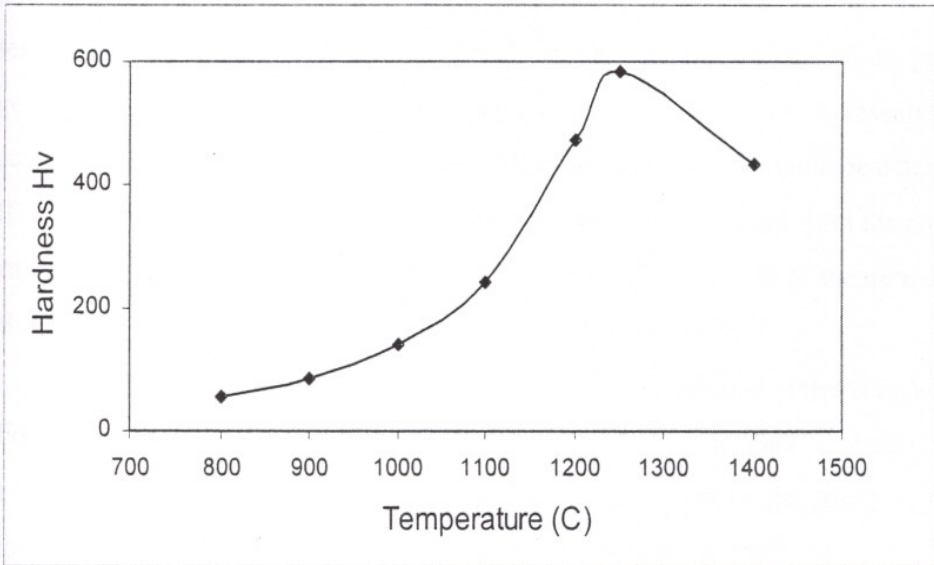


Figure 27. The variation of Vickers Hardness (Hv) of HA pellets with sintering temperature.

transformations. Although the density of the 1400°C sintered pellets was 97.2% of theoretical density, the microstructural observation by the optical microscope has shown that grain growth was excessive with the presence of cracks which may result in weaker mechanical properties. This is supported by the microhardness measurements given in Figure 27.

The Vickers hardness of the 800°C sintered ceramic was 55.6 and this value increases gradually to 139 at 1000°C. The hardness increased after 1000°C to a maximum value of 585 Hv at 1250°C as the microstructure develops and the ceramic becomes denser. The optical micrographs of the powder and the top surface of polished 1250°C sintered ceramic are given in Figures 28 and 29. The primary particles in the original powder was observed to be submicron in size but exact size determination from these optical microscope pictures was not possible. The highest magnification achievable was 1500X, therefore, the determination of particle size of submicron particles with accuracy was impossible. The grain sizes in the sintered sample were relatively uniform with sizes in the 1-5 μm also representing a crack-pore free dense surface.

The hardness for the 1400°C sample decreased to 435 Hv. This was reported previously for samples sintered above 1250-1400°C (21,19). The maximum hardness values for sintered dense HA ceramics are also reported to be about 600 Hv (10). The observation of the polished surfaces of 1400°C sintered ceramic has shown the presence of large grains and the pull out of grains during the polishing operation, representing weaker structure. The ceramic may also have a multiphase structure which should be determined by XRD. The microhardnesses of the 1450°C sintered ceramics prepared from the commercial alumina and zirconia powders were determined as 1718 Hv (97.21% of theoretical density, 3.98 g/cm^3) and 1460 Hv (99.4% of theoretical density, 6.08 g/cm^3).

The FTIR spectra for the as-received HA powder and 800°C sintered ceramic given in Figures 30 and 31 shows that the stretching band of OH^- appears at about 3572 cm^{-1} . The vibrational band of OH^- at 635 cm^{-1} can not be identified in the powder spectra but visible in the ceramic spectra. Phosphate peaks can be seen at 1048, 1091, 603, and 571 cm^{-1} (22). The peak slightly above 1600 cm^{-1} should be the H_2O peak. The 1250°C sintered ceramic FTIR spectra (Figure 32) was similar to that of 1400 °C. The FTIR spectra determined in this work matches with those reported previously for HA powders.

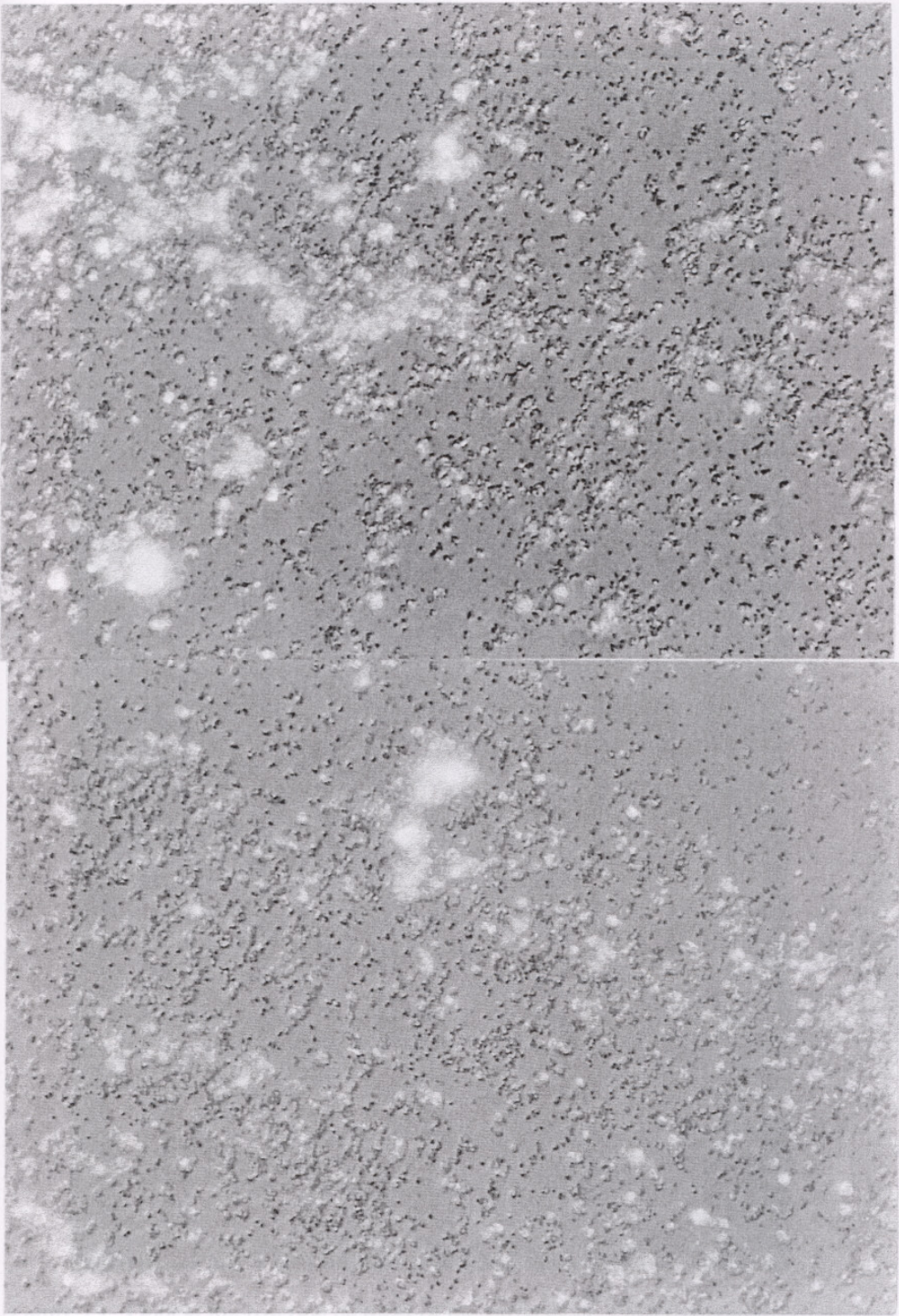


Figure 28. Optical microscope pictures of HA powders (750X).

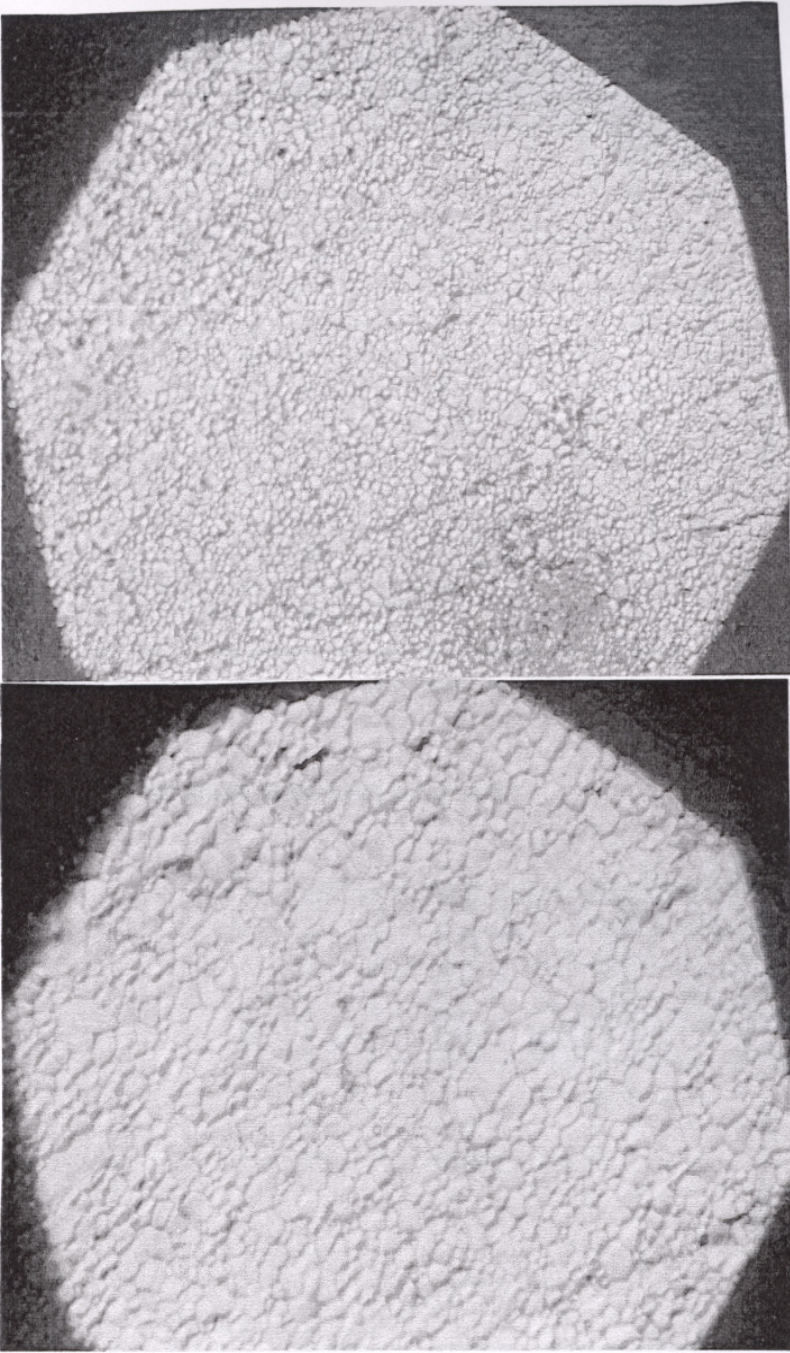


Figure 29. Optical microscope pictures of the surfaces of 1250°C sintered HA pellets, 750X and 1500 X.

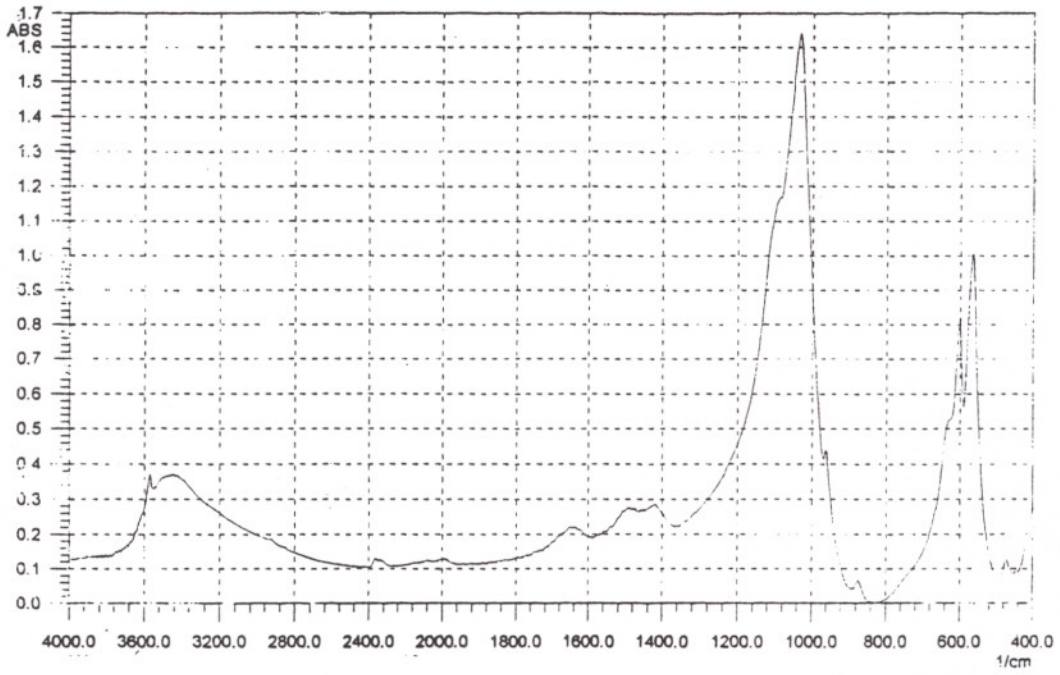


Figure 30. FTIR spectra of as-received HA powder.

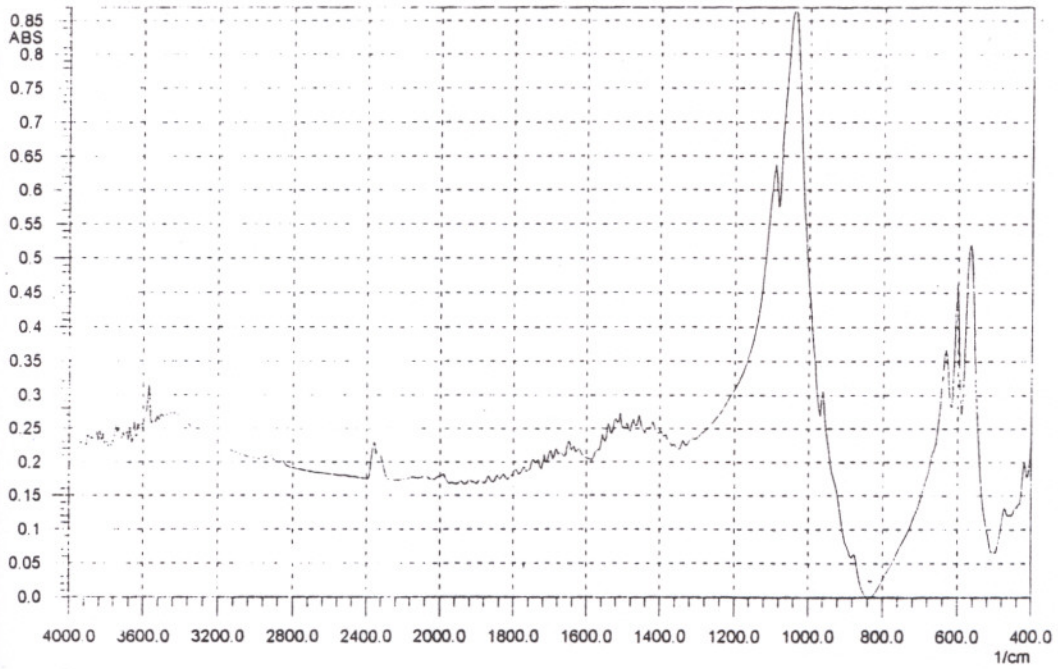


Figure 31. FTIR spectra of HA pellet heat treated at 800°C for 2 hours.

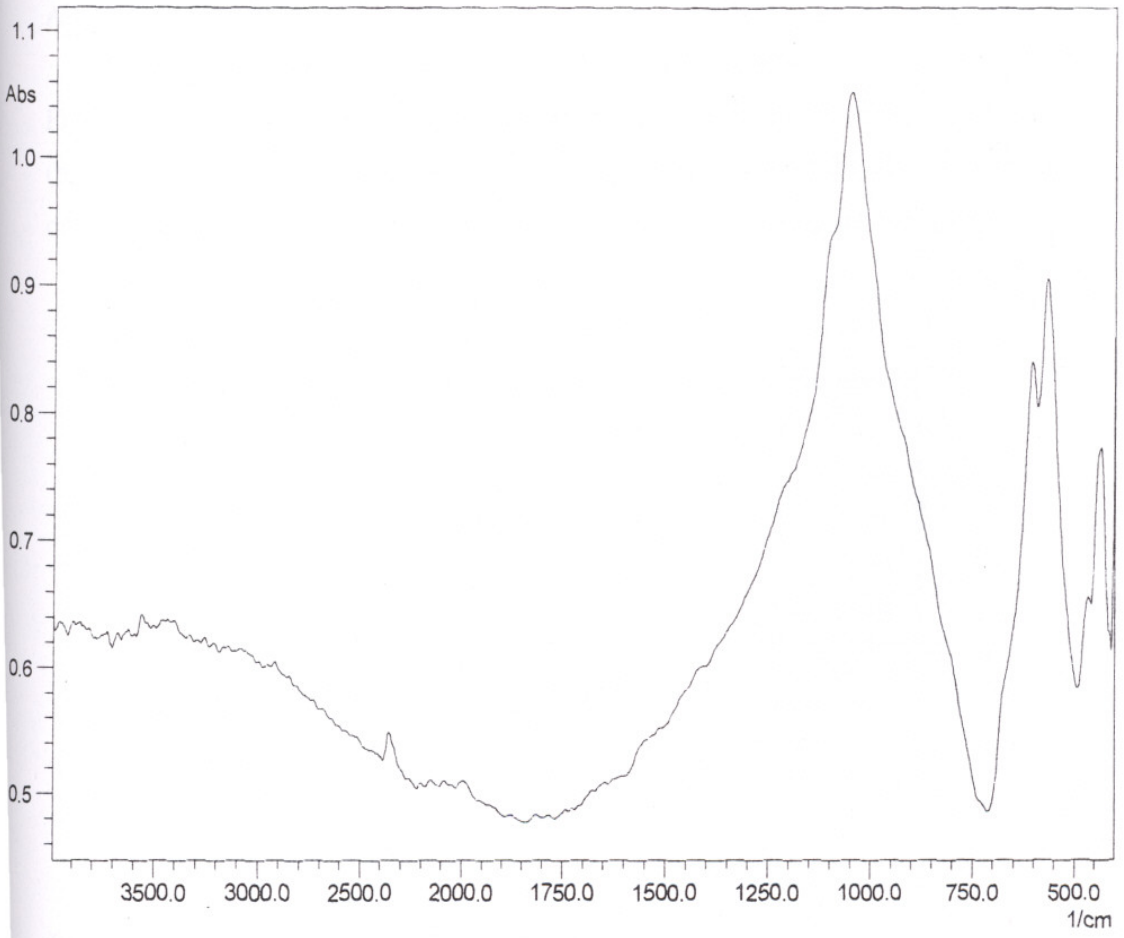


Figure 32. FTIR spectra of HA pellet heat treated at 1250°C.

6.2 Adsorption of BSA on HA and Ceramic Powders

Adsorption Kinetics

Uptake of BSA by HA at time scale for four different pH levels are given in Figures 33-36. The effect of pH on uptake profiles at a fixed initial BSA concentration ($p_0 = 1 \text{ mg BSA/ml}$) is summarized in Figure 37. Uptake curves for the adsorption of BSA onto commercial alumina and zirconia powders at $\text{pH} = 4.5$ are also given in Figure 38.

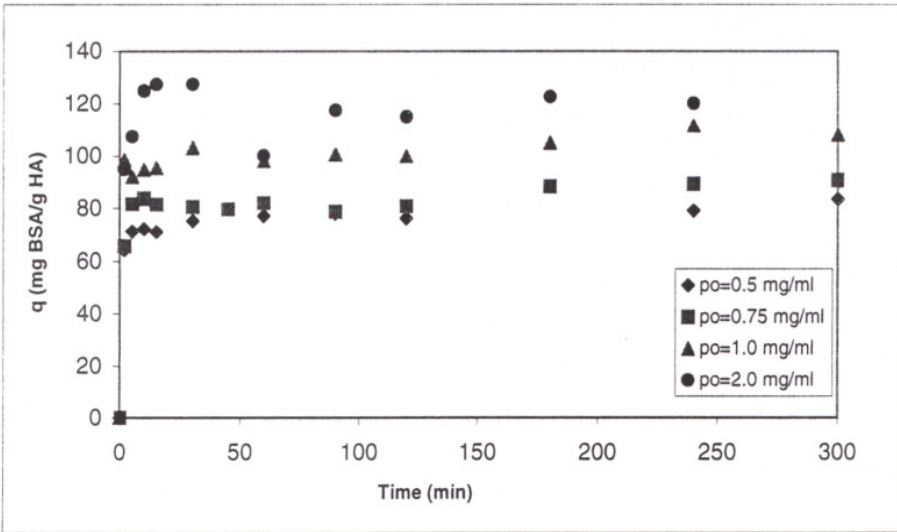


Figure 33. Uptake of BSA by HA at $\text{pH} = 4.7$.

As seen from the figures, there is an initial period which seems to be less than 2 minutes of rapid adsorption responsible for about 80% of total final adsorption. The amounts of BSA adsorbed on all surfaces are close to the respective saturation values in a few minutes. This stage is followed by a slower approach to a limiting final value in 5 hours. In general the amount of adsorption increases with the increase in the initial protein concentration (p_0). The increase in the p_0 from 0.5 to 1 and 1 to 2 mg BSA/ml have a progressively decreasing effect on the final amount of protein adsorbed as seen in Figure 33. The rate of adsorption in the first stage is considerably higher at all pH 's as seen in

Figure 37. The amount of final adsorption also decrease significantly (almost about 50%) with pH increase from 4.7 to 7.4.

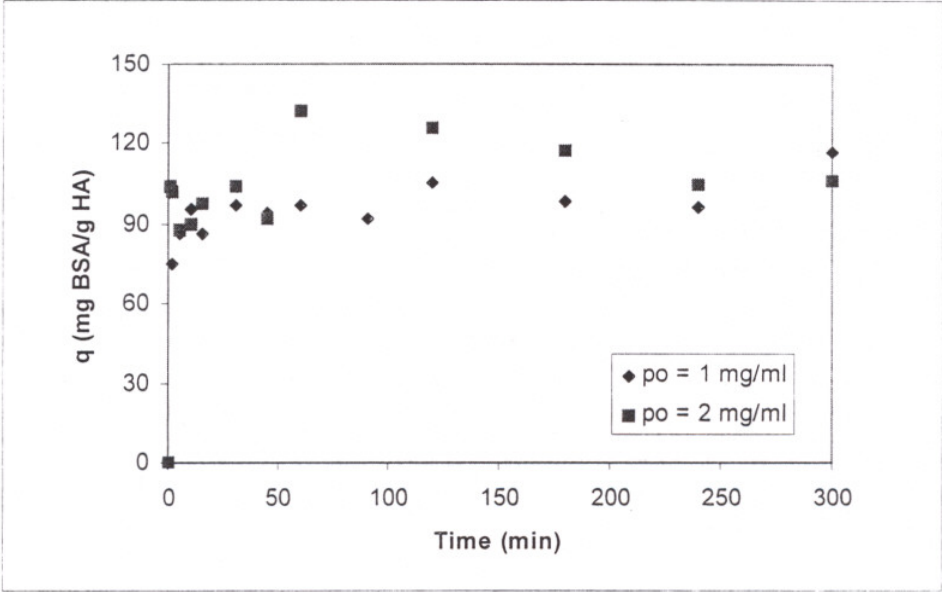


Figure 34. Uptake of BSA by HA at pH=5.6.

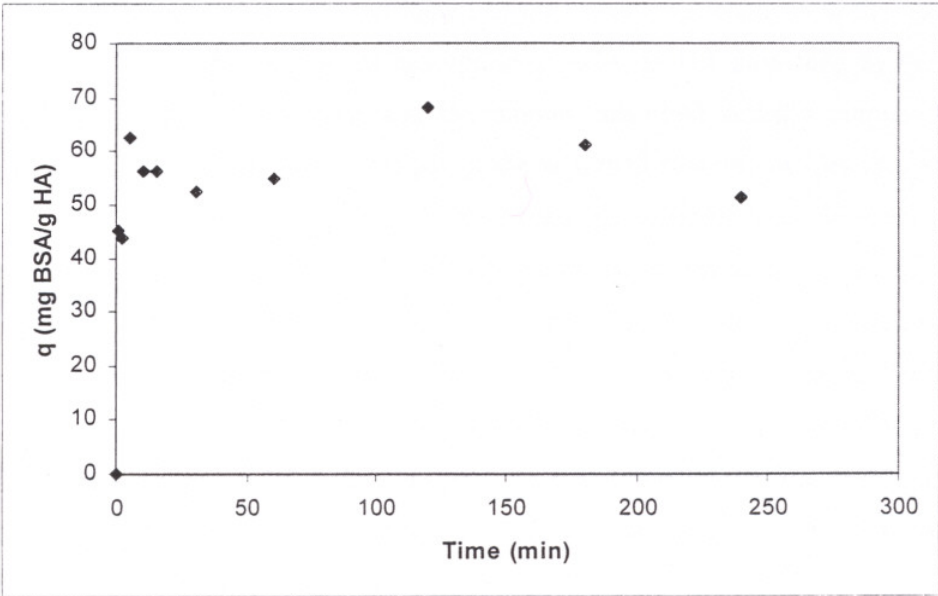


Figure 35. Uptake of BSA by HA at pH=6.6 with $p_o=1$ mg BSA/ml.

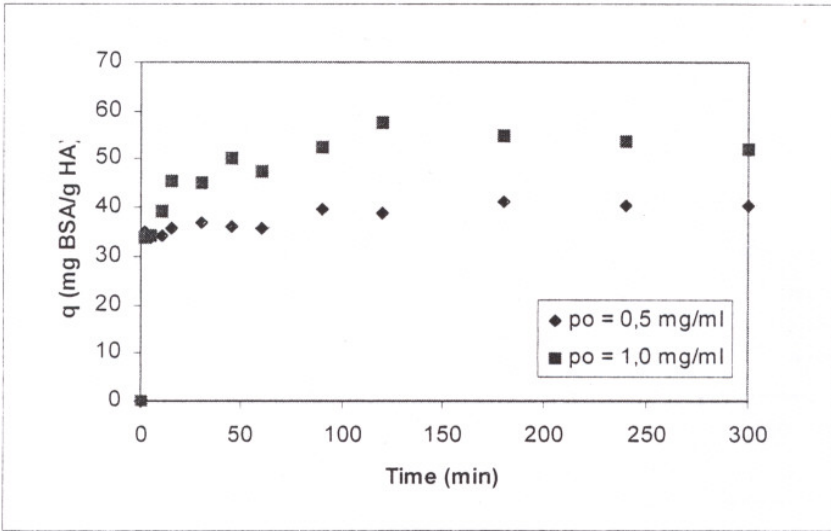


Figure 36. Uptake of BSA by HA at pH=7.4.

There seems to be a steady small increase in the amount of BSA adsorbed without a significant variation or fluctuation which was observed previously for BSA adsorption onto titanium and those fluctuations were attributed to conformational changes in the adsorbed protein (35). The time profiles for the adsorption of BSA on HA published by the same researchers had no such fluctuations and the amount adsorbed steadily increased to a limiting value(37). Conformational changes in the adsorbed protein was detected even if the time profiles had no fluctuations (33). Similar slight fluctuations in the BSA adsorption rate curves of two highest p_0 (1-2 mg BSA/ml) levels can be observed in Figures 33-38.

The uptakes of protein by alumina and zirconia at pH 4.5 are about 50% less than that on HA at $p_0= 1$ mg BSA/ml, seen in Figure 38. This difference may be due to the differences in partical size, surface area and surface characteristics. Alumina and zirconia are known to have about 0.2 μm average partical size (supplied by the company) and surface areas in the range of 10-20 m^2/g . The HA powder used in this work has fine submicron particles as was discussed in the previous section.

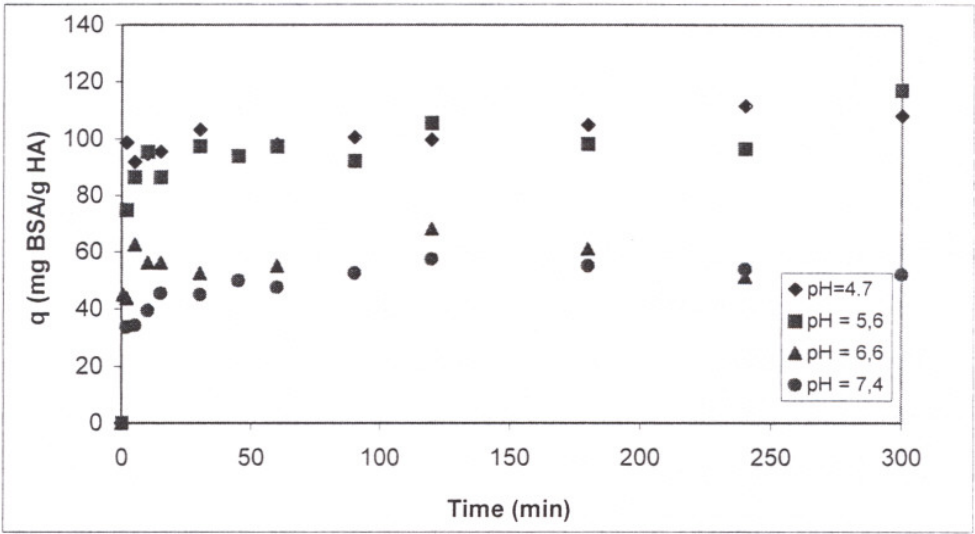


Figure 37. Uptake of BSA by HA at various pH values, $p_0 = 1 \text{ mg BSA/ml}$.

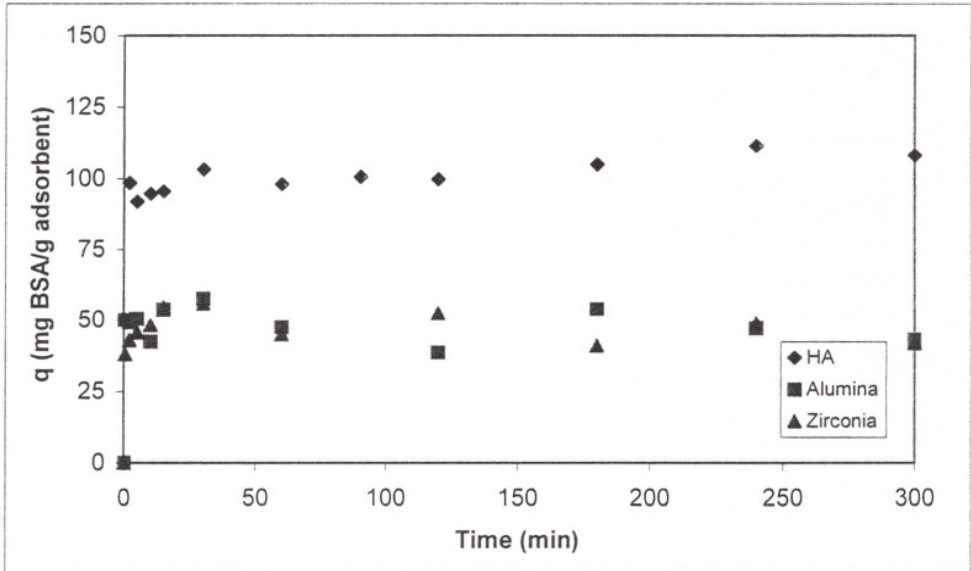


Figure 38. Uptake of BSA by alumina and zirconia powders at $\text{pH}=4.5$ and HA powders at $\text{pH}=4.7$ for comparison purposes ($p_0 = 1.0 \text{ mg BSA/ml sol.}$).

Adsorption Isotherms

Adsorption isotherms for BSA on HA at four different pH values are shown in Figure 39. Model lines for each pH value are also included in the Figure which were calculated using the Langmuir Model. Isotherms for the BSA/HA system at pH=7.4 in three different buffer solutions are given in Figure 40. Uptake of protein on alumina and zirconia at pH=4.5 as a function of equilibrium protein concentration is given in Figure 41 along with HA isotherm at pH=4.7. The equilibrium data were analyzed by using the Langmuir equation and the results are presented in Figures 42-44. The Langmuir parameters and regression coefficients are tabulated in Table 13.

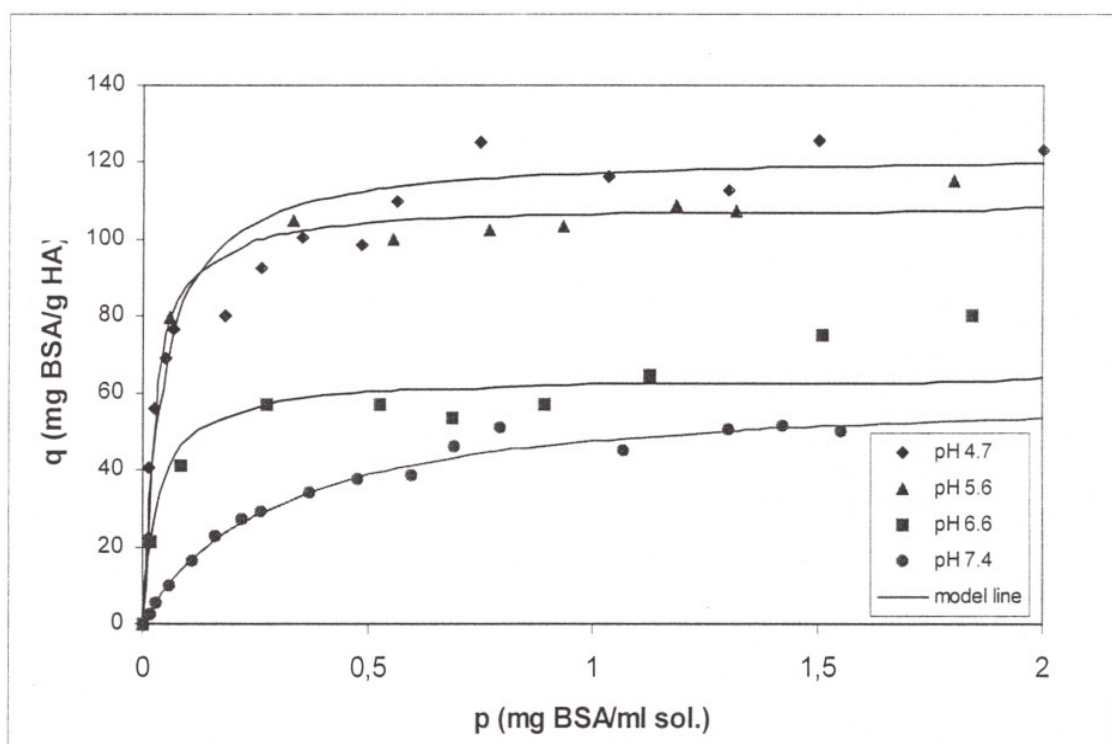


Figure 39. Adsorption isotherms for BSA onto HA for different pH values.

The maximum amount of BSA adsorbed (q_m) increases as the pH decreases. The affinity constant (K') did show a different trend. It is the highest at pH=5.6 and lowest at pH=7.4 as seen in Figure 43 and Table 13. It is interesting to note that q_m (maximum adsorption capacity) value is the highest (119 mg BSA/g HA) at pH=4.5 but the affinity constant is the second lowest (28 ml/mg BSA). The affinity constant values of pH 4.5 and 6.6 were close to each other. The q_m and K' are the lowest at pH=7.4. A linear approximation can be made for the adsorption isotherms for solution concentrations less than 0.05 mg BSA/ml. This linear approximation can even be extended to 0.1 mgBSA/ml at pH=7.4.

Table 13. The Langmuir parameters of the equilibrium data for BSA/HA adsorption.

PH	q_m Maximum Adsorption Capacity (mg BSA adsorbed/g HA)	K' Affinity Constant ml solution/ mg BSA	R^2 Regression Coefficient
4.5	119.0	28.0	0.930
5.6	108.7	46.1	0.910
6.6	64.0	31.2	0.962
7.4	61.3	3.5	0.998

Factors effective on protein adsorption on an adsorbent are complex. It is commonly accepted that ionic composition and strength of solution, pH, temperature and the functional groups on the protein and the adsorbent are all effective in protein adsorption.

Inflection points of the isotherms are located at different p (equilibrium solution concentration of BSA) values at different pH (Figure 39) which may be correlated to the affinities tabulated in Table 13. These differences in the affinities, q_m , and inflection points

can be explained through the surface characteristics and pI of both the adsorbate and the adsorbent. The isoelectric point (pI) of BSA is around pH 4.7-4.9 and pH=6-8.5 for HA (37). The surfaces of the adsorbate and the adsorbent are known to be positively charged below pI and negatively charged above pI. The surfaces of the adsorbate is taken to be negatively (except pH=4.7 where a surface charge close to zero may be expected) and the adsorbent is positively charged in the pH range investigated in this work.

The lowest affinity $K' = 3.5$ and the $q_m = 61$ values were determined at pH=7.4 which is actually the physiological pH for BSA/HA system. This may be due to the fact that adsorbate (HA) is very close to its PZC (point of zero charge) and the surface carries less net charge even though the protein is at its farthest pH from its pI (4.9) at which BSA carries maximum negative charge. Electrostatic attractions are at its lowest level and the electrostatic repulsions between negatively charged protein molecules are at their highest level at pH=7.4. Moreover, there may be a considerable level of competition between the ionized species for the available adsorption sites on the surface of HA. Addition of phosphate ions into the solution may lessen the available sites for protein binding. Sodium phosphate buffer solution was used to obtain the isotherm at this pH (7.4). It was reported that phosphate groups have a higher affinity than the COOH groups of protein for HA surface. Other studies in the presence of Na_2HPO_4 have shown similar results (37, 36).

At pH=6.6, there may be a significant level of positive charges on the adsorbent surface while the protein is negatively charged. Electrostatic interactions may play an important role for the attachment of protein on HA. Acidic proteins such as BSA would bind chiefly on calcium sites through its carboxylic groups which exchanges with the phosphate groups of the HA surface. The amount of BSA adsorbed at pH=6.6 was slightly higher than found at pH=7.4 while affinity constant (31.2 at pH=6.6) was considerably higher than that determined at pH=7.4. Also, ionic strength of buffer decreases compared to pH 7.4 (2.22 mM Na_2HPO_4 at pH 6.6 and 5.5 mM Na_2HPO_4 at pH 7.4) due to a decreasing concentration in divalent phosphate species of the buffer.

At pH=5.6, the affinity constant is found to be the highest, on the other hand q_m value is slightly lower than that of pH=4.7. It can be thought that BSA strongly binds to the HA surface through its negatively charged carboxyl groups and similarly attracted by calcium sites on HA. Among the four pH levels investigated in this work, the pH=5.6

isotherm is the steepest at very low solution concentration. This may be explained by both adsorbate and adsorbent being relatively away from their point of zero charge pH values and the surfaces having opposite charges.

Maximum adsorption occurred was observed at a pH value close to the pI of BSA although BSA carries approximately zero net charge which would minimize electrostatic repulsions/attractions with an ionic surface (36). Similar results have been also found in this study and adsorption was observed to be the highest for the smallest net charge on the protein side of the BSA/HA system. This may be due to a minimum intramolecular and/or lateral repulsion of the adsorbed protein molecules. Our findings are in good agreement with the results reported previously (34). As the pH approaches the isoelectric point of BSA, the charge on the molecule and the degree of hydration decrease, short-range attractive forces play an important role (37).

Three-dimensional tertiary structure in proteins is maintained by ionic bonds, hydrogen bonds, -S-S- bridges, van der Waals forces and hydrophobic interactions. Larger globular proteins tend to have a higher percentage of hydrophobic amino acids than do smaller proteins. Hydrophobic interactions are considered to be a major driving force in the maintenance of protein conformation. Hydrophobic interactions cause nonpolar side chains to cling together in polar solvent, especially water. These groups are pushed together by their expulsion from the polar medium. Hydrophobic interactions may involve the side chains of adjacent different molecules or they may occur between the side chains on the same protein molecule. Once the chains are brought close together, van der Waals attractive forces can assist in holding them together.

A protein with no net charge (at its pI) will have maximum hydrophobicity (43). Maximum adsorption for some proteins near their isoelectric points has been argued to be due to the minimal denaturation where the protein molecule exhibits its most compact form (36). Albumin has 55% nonpolar amino acids and therefore hydrophobic interactions are likely to have a significant effect on the determination of the form of the molecule and the adsorption processes. Maximum adsorption of BSA on HA was observed at pH=4.7 and this can be attributed to the hydrophobic effects.

Regression coefficients (R^2) as well as q_m and K' are given in Table 13. All regression coefficients are > 0.910 which is an indication of the well fit of the data to the

model. The best fit ($R^2=0.998$) was obtained for $\text{pH}=7.4$ as seen in Figure 42. For other pH values a good fit was not observed due to the fact that the experimental points were not located on a smooth plateau in the isotherms. The initial stages of the adsorption where low surface coverages are present most closely reflect the affinity of the BSA molecule toward the adsorbate because the lateral interactions between protein molecules are insignificant. Intramolecular attraction and/or repulsion, rearrangement of the molecules on the binding site may become more significant at higher concentration.

The regression coefficient obtained at $\text{pH}=6.6$ was higher than those at 5.6 and 4.7. The data seems to fit a lot better up to an equilibrium solution concentration of 1 mg BSA/ml at this pH (Figure 39). The amount of BSA adsorbed is above the level predicted by the model curve above the solution concentration of about 1.5 mg BSA/ml. At low BSA concentrations, the surface is not saturated and the adsorbed molecules are randomly oriented on the surface. Above 1.0 mg BSA/ml equilibrium solution concentration lateral interactions between molecules become important. This may cause the ordering of protein molecules on the surface, hence there is more room on the surface for further adsorption.

A similar behaviour was observed for $\text{pH}=5.6$ in the adsorption isotherm above $p=1.3$ mg BSA/ml. The saturation level (the concentration level at which the q value becomes steady) for $\text{pH}=4.7$ was obtained at a relatively higher p value (0.6) (Figure 39). The affinity constant is smaller than that of $\text{pH}=5.6$. The shallow curvature of isotherms indicates a lower affinity of adsorbate and adsorbent. The affinity is related to the net charge of the protein and adsorbent. At $\text{pH}=4.7$ adsorption is not due to the electrostatic interactions of protein and HA surface. At $\text{pH}=7.4$, the adsorption isotherms reaches to a plateau gradually. Discontinuities in the albumin adsorption isotherms have been reported previously (35, 36) whereas continuous isotherms without steps were reported for BSA adsorption on HA powder and described by the Langmuir model in another work (37). In the latter work, adsorption isotherms were obtained up to an equilibrium concentration of 0.8 mg BSA/ml (2 mg BSA/ml in this work) which may be the reason for the absence of discontinuities.

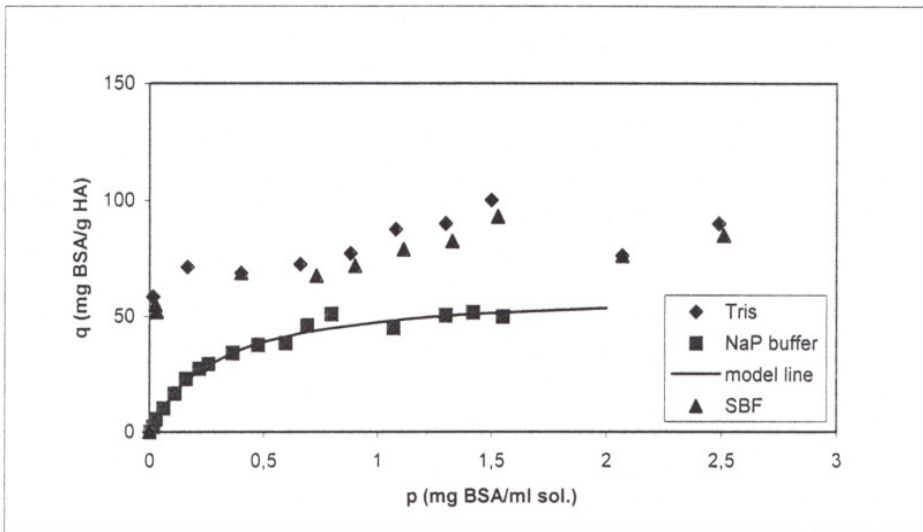


Figure 40. Adsorption isotherms for BSA onto HA at pH=7.4 for Tris, NaP and SBF buffer solutions.

Adsorption isotherms of BSA on HA at pH=7.4 in sodium phosphate, SBF (simulated body fluid, the compositions are given in the experimental section), and tris buffer solutions are given in Figure 40. The amounts of BSA adsorbed on HA in tris and SBF buffer solutions are higher than those of sodium phosphate buffer. These differences may be mainly due to the differences in the nature of ions in these buffer solutions. The presence of higher phosphate ion concentration in the sodium phosphate buffer may also have an effect on this difference because of the higher affinity of phosphate ion than the carboxyl groups of the proteins for the Ca sites on the HA surface as was discussed previously. It was reported that the strength of phosphate bonds was more than 20 times greater than that of carboxyl bond (37, 43).

There seems to be a slightly more adsorption observed in tris solution than that of SBF. This could be due to the presence of various ions in the SBF solution. As mentioned before phosphate ions in SBF reduce adsorption while calcium-ions bridging between BSA and HA may enhance adsorption. It was reported that divalent cations (Ca^{2+} , Mg^{2+}) enhance acidic protein adsorption and create new adsorption links (36, 37). There are significant amounts of chloride (Cl^-) and sodium (Na^+) ions in the SBF solution. Cl^- ions have no

amounts of chloride (Cl^-) and sodium (Na^+) ions in the SBF solution. Cl^- ions have no ability to form complexes with calcium (Ca^{2+}) and Na^+ can bind to phosphate groups of HA. Hughes et al (37) have shown that the maximum amount of BSA adsorbed (q_m) did not differ significantly from the amount adsorbed in the absence of NaCl . It can be reported that some ions enhance adsorption while the others reduce adsorption. Adsorption of BSA in tris and SBF solutions did not differ greatly. Isotherms can not be described with the Langmuir model.

Adsorption isotherms of BSA on alumina and zirconia powders at $\text{pH}=4.5$ and on HA at $\text{pH} 4.7$ are shown in Figure 41. Langmuir isotherm model has been used to describe the adsorption of BSA on zirconia and HA. Langmuir parameters of equilibrium data for BSA/zirconia adsorption have been calculated as: $q_m=57.8 \text{ mg BSA/g zirconia}$, $K'=3.32 \text{ ml/mg}$, and $R^2=0.9245$. Both of them didn't give a good fit to Langmuir model.

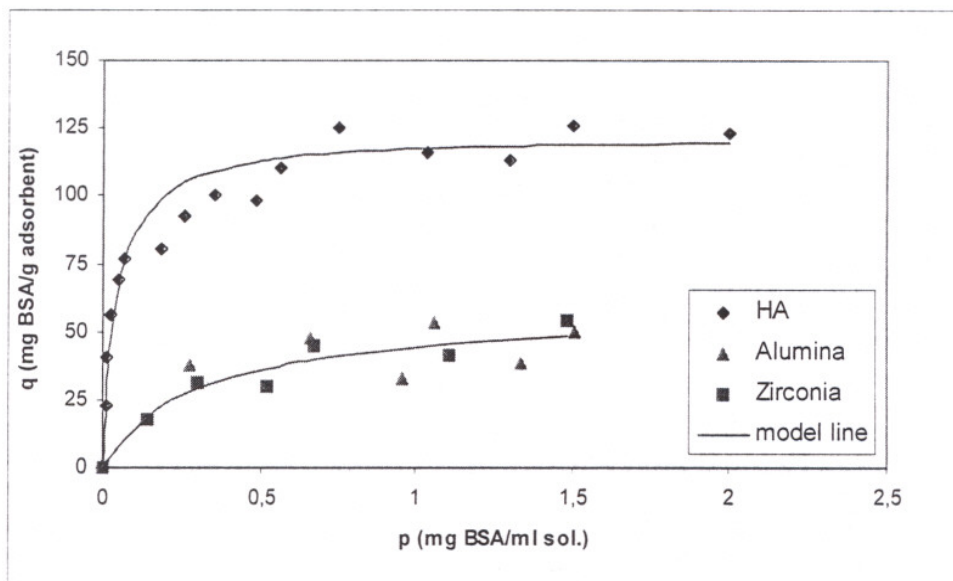


Figure 41. Adsorption isotherms for BSA onto alumina and zirconia powders at $\text{pH}=4.5$ and HA powders at $\text{pH}=4.7$ for comparison purposes.

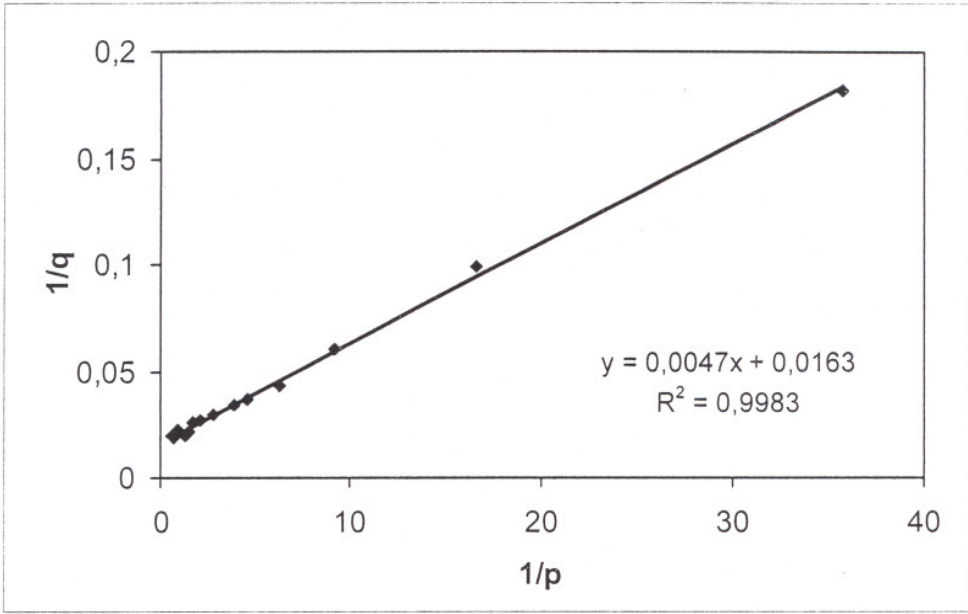


Figure 42. Double reciprocal plot for BSA adsorption on HA at pH=7.4.

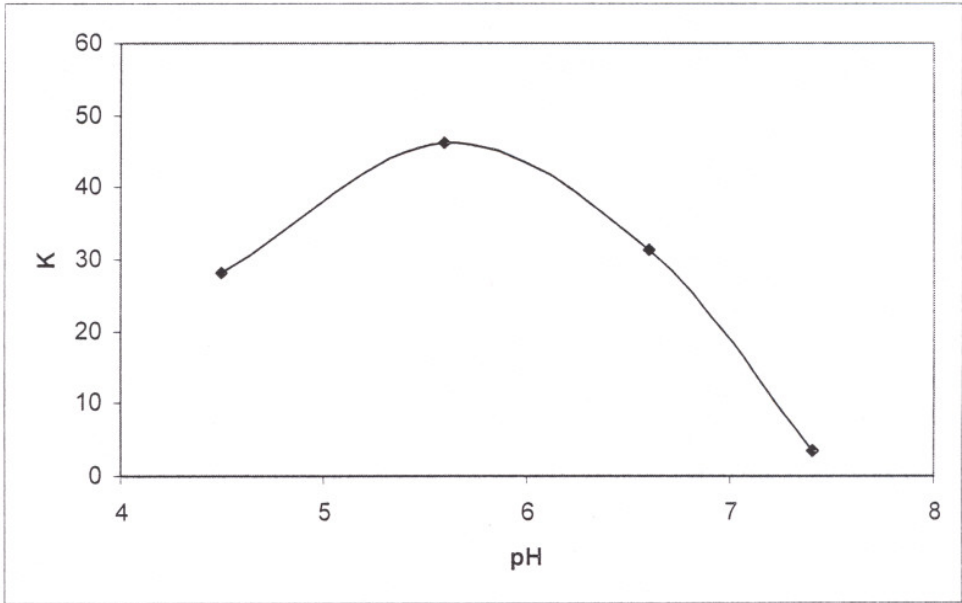


Figure 43. The variation of affinity constant with pH for BSA adsorption on HA.

Although the adsorption isotherm of BSA on alumina is similar to BSA on zirconia, the Langmuir Equation did not represent the isotherm. The regression coefficient was low (~ 0.7). The model line included in Figure 41 is for the zirconia/BSA system. Alumina and zirconia both have positive net surface charges at $\text{pH}=4.5$. Amount of BSA adsorbed on HA is about 2.5 times higher than those of zirconia and alumina. This difference may be due to the differences in surface characteristics and area. Also it should be kept in mind that the densities of these three powders are different (3.16, 3.98, 6.08 respectively for HA, alumina and zirconia).

The maximum adsorption capacity q_m and the variation of the amount of BSA adsorbed with pH are presented in Figures 44 and 45. Both curves show the presence of two pH regions (above and below a pH of about 5.8) where the calculated q_m and experimental q values are considerably different. Unfolding may occur with increasing negative charge (increasing pH) and with the electrostatic repulsion of protein molecules the distance between adjacent molecules on the surface increases. Also the surface of HA carries less net charge. These may cause a significant decrease in the adsorbed amount of protein with the increase in pH .

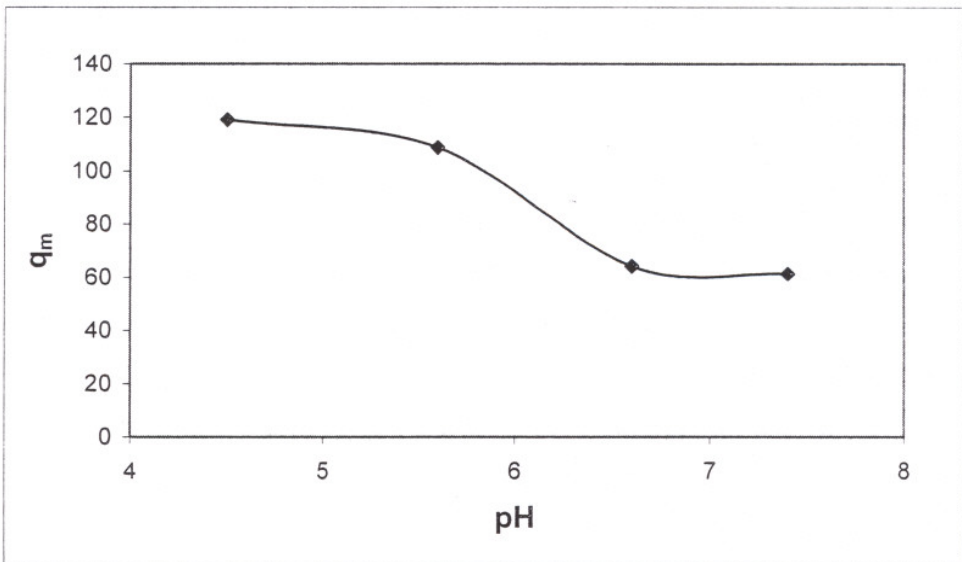


Figure 44. The variation of maximum adsorption capacity with pH for BSA adsorption on HA.

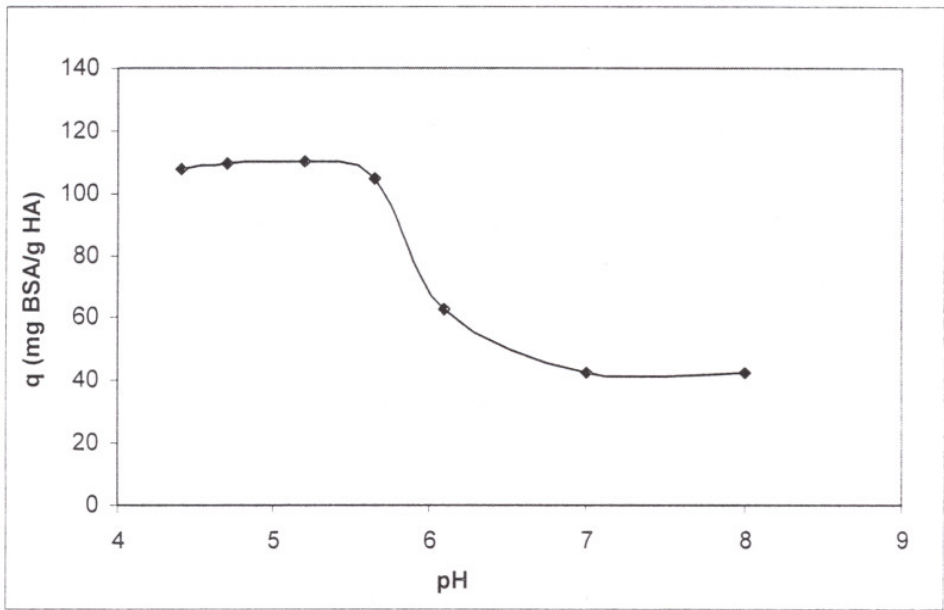


Figure 45. The variation of amount of BSA adsorbed on HA with pH.

($p_0 = 1.0$ mg BSA/ml sol.).

A review of the recent research on the adsorption of BSA on various adsorbents shows that there is a tendency of a decrease in adsorption with increasing pH. Increasing electrostatic repulsions between the protein molecules beyond the pI of BSA have been reported in a number of studies (31,35-37, 45).

The variation of the final BSA concentration in solution with HA solids loading (different solid/liquid ratios) at pH=4.7 and a fixed initial protein concentration ($p_0=1.0$ mg BSA/ml solution) is presented in Figure 46a. The same information is presented differently in the form of the percentage of the initial amount of protein adsorbed at each HA loading in Figure 46b. These figures clearly show that beyond a certain solids loading (750 mg HA/50 ml solution) , the addition of more HA has no effect on the recovery of protein from the solution. These curves can be used to estimate the necessary amount of the solids for a specific optimum recovery of the protein from a solution. The solids loading for the main part of the adsorption experiments in this work was set at 200 mg HA/50 ml solution which represents about 45% recovery of the protein from the solution with a $p_0=1$ mg BSA/ml solution. This represents a proper choice of solids loading since all the

concentration determinations were made in the supernatants. A higher solids loading in the 500-750 mg HA/50 ml solution range would make adsorption studies difficult where the low initial protein concentrations are used.

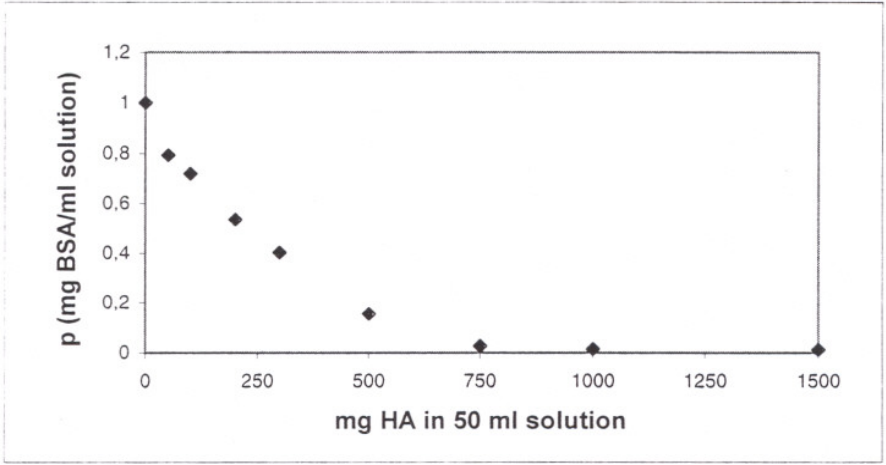


Figure 46a. The variation of final concentration of BSA in solution with HA solids loading (pH= 4.7 and $p_0 = 1.0$ mg BSA/ml sol.).

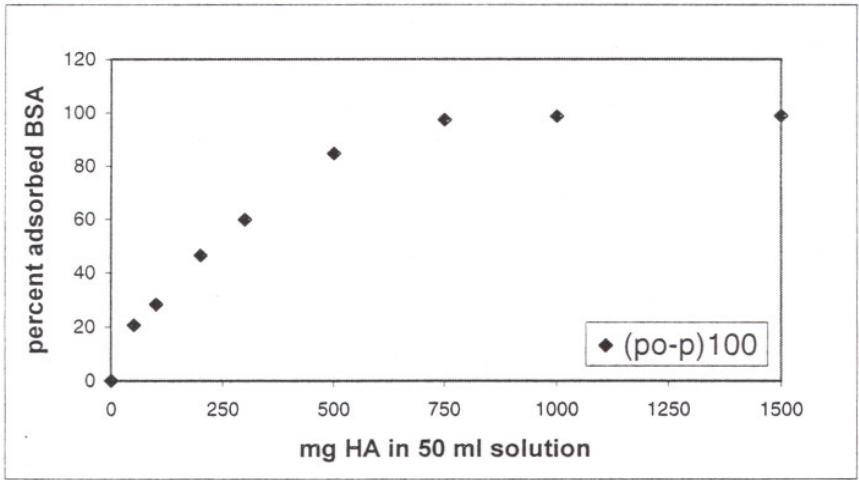


Figure 46b. The variation of percent adsorbed BSA in the solution with HA solids loading (pH= 4.7 and $p_0 = 1.0$ mg BSA/ml sol.).

CHAPTER VII

CONCLUSIONS AND RECOMMENDATIONS

In this study the preparation and characterization of HA powders and ceramics by using a series of techniques and the adsorption behaviour of BSA on HA surfaces was investigated.

The sintering studies have shown that it is possible to prepare dense and porous HA ceramics in the 800-1250°C for different applications. The densities of the 1200-1250°C sintered ceramics were close to the theoretical density with a uniform microstructure with fine grains. The microhardness was about at its maximum for these ceramics. A more detailed sintering study along with microhardness-compression and tensile testing would give a better understanding of these ceramics in the 1100-1250°C. The microhardness of the ceramics was observed to increase with the increase in density up to a maximum of 585 Hv with less than 3% residual porosity.

The commercial powder and the 1250°C dense ceramic were determined to be almost phase pure and identical with a low level of CaO impurity. The preparation of a finer pure powder along with the addition of secondary phases like whiskers, controlled morphology-size pore generating additives, zirconia and alumina may yield interesting biomaterials which are the current research areas worldwide. The Ca/P ratio in these powders controlled and determined by using techniques like ICP.

The adsorption of proteins is the first phase of a number of reactions right after an implant is placed in a human body. Moreover, the nature of adsorbed protein on biomaterials is believed to be responsible for the host response. The adsorption of proteins on HA and other solids is important in various fields like dental applications, biocompatibility of implants, protein separation-purification etc.

The present study has provided valuable information on the BSA/HA adsorption, contributing to a better understanding of adsorption mechanism. The effects of parameters such as pH, time, protein concentration, the nature and content of ionic species in the adsorption environment all at 37°C were investigated.

Batch adsorption kinetic studies were carried out in the 4.5-7.4 pH range for various initial protein concentrations in the 0.5-2.0 mg BSA/ml solution range. At all pH values,

the rate of adsorption was very fast in the first two minutes where almost 80% of total adsorption was completed. The rate of adsorption in the 0-120 seconds interval should be investigated by using an almost instant separation technique for the HA/supernatant which was accomplished by centrifugation for a better understanding of the adsorption process in that time interval. The use of pellets which will not disintegrate during adsorption may make the sampling a lot easier and quicker in the 0-120 seconds time interval. This may also help in a better understanding of diffusional resistances.

Uptake of BSA by HA increases with an increase in initial BSA concentration. The highest uptake obtained with initial BSA concentration p_0 (= 2 mg BSA/ml) is around 125 mg BSA/g HA at pH=4.7 while the minimum uptake was found to be 42 mg BSA/g HA at pH = 7.4 with an initial concentration of 0.5 mg BSA/ml. The amount of BSA adsorbed did not vary significantly with time and almost no fluctuations were observed.

Adsorption isotherms were obtained for pH 4.7-7.4 and described by the Langmuir model. The Langmuir parameters: q_m (maximum amount of protein adsorbed, mg BSA/g HA) and K' (affinity constant) depend on pH, a decrease in pH leads to an increase in adsorption but K' is the highest and lowest at pH 5.6 and pH 7.4, respectively. The Langmuir model did not represent adsorption isotherms obtained in Tris and simulated body fluid (SBF). The amounts of BSA adsorbed on HA in Tris and SBF solution did not differ. The presence of phosphate ions in buffer solution (pH=7.4) leads to a decrease in adsorption.

Dimensions of mg/m^2 adsorbent is commonly used for the expression of q . Results of this work would be compared with the results of published research if the surface area of HA was determined. The amount of BSA adsorbed at equilibrium in the pH 4.5-5.8 pH range was twice of that in the 6-8 pH range. A maximum recovery of BSA from the solution phase was obtained with 750 mg HA solids loading into 50 ml solution with an initial protein concentration p_0 (1 mg BSA/ml) at pH4.7. The amounts of BSA adsorbed on alumina and zirconia at pH 4.7 are 50% less than that of HA.

Desorption studies can be carried out in order to understand the mechanism and interactions involved in the binding of protein. Desorption may be performed by adding chloride and phosphate ions into the solution to elute the protein from the calcium sites on the HA surface. It is expected that chloride ions may not have significant effect on

desorption if the binding of protein occurs only at calcium sites whereas phosphate ions do. Further research can be carried out with the human blood plasma to get a better understanding of the competitive protein adsorption processes.

REFERENCES

1. L.L.Hench, "Medical Materials for the next millennium", 13-19, *MRS Bulletin*, May 1999.
2. P.Ducheyne, "Stimulation of biological function with bioactive glass", 43-49, *MRS Bulletin*, November 1998.
3. L.L.Hench and J.Wilson, "Bioceramics", 62-74, *MRS Bulletin*, September 1991.
4. D.H. Kohn and P. Ducheyne, "Materials for bone and joint replacement", pp.31-109 in *Medical and Dental Materials, Volume 14*, Materials Science and Technology: A Comprehensive Treatment, Edited by R.W. Cahn, P. Haasen and E.J. Kramer, VCH, New York, 1992.
5. D.F. Williams, "Biofunctionality and biocompatibility", pp.1-28 in *Medical and Dental Materials, Volume 14*, Materials Science and Technology: A Comprehensive Treatment, Edited by R.W. Cahn, P. Haasen and E.J. Kramer, VCH, New York, 1992.
6. M.N. Helmus, "Overview of biomedical materials", pp.33-38, *MRS Bulletin*, September 1991.
7. J.B.Park and R.S.Lakes, "Biomaterials: An Introduction", Plenum Press, New York, 1992.
8. W.Suchanek and M. Yoshimura, "Processing and properties of hydroxyapatite-based biomaterials for use as hard tissue replacement implants", Vol. 13, No.1, 94-115, *J.Mater. Res.*, 1998.
9. S.K.Ritter, "Boning Up", *Chemical and Engineering News*, August 25, 1997.
10. L.L.Hench, "Bioceramics", pp.1705-28, Vol.81, No.7, *J. Am.Ceram.Soc.*, 1998.
11. F. Williams "Materials for oral and maxillofacial surgery", pp.260-285 in *Medical and Dental Materials, Volume 14*, Materials Science and Technology: A Comprehensive Treatment, Edited by R.W. Cahn, P. Haasen and E.J. Kramer, VCH, New York, 1992.
12. A.Slosarczyk, E. Stobierska, Z.Paszkiwicz and M. Gawlicki, "Calcium phosphate materials prepared from precipitates with various calcium:phosphorus molar ratios", 2539-44, Vol.79[10], *J.Am.Cer. Soc.*, 1996.

13. P. Layrolle, A. Ito, and T. Tateishi, "Sol-Gel synthesis of amorphous calcium phosphate and sintering into microporous hydroxyapatite bioceramics", 1421-28, 81[6], *J. Am. Ceram. Soc.*, 1998.
14. S.A. Bouali, C. Rey, A. Lebugle, and D. Bernache, "Surface modifications of hydroxyapatite ceramics in aqueous media", pp.269-272, Vol.15, No.4, *Biomaterials*, 1994.
15. M. Toriyama, Y. Kawamoto, T. Suzuki, Y. Yokogawa, K. Nishizawa, and H. Nagae, "Synthesis of hydroxyapatite by an oxidative decomposition method of calcium chelate", 939-943, Vol.100, *J. of the Ceram. Soc. Jpn. Int. Edition*, 1992.
16. F. Nagata, Y. Yokogawa, M. Toriyama, Y. Kawamoto, T. Suzuki, K. Nishizawa and H. Nagae, "Hydrothermal synthesis of plate-like hydroxyapatite crystals", pp.11-14, Advanced Materials '93 II/A: Biomaterials, Organic and Intelligent Materials, *Trans. Mat. Res. Soc. Jpn. Volume 15A*, Elsevier Science, 1994.
17. H. Monna and T. Kamiya, "Preparation of hydroxyapatite by the hydrolysis of brushite", pp.4247-4250, Vol.22, *J. Materials Science*, 1987.
18. I.H. Arita, D.S. Wilkinson, M.A. Mondragon and V.M. Castano, "Chemistry and sintering behaviour of thin hydroxyapatite ceramics with controlled porosity", pp. 403-408, Vol.16, *Biomaterials*, 1995.
19. P. Van Landuyt, F. Li, J.P. Keustermans, J.M. Streydio, F. Delannay and E. Munting, "The influence of high sintering temperatures on the mechanical properties of hydroxylapatite", pp.8-13, Vol.6, *Journal of Materials Science: Materials in Medicine*, 1995.
20. A.J. Ruys, M. Wei, C.C. Sorrell, M.R. Dickson, A. Brandwood and B. K. Milthorpe, "Sintering effects on the strength of hydroxyapatite", pp.409-415, Vol.16, *Biomaterials*, 1995.
21. S. Best and W. Bonfield, "Processing behaviour of hydroxyapatite powders with contrasting morphology", 516-521, vol.5, *Journal of Materials Science: Materials in Medicine*, 1994.
22. C.J. Liao, F.H. Lin, K.S. Chen and J.S. Sun, "Thermal decomposition and reconstitution of hydroxyapatite in air atmosphere", pp.1807-1813, Vol.20, *Biomaterials*, 1999.

23. K.S. Sing, "Reporting physisorption data for gas/solid systems", p.605, in Pure and Applied Chemistry, Singwork, London, 1985.
24. R.E.Treybal, "Mass-Transfer Operations", McGraw Hill, Third Edition.
25. D.M.Ruthven, "Principles of Adsorption and Adsorption Processes", John Wiley, New York, 1984.
26. I.J.Krijgsman, "Product Recovery in Bioprocess Technology", Butterworth-Heinemann, Oxford, 1992.
27. P.A.Belter, E.L.Cussler, and W.S.Hu, "Bioseparations: Downstream Processing for Biotechnology", John Wiley, New York, 1988.
28. G.H.Cowan, "Development of physical and mathematical modelling methods for scale-up of batch stirred tank and packed-bed column adsorption and chromatographic units", Nato ASI Adsorption: Science and Technology, Vimerio, Portugal, July 17-29, 1988.
29. F. Franks, "Protein Biotechnology: Isolation, Characterization and Stabilization", Chapter I, pp.1-20, Humana Press, Totowa, New Jersey, 1993.
30. J.E.Bailey and D.F.Ollis, "Biochemical Engineering Fundamentals", Second Edition, McGraw Hill, New York, 1986.
31. A. Krajewski, R. Malavolti, and A. Piancastelli, "Albumin adhesion on some biological and non-biological glasses and connection with their Z-potentials", 17: 53-60, *Biomaterials*, 1996.
32. J.P.Van der Wiel and J.A.Wesselingh, "Continuous adsorption in biotechnology",
33. H.Zeng, K.K.Chittur, and W.R.Lacefield, "Analysis of bovine serum albumin adsorption on calcium phosphate and titanium surfaces", pp.377-384, Vol.20, *Biomaterials*, 1999.
34. M.Wahlgren and T.Arnebront, "Protein adsorption to solid surfaces", pp201-208, Vol.9, *TIBTECH*, June 1991.
35. D.T.H. Wassell and G. Embery, "Adsorption of bovine serum albumin onto titanium powder", 17:859-864, *Biomaterials*, 1996.
36. C.Forgues, M.Bailly, and G.Grevillot, "Adsorption of BSA and hemoglobin on hydroxyapatite support: Equilibria and multicomponent dynamic adsorption", pp.5-16, Vol.4, *Adsorption*, 1998.

37. D.T.H. Wassell, R.C. Hall, and G. Embery," Adsorption of bovine serum albumin onto hydroxyapatite", 16:697-702, *Biomaterials*, 1995.
38. V. Hlady and H.F. Milhofer, "Adsorption of human serum albumin on precipitated hydroxyapatite" 69(3): 460-68, *J. Colloid Interface Science*, 1979.
39. J.Talbot, "Time dependent desorption: A memory function approach", pp.89-94, Vol.2, *Adsorption*, 1996.
40. M.E. Soderquist, and A.G. Walton, "Structural changes in Proteins adsorbed on polymer surfaces", 75(2): 386-397, *J. Colloid Interface Science*, 1980.
41. J.Sefton, M.Lambert, M.Wilson, and H.N.Newman, "Adsorption/desorption of amine fluorides to hydroxyapatite", pp.37-46, Vol.17, No.1, *Biomaterials*, 1997.
42. L.Feng and J.D.Andrade, "Protein adsorption on low temperature isotropic carbon: III. Isotherms, competitiveness, desorption and exchange of human albumin and fibrinogen", pp.323-333, vol.15, No.5, *Biomaterials*, 1994.
43. D.Rickwood and B.D. Haues, "Protein purification applications: A practical approach", Edited by E.L.V. Harris and S. Angel, IRL Press , Oxford, 1990.
44. J.M. Oliviera, R.N. Correia, and M.H. Fernandes, "Surface modifications of a glass and a glass-ceramic of the MgO-3CaO.P₂O₅-SiO₂ system in a simulated body fluid", pp.849-54, Vol.16, No.11, *Biomaterials*, 1995.
45. A. Krajewski, A. Piancastelli, and R. Malavolti"Albumin adhesion on ceramics and correlation with their Z-potential", pp.637-641, vol.19, *Biomaterials*, 1998

İZMİR YÜKSEK TEKNOLOJİ ENSTİTÜSÜ
REKTÖRLÜĞÜ
Kütüphane ve Dokümantasyon Daire Bşk.

APPENDIX A

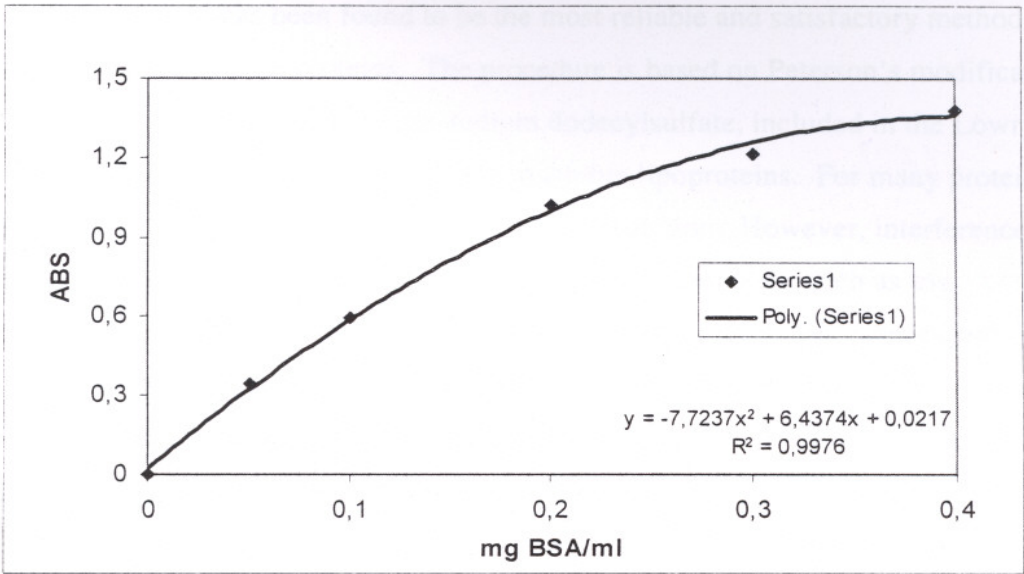


Figure 47a. Calibration curve for direct procedure of Lowry assay.

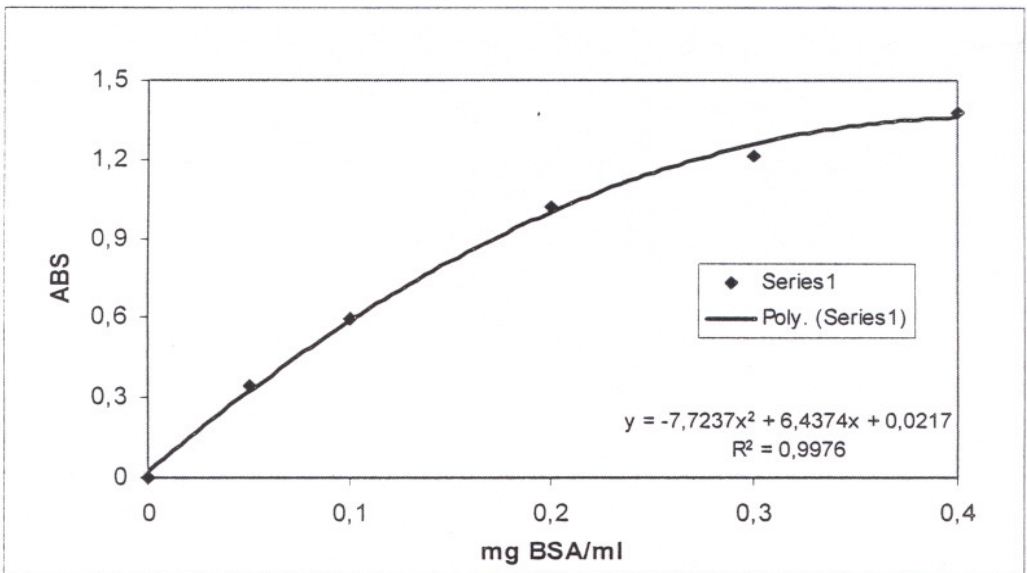


Figure 47b. Calibration curve for indirect procedure of Lowry assay.

Lowry Method

Lowry method has been found to be the most reliable and satisfactory method for the determination of soluble proteins. The procedure is based on Peterson's modification of the micro-Lowry method and utilizes sodium dodecylsulfate, included in the Lowry reagent, to facilitate the solution of relatively insoluble lipoproteins. For many proteins, the Lowry reaction can be run directly on the protein solution. However, interference in the direct Lowry procedure is caused by commonly used chemicals, such as tris, ammonium sulfate, EDTA, sucrose, citrate, etc. An alkaline cupric tartarate reagent complexes with the peptide bonds and forms a blue color when phenol reagent is added. Absorbance is determined at a suitable wavelength between 500 nm and 800 nm. In this work, the wavelength chosen was 750 nm. The protein concentration was determined from a calibration curve. Lowry reagent contains copper sulfate, sodium tartarate, sodium carbonate and sodium hydroxide in certain proportions with Folin-Ciocalteu's phenol reagent (sodium tungstate, sodium molybdate, phosphoric and sulfuric acid) in water.

APPENDIX B

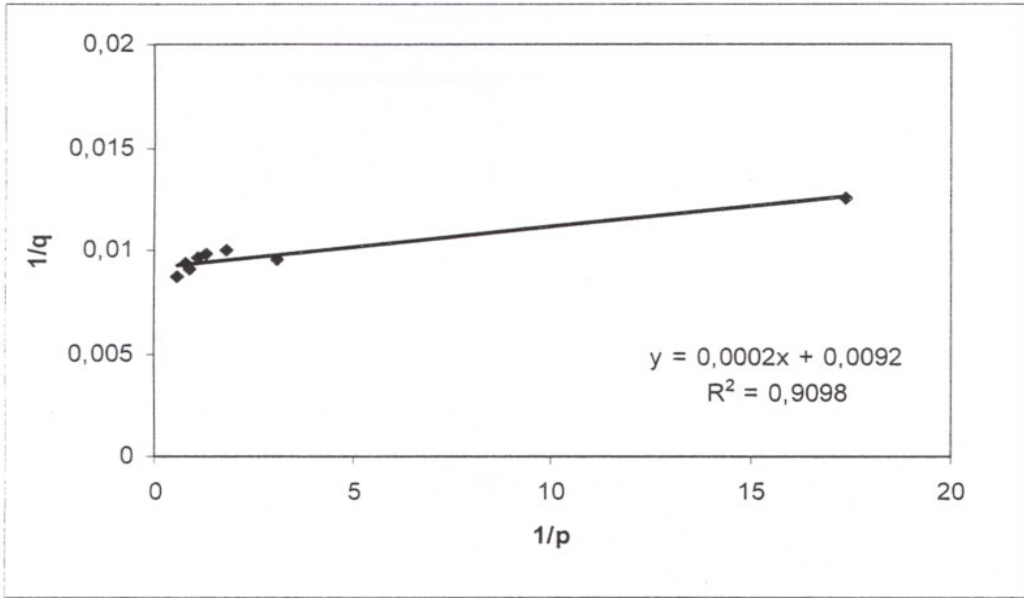


Figure 48. Double reciprocal plot for BSA adsorption on HA at pH=5.6.

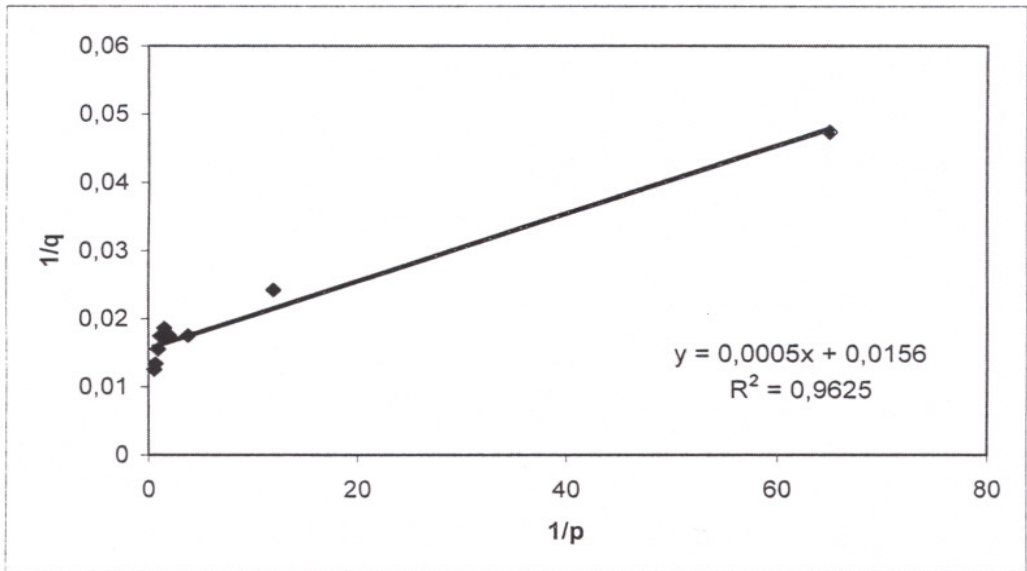


Figure 49. Double reciprocal plot for BSA adsorption on HA at pH=6.6.

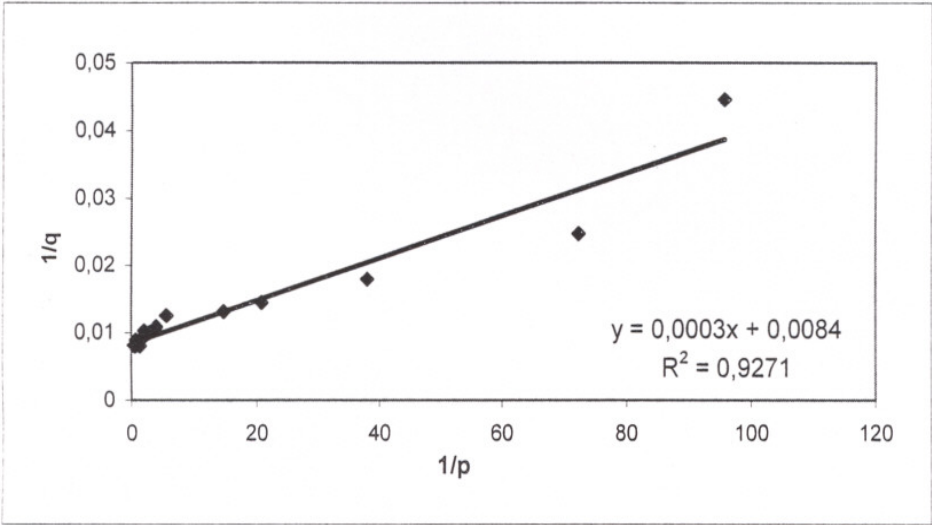


Figure 50. Double reciprocal plot for BSA adsorption on HA at pH=4.7.

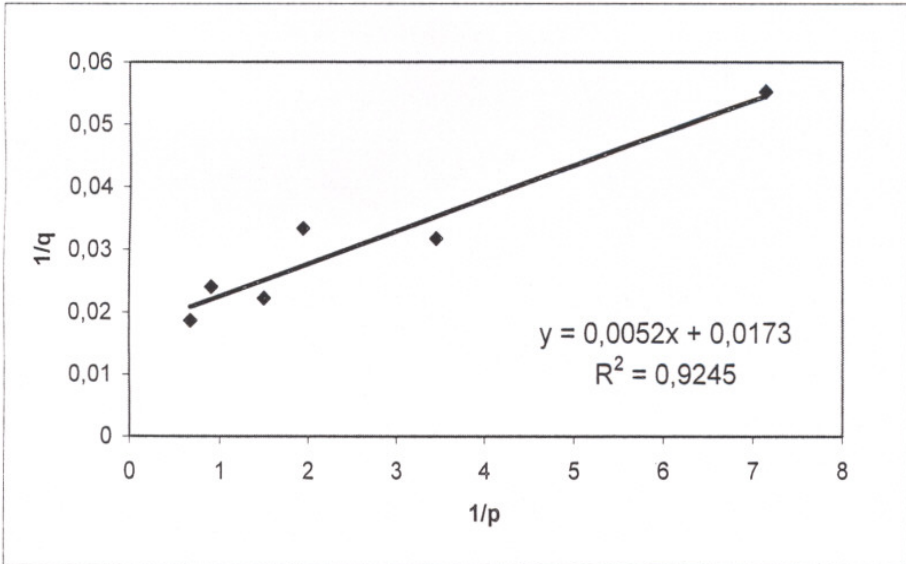


Figure 51. Double reciprocal plot for BSA adsorption on zirconia at pH=4.5.